POLITECNICO DI TORINO

Corso di Laurea Magistrale in Ingegneria Energetica e Nucleare

Tesi di Laurea Magistrale

Process modelling of a Direct Air Capture (DAC) system based on the Kraft process

Relatore

Prof. Andrea Lanzini

Correlatore

Ing. Giulio Buffo

Candidato

Stefano Bianchi

Dicembre 2018

Abstract

Socio-political interests of reducing GHG emissions towards the environment have led to significant technological improvement of efficient methods to capture CO_2, then dispatched to either sequestration (CCS) or re-utilization (CCU) applications. In this framework, this thesis proposes the modelling of a Direct Air Capture (DAC) process using chemicals. Starting from a reference layout based on the Kraft process, the aim of this paper is to simulate the whole process, considering the main assumptions and theoretical solutions adopted in the analysis, and to discuss the primary energy requirements and thus the energy feasibility of such a solution.

The base process found in literature has been reproduced on the commercial software Aspen Plus® after being subdivided in specific sections, depending on the main chemical reactions that occur in each of them. The CO_2 stream delivered after the compression section is at 45°C and 150 bar and can be considered for both CCS and CCU applications.

Once the model was completed, a specific analysis has been performed to evaluate the energy performance of the simulated plant. The electricity demand of the global system is satisfied by the internal production of electric power from a combined cycle in the power island section. Thus, excluding the need for electricity, the total primary energy input has been evaluated in 1.97 $kWh/mol_{CO2,\ captured}$, under the hypotheses of adopting an adiabatic calciner, natural gas rather than pure methane for feeding the calciner and the power island, and after applying the pinch analysis to study a possible heat recovery network between the streams of the plant. This analysis highlighted the possibility of recovering almost 90% of the heat generated in the plant, which otherwise would have been supplied by an external thermal source.

Being the modelled plant still at the pilot state, the lack of reliable data about capital and operating costs of the components did not allow perform a detailed techno-economic assessment. Nevertheless, all the main technical results of this thesis are validated by the data and the results of several papers found in literature.

Table of contents

List of figures

List of tables

List of acronyms

CCS	Carbon Capture and Storage
CCU	Carbon Capture and Utilization
CE	Carbon Engineering
DAC	Direct Air Capture
EU	European Union
GHG	Greenhouse Gas
IPCC	International Panel for Climate Change
MEA	Monoethanolamine
RCP	Representative Concentration Pathways
SET Plan	Strategic Energy Technology Plan
UN	United Nations
UNFCCC	United Nations Framework Convention on Climate Change

1. Introduction

The amount of greenhouse gas emissions emitted every year in the atmosphere is recognized as one of today's most important problems. More specifically, the emissions from anthropogenic sources have been the main cause of the increased attention on the world climate changes. In the Intergovernmental Panel for Climate Change (IPCC) Synthesis Report published in 2014, scientists stated that "anthropogenic greenhouse gas emissions have increased since the pre-industrial era, driven largely by economic and population growth, and are now higher than ever. This has led to atmospheric concentrations of carbon dioxide, methane and nitrous oxide that are unprecedented in at least the last 800,000 years" [1]. This issue is also well represented in a chart, shown here in Figure 1.1, where the total annual anthropogenic GHG emissions by gases trend is clearly increasing.

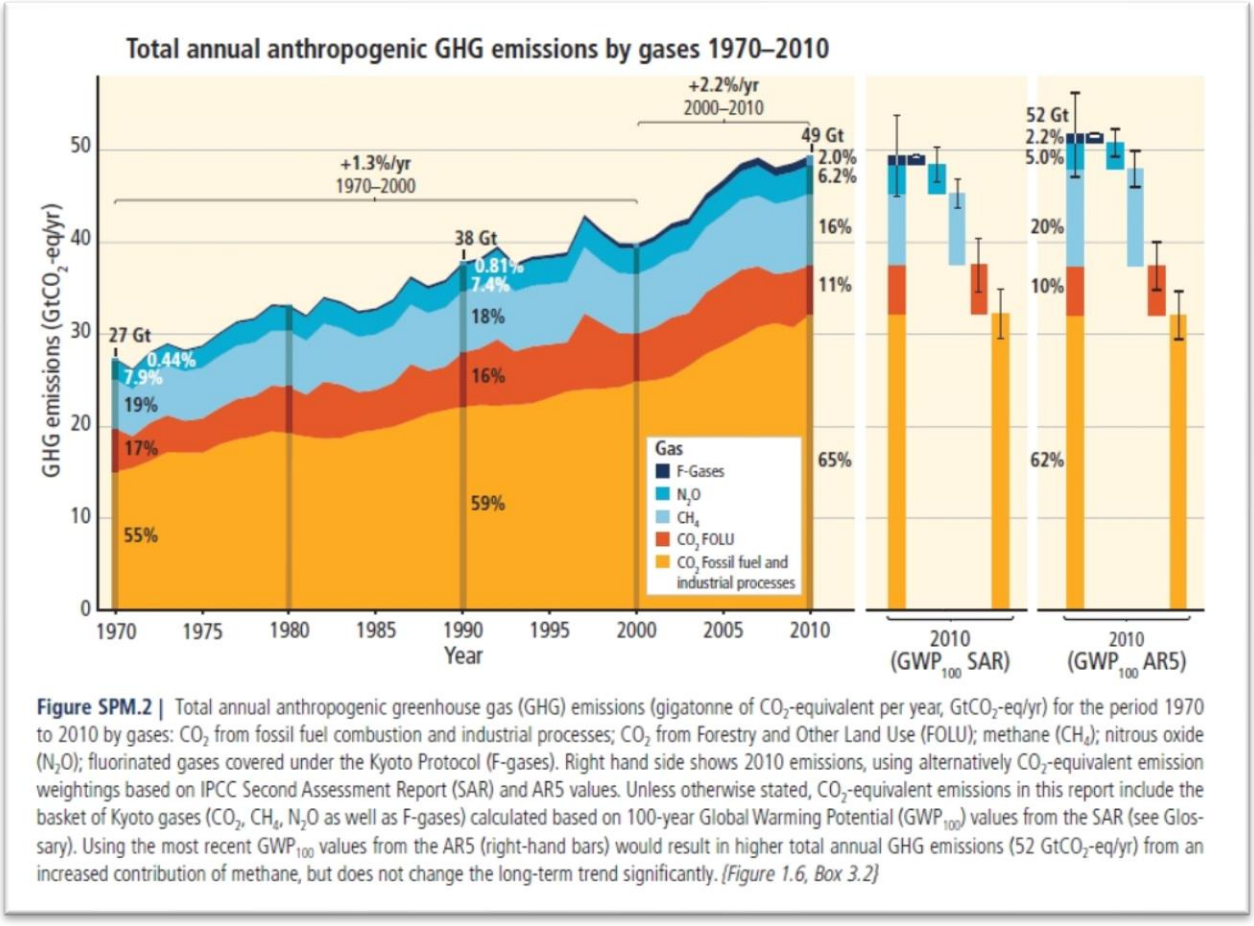

Figure SPM.2 | Total annual anthropogenic greenhouse gas (GHG) emissions (gigatonne of CO_2-equivalent per year, $GtCO_2$-eq/yr) for the period 1970 to 2010 by gases: CO_2 from fossil fuel combustion and industrial processes; CO_2 from Forestry and Other Land Use (FOLU); methane (CH_4); nitrous oxide (N_2O); fluorinated gases covered under the Kyoto Protocol (F-gases). Right hand side shows 2010 emissions, using alternatively CO_2-equivalent emission weightings based on IPCC Second Assessment Report (SAR) and AR5 values. Unless otherwise stated, CO_2-equivalent emissions in this report include the basket of Kyoto gases (CO_2, CH_4, N_2O as well as F-gases) calculated based on 100-year Global Warming Potential (GWP_{100}) values from the SAR (see Glossary). Using the most recent GWP_{100} values from the AR5 (right-hand bars) would result in higher total annual GHG emissions (52 $GtCO_2$-eq/yr) from an increased contribution of methane, but does not change the long-term trend significantly. *{Figure 1.6, Box 3.2}*

Figure 1.1 – Anthropogenic GHG emission in the period 1970-2010 [1]

It is worth noting that the total anthropogenic GHG emission have increased year by year from 1970 to 2010, but it is to be underlined that the major increases happened in the first ten years of the XXI century, a very narrow period. At the beginning of the year 2010, anthropogenic GHG emissions have reached 49 ± 4.5 $GtCO_2$-eq/yr. In particular, CO_2 emitted from fossil fuel combustion and industrial processes contributed to about 78% of the total GHG emissions increase of the last 40 years. These emissions are mainly related to population size, economic activity, lifestyle, energy use, technology and climate policy [1].

Keeping as a reference the data about CO_2 emissions provided by the last IPCC Report on Climate Change in 2014, the future scenario is very alarming. As it is possible to see in the next Figure 1.2, the trend will be of continuous growth, with the estimate of almost 150 $GtCO_2$-eq/yr in less than one century.

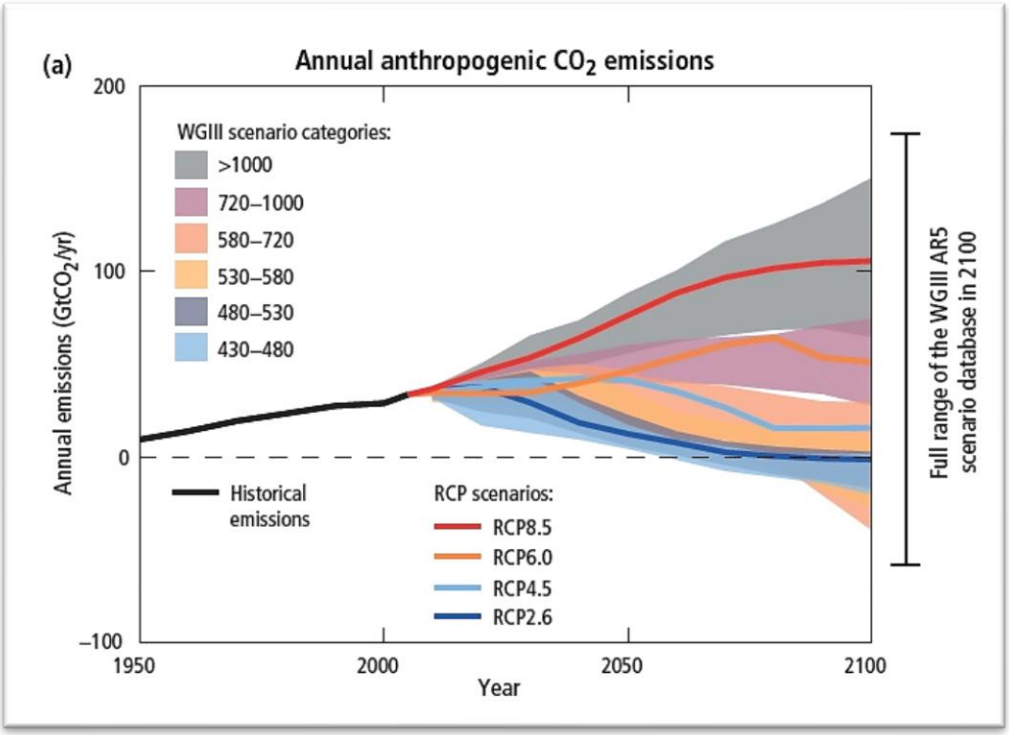

Figure 1.2 - Future trend of anthropogenic CO2 emissions [1]

The RCPs (Representative Concentration Pathways) scenarios (8.5, 6.0, 4.5 and 2.6 in Figure 1.2) are very useful to understand the relation between the future trend of carbon dioxide concentration and the associated global surface temperature change.

The trend of global surface temperature change is clearly visible in the following Figure 1.3, where an increase of the global surface temperature is associated to each RCP shown before, with a certain degree of probability of happening.

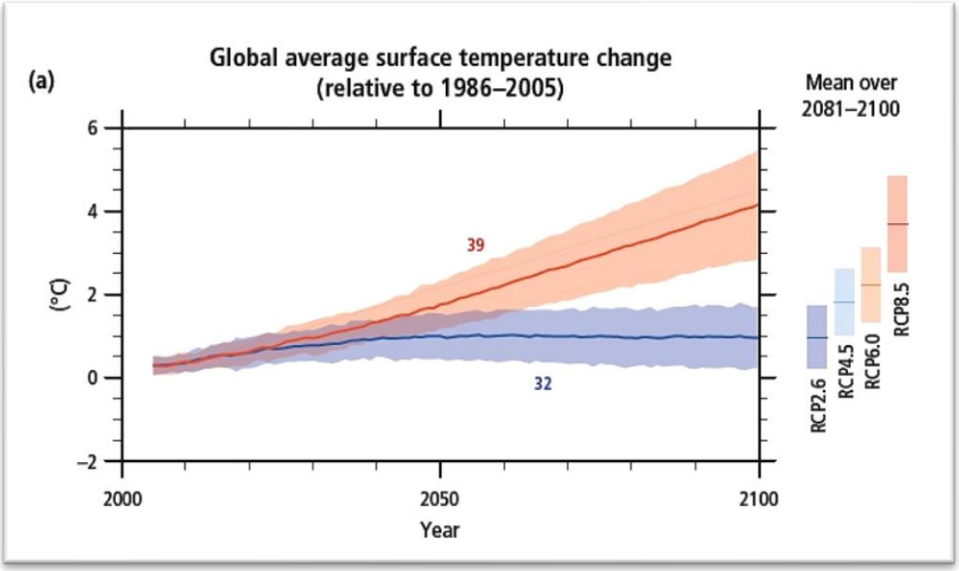

Figure 1.3 - Future scenarios for surface temperature change [1]

Global surface temperature change for the end of the XXI century (2081-2100) is expected to likely exceed 1.5°C for RCP4.5, RCP6.0 and RCP8.5 (*high confidence*). Warming is likely to exceed 2°C for RCP6.0 and RCP8.5 (*high confidence*), more likely not to exceed 2°C for RCP4.5 (*medium confidence*), but unlikely to exceed 2°C for RCP2.6 (*medium confidence*) [1].

As mentioned above, the atmospheric concentration of carbon dioxide has increased from 280 ppm in the pre-industrial age to more than 370 ppm now, and, as seen in the previous figures, is expected to increase steeply in the future [2].

Moreover, the increase of carbon dioxide emissions is not an isolated issue and the relation between CO_2 concentration in atmosphere and the increase in temperature of the earth during the last centuries is now an established fact and clearly visible in Figure 1.2 and Figure 1.3. From now on, future climate will depend on committed warming caused by past anthropogenic emissions, as well as future anthropogenic emissions and natural climate variability. With *medium confidence*, the IPCC has reported that the global mean surface temperature change for the period 2016-2035 relative to 1986-2005 will likely be in the range 0.3°C to 0.7°C, assuming that no major volcanic eruptions or changes in some natural sources or total solar irradiance will happen [1].

The seriousness of the situation has been recognised, probably for the very first time, by almost all nations of the world on 12th December 2015 with the so called 'Paris Agreement'. It is an agreement within the United Nations Framework Convention on Climate Change (UNFCCC), dealing with GHG emissions mitigation, adaptation, and finance, starting in the year 2020. The Paris Agreement is proposed to undertake for the first-time ambitious efforts to tackle climate change and adapt to its effects. Its central goal is to keep the global temperature rise at the end of this century below 2°C with respect to pre-industrial levels and to pursue efforts to limit the temperature increase even further to 1.5°C [3].

Considering all this, one of the straightforward ways to keep the overall CO_2 emissions in the atmosphere below unsustainable levels is the introduction of new techniques to capture CO_2: if combined with the energy transition toward sustainable energy sources, the reduction of CO_2 emissions can mitigate the climate changes stressed in this worrying scenario.

1.1 Energy transition and reduction of CO_2 emissions

In a period of energy transition like the XXI century, the importance of renewable energy sources is increasing every day. The theme of sustainable development has been now considered as one of the most important goals of these decades and not by chance it has been thoroughly described in the 'UN 2030 Agenda for Sustainable Development' published on September 25th, 2015. Countries adopted a set of goals to tackle poverty, protect the planet and ensure prosperity for all as part of a new sustainable development agenda. Each goal has specific targets to be achieved before the next 15 years [4].

Figure 1.4 shows the 17 Sustainable Development Goals reported in the 2030 Agenda, aiming to promote the development in different social, economic and environmental areas: integrated processes should drive and support the pathways to these Goals in a sustainable manner, including international cooperation in the political and institutional context.

Figure 1.4 – The 17 Sustainable Development Goals

As it is clear, the number 13 is strictly connected to the topic of this thesis work, as it refers directly to climate action; but many others are related to clean-energy production, innovation and responsible consumption and production (number 7, 9 and 12). About this, the EU has implemented a specific program focused on the energy sector, generically called 'EU SET plan' [5]. It has been the research and innovation pillar of the EU's energy and climate policy since 2007 but with the last revision in 2015 the SET-Plan has adapted its structure and processes to effectively accelerate the transformation of the EU's energy system. Particularly, the plan focuses on the following ten 'key actions' [5]:

1. Develop performant renewable technologies integrated in the energy system;
2. reduce the cost of key renewable technologies;
3. create new technologies and services for consumers;
4. increase the resilience and security of the energy system;
5. develop energy efficient materials and technologies for buildings;
6. improve energy efficiency for industry;
7. become competitive in the global battery sector (e-mobility);
8. strengthen market take-up of renewable fuels;
9. drive ambition in carbon capture and storage/use deployment;
10. increase safety in the use of nuclear energy.

For each of the ten key actions, a specific target has been defined and seven implementation plans have been adopted until January 2018. Specifically, the ninth of them is directly connected to a very innovative and increasingly considered topic like the Carbon Capture Storage and Use (CCS/U).

Figure 1.5 is taken directly from the EU's website in the SET Plan section [5], and contains all the points listed before.

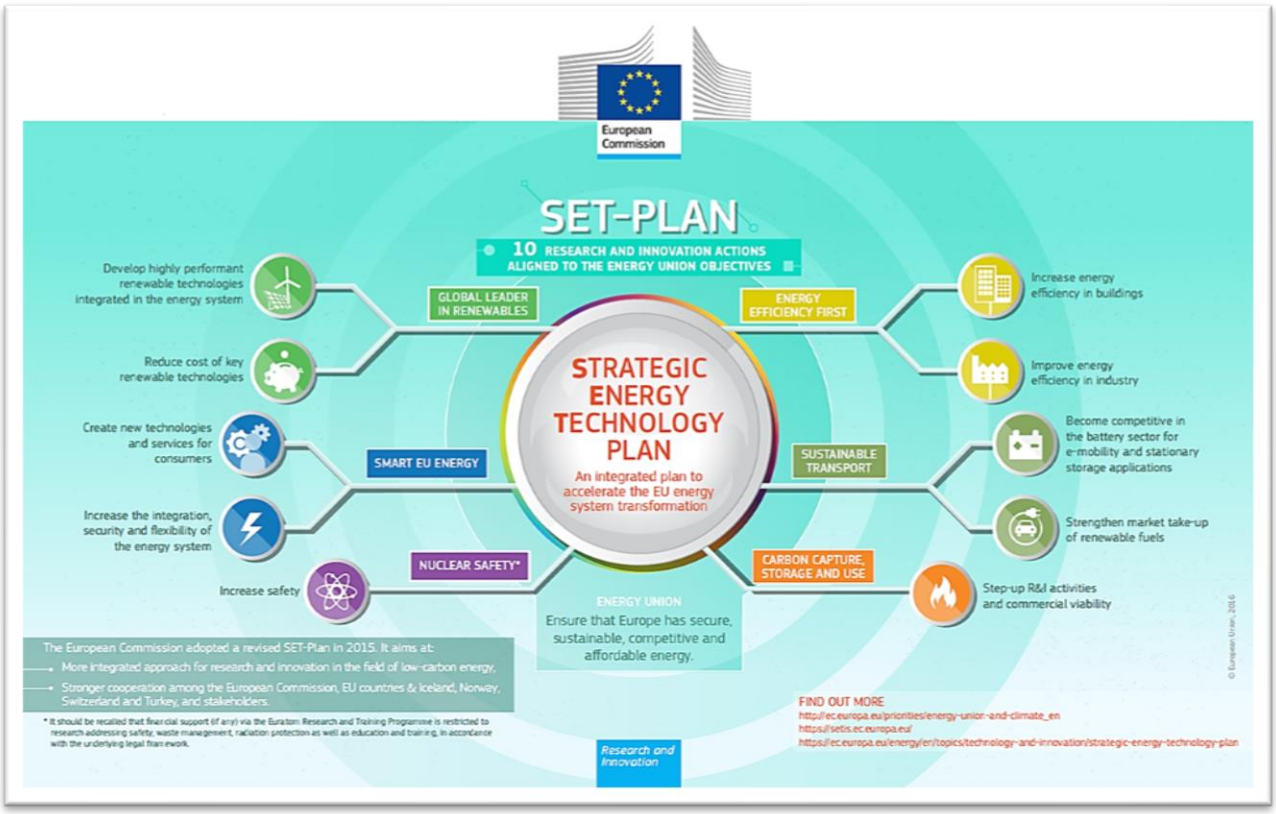

Figure 1.5 – EU's Set-Plan, main key actions [6]

With these final goals, the line to follow is clearly drawn and leads to a more responsible way to produce and use the energy. Indeed, the increase of the efficiency of the energy chain and the introduction of renewable energy sources are the major keys for a sustainable development. Of course, improving process efficiency to reduce the amount of CO_2 emissions and implementing systems capable to separate CO_2 and the other GHG requires a great technological effort and a big expenditure in terms of time and money. Moreover, despite the significant deployment in the last years, the use of renewable energy sources still faces different and already known

drawbacks like the difficulty of predicting the generated power and their availability on medium-long term [6].

Especially the renewable energy sources have been taken into account since they are low-cost energy sources and they can be an alternative to fossil sources, especially considering significant fluctuation of fossil fuel prices in today's global energy market. Despite their strengths, renewable sources still present drawbacks in the field of national energy security due to their intermittence and to possible network congestion problems [7]. The energy transition appears to be of primary importance to reach the set goals: to make it possible all the most energy-intensive sectors have been analysed. As a result of these studies, it has been shown that the transportation sector contributes to about 22% of global emissions worldwide [7], as the majority of GHG emissions in this sector is related to CO_2 produced by the engines burning fossil-based fuels like gasoline and diesel.

1.2 Pathways for CO_2 capture and final disposal via storage (CCS) or utilization (CCU)

In the previous sections, the importance of a reduction of carbon dioxide emissions has been underlined by all the references taken into consideration. In fact, despite all the efforts to minimize CO_2 emissions, tens of billions of CO_2 are still released every year. CO_2 capture was proposed in 2005 by the IPCC as a technology necessary to decelerate the growth of the atmospheric CO_2 concentration [8], and during the years more than one method for capturing CO_2 has been proposed and developed.

There are several approaches to capture CO_2. Some rely on capturing CO_2 close to the source of emissions, other rely on recapturing it out of the atmosphere, possibly long after its emissions [2]. Conventional CO_2 capture is usually considered for CO_2 emissions from large stationary sources, such as fossil-fuel-based power plant, cement plants, oil refineries and iron or steel industry installation [9]. Carbon capture can be implemented according to the different processes in which it is carried out, that are listed below:

1. **Pre-combustion.** It is usually adopted when starting from natural gas or syngas (a gas mixture made mostly of CO and H_2). A pre-combustion system involves first converting solid, liquid or gaseous fuel into a mixture of hydrogen and carbon dioxide using one of several processes such as 'gasification' or 'reforming' [1].

2. **Oxy-fuel or carbonation-calcination.** This process is carried out by combustion with pure oxygen instead of air. It gives benefits in terms of CO_2 concentration in flue gases (flue gases volume is considerably reduced by using O_2 instead of air and CO_2 concomitantly increased up to 90%) but there are drawbacks related mainly to the very high costs to obtain pure oxygen from air separation units.
3. **Post-combustion.** In this case, carbon dioxide is captured from flue gases released after the combustion. This is the process held in greater consideration due to the advantage of not having to make changes to the combustion facilities even if the major drawback is the lower CO_2 concentration in flue gases (between 4 vol % and 13-15 vol % depending on the fossil fuel used in the power plant) [10]. This CO_2 capture system is usually constituted by a separated plant, especially when liquid amine absorption techniques are used. This method will be resumed and described in more details in the next section.

Once the carbon dioxide has been separated by other gases (e.g. air, other flue gases), two main approaches have been deemed worthy of attention in the last twenty years to store or re-use it. Carbon Capture Storage (CCS) concept was the first considered as a possible solution to mitigate the impact of CO_2 in the atmosphere, while Carbon Capture Utilisation (CCU) concept has been introduced in the following years with the aim of giving an energetic value also to the captured CO_2. CCS is a set of technologies organized in order to capture wasted CO_2, to transport it from large point sources to a storage site where it is injected down wells and then permanently trapped in porous geological formations deep below the surface [11]. Instead of injecting CO_2 down in geological formations, other solutions are the storage into oceans, into mineral carbonates or using it for industrial processes. Moreover, the IPCC report about carbon dioxide capture and storage considers “CCS as an option in the portfolio mitigation actions for stabilization of atmospheric greenhouse gas concentrations”, since CCS has the potential to reduce overall mitigation costs and increase flexibility in achieving GHG emission reductions [8].

However, CCS requires high investment costs (mainly for the carbon dioxide compression and for the construction of injection wells in the ground) and poses risks associated with the need for long-term storage and potential leakage of CO_2 [12]. In this framework, Carbon Capture and Utilization (CCU) concept is being proposed as a complementary technology to CCS with the aim of both reducing CO_2 emissions and consumption of fossil resources by utilising CO_2 as a feedstock for the production of chemicals and synthetic fuels [12]. The value-added products

generated by the conversion of CO_2 can be then enhanced for many other applications and the fuels produced could be a possible and valid alternative to the traditional fossil fuels.

Based on CCU concept, there are some interesting projects like *ICO2chem*, that aims to study a possible combination between carbon capture and new and innovative processes to produce chemicals and synthetic fuel. For example, *ICO2chem* aims to reuse the captured CO_2 into the SOEC (Solid Oxide Electrolyser Cell) technology or alternatively in a Reverse Water-Gas Shift reactor, followed by a Fischer-Tropsch (FT) synthesis unit. The aim of these works is not only the reduction of the global CO_2 emissions, but also the re-utilisation of the captured carbon dioxide as a significant source for the synthesis processes of different commodities, mainly fuels and chemicals. Indeed, the technologies analysed in these projects firstly aim to propose an alternative process to the traditional production of the transportation fuels and secondly are capable of producing alternative products for the chemical sector. In this sense, Fischer-Tropsch process can easily yield chemical products that have properties like those of fuels but constituted by a number of carbon atoms higher than the fuels. At the end, the idea is to produce CO_2-neutral fuels and chemicals with two main consequences: reduction of the dependency on fossil fuel in the energy and chemical sectors and the consequent reduction of CO_2 yearly emissions.

1.3 Thermodynamics of Direct Air Capture

DAC is only one of the possibilities to separate the carbon dioxide from a gaseous mixture. However, the separation of a mixture under isothermal and isobaric conditions requires a minimum amount of energy [13]. In this paragraph, a brief description of how to calculate this work is provided since the value obtained here will be compared with the energy performance of the model realized in this thesis.

First, the minimum thermodynamic work required to separate CO_2 can be written for the following simplified system:

The theoretical minimum work of separation is equal to the difference between the work potential of the product and feed streams, which is equal to the difference in stream exergy [13]:

$$W_{min} = \pm \sum_{i} \Psi_i \qquad \text{(eq. 1-1)}$$

where Ψ_i is the exergy of the stream *i*.

As written above, if isothermal and isobaric processes are considered, the change in work potential equals the change in the Gibbs free energy [13]. The reference scheme shown before is the simplest case of separation of one feed stream (stream 1), which consists of *n* substances, into two product streams (stream 2 and 3). All streams consist of ideal mixtures. For this kind of system, the minimum thermodynamic work can be determined by applying the following equation [14]:

$$W_{min} = -\sum_{i=1}^{3} RTN_i \left(\pm \sum_{k=1}^{n} X_{i,k} ln X_{i,k}\right) \qquad \text{(eq. 1-2)}$$

where:

- N_i is the molar flow rate of stream *j;*
- $X_{i;k}$ denotes the molar concentration of substance *k* in stream *j*.

According to the previous equation, the theoretical minimum work required to separate a stream of air with 400 ppm CO_2 (this is CO_2 concentration considered for the developed model) into one stream poor of CO_2 and a second stream of highly concentrated (e.g. 99% purity) CO_2, all at the same temperature and pressure, is about 20 kJ/mol$_{CO2}$, or 0.126 kWh/kg. Of course, no real process can operate by expending only the theoretical minimum work, because reversibility (necessary assumption to achieve minimum work) requires infinitesimal mass transport driving forces, which in turn imply theoretical equipment of infinite size and cost [14].

The value found before is confirmed by a sensitivity analysis that can be realized for different CO_2 capture ratio. In the Table 1.1, the values calculated in the sensitivity analysis are shown.

Table 1.1 – CO_2 capture. Sensitivity analysis

Sensitivity analysis	
% CO_2	Capture work [kWh/kg_CO_2]
3.6%	0.065
50.00%	0.021
30.00%	0.031
20.00%	0.038
15.00%	0.043
10.00%	0.049
5.00%	0.060
3.60%	0.065
1.00%	0.085
0.04%	0.133

The resulting chart is provided in Figure 1.6:

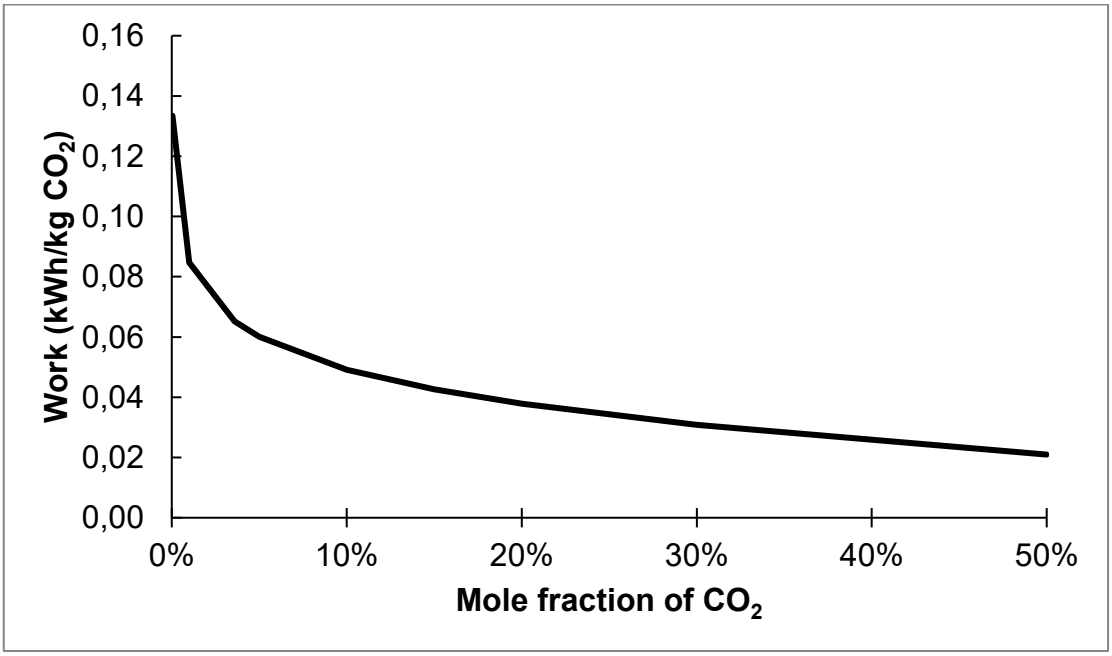

Figure 1.6 – Minimum thermodynamic work for capturing CO_2

The minimum theoretical work is therefore an important benchmark to evaluate the feasibility of a CO_2 capture system from an energetic point of view. Considering that this thesis work aims

at evaluating the energetic feasibility of a system for direct capture of CO_2 from ambient air, it is worth noting (Figure 1.7) the difference between the minimum theoretical work required for CO_2 capture at a temperature of 298 K from a flue gas stream containing 12% of CO_2, and from air with a CO_2 concentration of 400 ppm (e.g. air capture), at different fractions of capture [13].

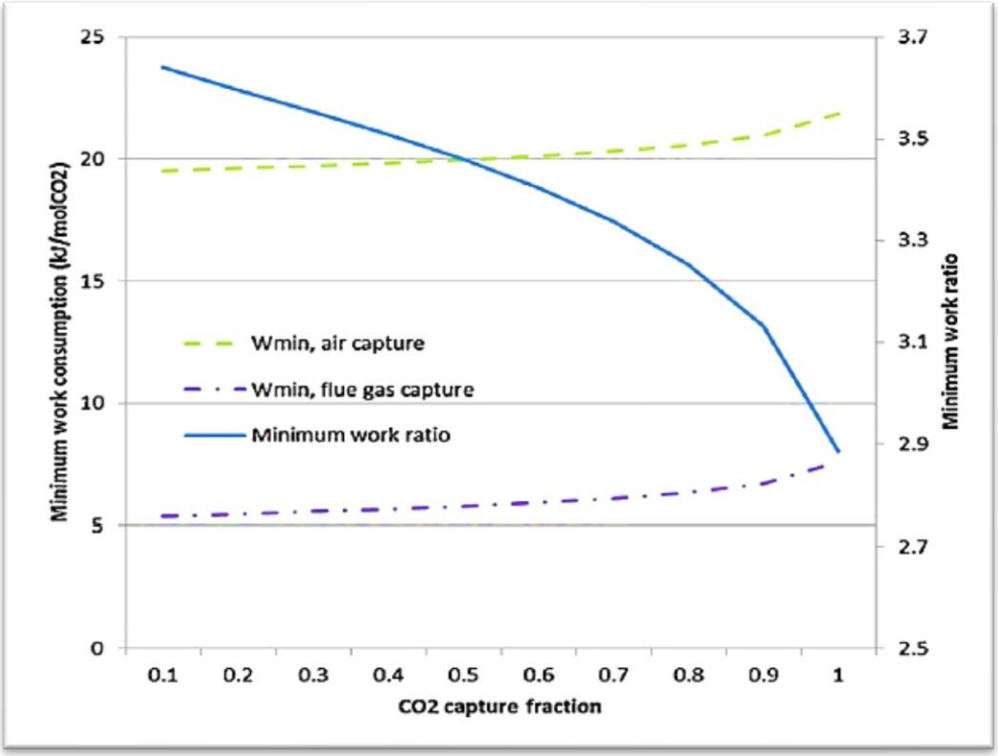

Figure 1.7 – Minimum theoretical work for CO_2 capture from either flue gas or air [14]

On average, the minimum energy requirement for air capture is about three-fold that for flue gas capture and the relative difficulty increases with the reduction in the fraction of capture [13]. This is a first comment that will be considered in the final chapter dedicated to comparing the energy performances of different plants.

1.4 Thesis outline and goals

After a brief introduction about the current situation contained in the 1st chapter and having been determined the minimum work for separating the CO_2 from a gas mixture, the 2nd chapter is focused on the state-of-the-art of the main technologies considered in the field of carbon capture. Mainly the post-combustion method and direct air capture have been analysed to provide a general but however sufficiently detailed idea about the contest.

The 3rd chapter is fully dedicated to the description of the DAC model realized in the thesis work. The theoretical framework on which the process is based, concerning chemistry, thermodynamics and mass transfer is firstly explored while the second part of the chapter contains all the considerations important for a complete understanding of the model, including descriptions of components and design specifications.

Finally, in the 4th chapter, all the results obtained from software simulation are described with the techniques employed to read them. Furthermore, some possible future developments of this work are proposed with the aim of stimulating further insights.

2. State-of-the-art of technologies for carbon capture

In section 1.2, the three main technologies considered today for carbon capture have been shown. In the next two paragraphs a more detailed description of the post-combustion process will be carried out and the Direct Air Capture (DAC) process will be also introduced.

In this work, only post-combustion process will be analysed in more details since both pre-combustion and oxy-fuel combustion are characterized by too significant drawbacks (from both economic and technical points of view) which have not yet been overcome. In particular, in the pre-combustion process, CO_2 capture is relatively easy because its volumetric concentration in the starting gas mixture ranges between 15 and 60% [9], but problems all lie in the first steps of fuel preparation for coal gasification and steam reforming which are still challenging and expensive. The oxy-fuel process is even more complicated and expensive: as described before, the use of oxygen instead of air as oxidising agent for the combustion of a fuel leads to an increase of CO_2 concentration in the final exhausts due to a reduction of the total flue gas volume and it is an important advantage. At the same time, however, the costs associated to the oxygen production must be considered. Oxygen is usually separated from the other air components by using pressure swing adsorption or membrane separation, but these plants are able to separate oxygen at a relatively low quality (~93 ÷ 95% for adsorption and 30÷40% for membranes). Power production plants need high quantity of air (or oxygen in the case of oxy-fuel combustion) and the purity of oxygen must be very high to obtain a concentrated CO_2 in the flue gases. Therefore, the only possibility regarding the oxygen production is the cryogenic air separation unit. In this

case, the costs for the construction and use of the plant would be too high and the oxy-fuel combustion process would not be convenient, especially from the economic point of view.

These are the main reasons for which the post-combustion process is the one that holds the highest consideration in the field of carbon capture. To sum up, in the following Table 2.1 typical pressures, temperatures, and CO_2 concentrations of the different gas streams used in CCS technologies are shown [9],[10].

Table 2.1 – Comparison between carbon capture technologies

	Syngas (PRE-COMBUSTION)	**OXY-FUEL COMBUSTION**	**Flue gas (POST-COMBUSTION)**
Pressure [atm]	> 5	> 50	1
Temperature [°C]	> 100	< 50	< 100
CO_2 concentration [vol %]	~ 35	> 90	4-14

2.1 Post-combustion CO_2 capture

A typical post-combustion plant layout is depicted in Figure 2.1 in next page.

These kinds of plants can capture CO_2 from flue gas released after combustion. The major advantage of this solution is related to the possibility of not retrofitting the existing combustion facilities and managing high amounts of flue gas. Typically, the flue gas needs to be treated to a great extent since impurities such as SO_2 and NO_x constitute a significant problem for the separation process [9]. The problems associated to these acid gases refer to their reactivity toward amines, which are the main compounds used for post-combustion CO_2 capture.

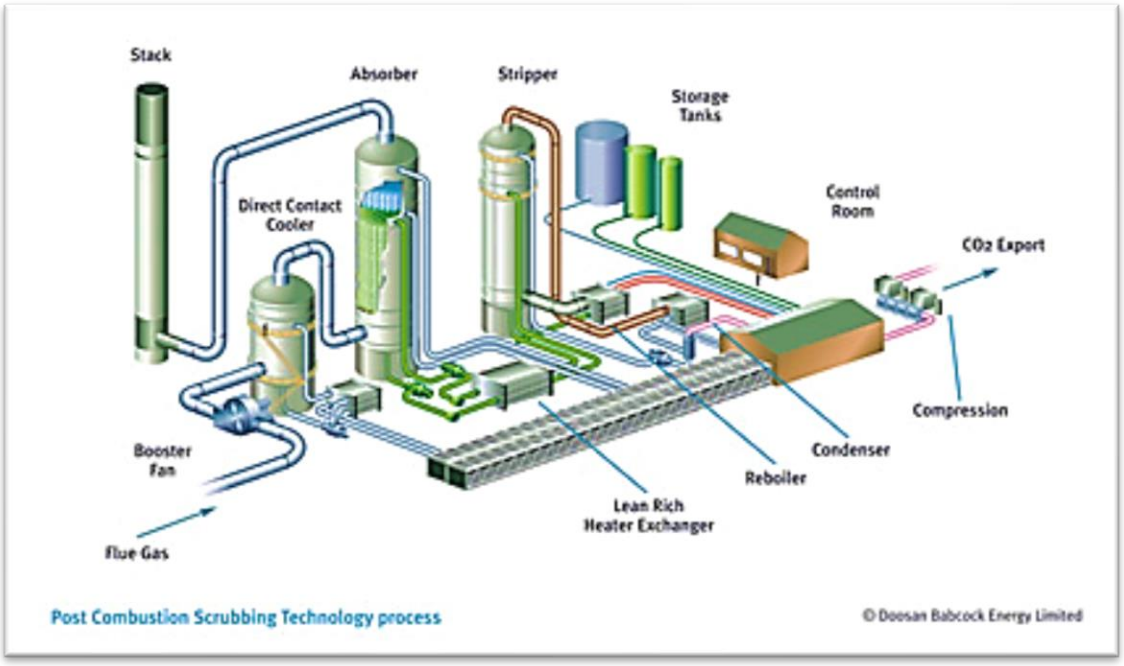

Figure 2.1 – Layout of a post-combustion carbon capture process [16]

The following section is dedicated to the amine-based post-combustion capture and the process is described more in detail because it will be useful to understand at least the behaviour of the absorber column present in the plant modelled in chapter 3 of this work. The absorber used in the Direct Air Capture (DAC) plant works in fact with a liquid solution of water and solvent that can be assimilated (from the point of view of the separation of CO_2) to the solution of water and amines used in post-combustion capture. A better explanation can therefore be helpful for a further correct understanding of the capture process.

2.1.1 Amine-based post-combustion capture

Figure 2.2 shows a typical and generic system for CO_2 capture. Starting from this very general conceptual scheme, each carbon capture system can be developed following different ideas and depending on the specific design choices.

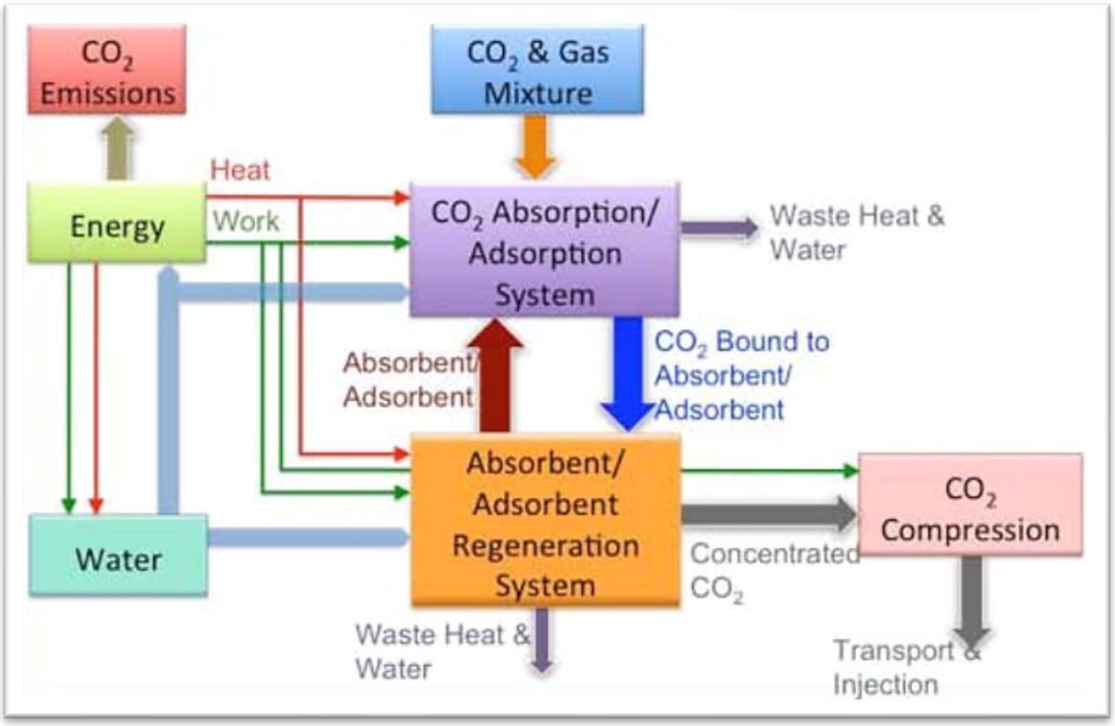

Figure 2.2 – Generic system for CO_2 capture [17]

The first key component is the carbon dioxide absorption/adsorption system, where the CO_2 is separated from a CO_2-rich gas mixture. Once the CO_2 has been chemically bounded to other molecules, there is the absorbent/adsorbent regeneration system. It is responsible for the regeneration of the solvent and for the release of CO_2 in concentrated form. Then, the compression of carbon dioxide occurs, before being sent to the transport/injection system. The global process is driven by some energy inputs in form of heat and work, and water, to compensate water losses that are always present in these processes.

To date, large-scale post-combustion CO_2 separation processes have been mainly based on liquid amine absorption techniques [9]. This process is also called 'amine scrubbing' and consists of a chemical absorption of the CO_2 contained into flue gas using amines. Aqueous solutions of monoethanolamine (MEA), diethanolamine (DEA), and methyldiethanolamine (MDEA) have been successfully used to capture carbon dioxide on a large scale [9]. Amines are organic compounds based on a nitrogen atom; they are formally derived from ammonia (NH_3), in which one or more atoms of hydrogen have been replaced with an alkyl or aryl group [15]. Depending on the number of hydrogen atoms, amines are classified in primary, secondary and tertiary. The choice of using amines to capture CO_2 from flue gas is due to the strong covalent bonds that form

when the amines and CO_2 come into contact. Furthermore, MEA is the most simple and the most used amine in the field of chemical absorption [16].

Looking at the plant layout shown in Figure 2.1, a brief description of its functioning is reported here following. The whole process can be subdivided in two main sections: the absorption of CO_2 and the regeneration of the solvent which leads to a concentrated CO_2 stream.

The absorption phenomenon occurs inside the absorber, which is typically a packed column. A packed column is a pressure vessel provided with a packing section, where the packing bed is usually a hollow tube or pipe or other vessel that is filled with a packing material. The purpose of a packed bed is usually to improve contact between two phases in chemical or similar processes. In this specific case, the absorber is responsible for the separation of carbon dioxide from flue gas (or eventually biogas if the plant is a biogas upgrading plant). The separation occurs when the CO_2 rich flue gas that enters the absorber from the bottom section is put in contact with the solvent, circulated in counter current with respect to the stream of gas. The solvent is constituted by a solution of water and a type of amine (usually MEA). Thanks to its characteristics, the molecules of amine in the solvent react with the molecules of CO_2 contained in the flue gas. This reaction is very selective, which means that amines can bind with CO_2 more than with other gaseous species, leaving the other gas components almost unaltered. The absorber works at low temperature (the temperature difference between the bottom and the top section is about 20÷30°C), and the driving force of the process is the chemical affinity between CO_2 and amines, not the absorber pressure. The working pressure is slightly more than the atmospheric one [17], [18], and it is due to avoid the possibility that some leakage of solvent could cause a depressurization into the absorber. Therefore, it is operated at a pressure in the range of 1-2 bar.

The second section refers to the regeneration of the solvent which is also linked to the separation of CO_2. In a typical amine scrubbing process, the regeneration step occurs in a stripper (usually operated at a pressure of 1.5-3 bar and a temperature of 105-160 °C) [17], [18], but the solvent regeneration process can be very different depending on the solvent used. For example, in the work object of this thesis, the regeneration of the solvent occurs by linking two chemical loops that will be analysed in the following sections, and it will be seen that it is of course not possible to regenerate the solvent using a single component only. In the stripper, high temperature is necessary to enhance the reaction of desorption between CO_2 and the solvent. The stripper is constituted by a packing material, used to put in contact the CO_2-rich solvent that comes from

the top of the column together with a stream of steam coming from the bottom of the stripper. In this way, the carbon dioxide breaks bonds with the solvent and it is released. Strippers used in this process are typically equipped with a reboiler in the bottom part that has more than one role [17]:

- it increases the temperature to reach the set thermodynamic conditions;
- it provides the heat necessary for the endothermic desorption reaction;
- it generates steam to reduce the partial pressure of CO_2 in the column, improving the kinetic of desorption.

This is a general description of a typical amine-based post-combustion capture and it will be mentioned again during the description of the different components in the DAC plant.

2.2 Direct Air Capture (DAC)

This section is fully dedicated to the central theme of this thesis work. Direct Air Capture (DAC) concept is shown starting from a general overview; then, a DAC plant layout will be described into details, with all the comments and remarks necessary to reach a complete understanding of the whole process.

DAC is the acronym used to indicate the direct capture of CO_2 from air. It involves a system in which ambient air flows over a chemical sorbent that selectively removes CO_2 [19]. Then, as for other capture concepts, CO_2 is released as a concentrated stream for disposal or reuse at the end of the sorbent regeneration, but the very big different with respect to the other capture processes is in the absorption phase. Since DAC has elements in common with post-combustion CO_2 capture from flue gas (e.g. the use of a liquid sorbent), it is generally considered in comparison with this concept. However, they are two different technologies with different end goals; DAC is proposed to extract CO_2 from the atmosphere, while post-combustion capture is meant to scrub and purify CO_2 from an exhaust gas [19]. Even if the environmental community tends to compare DAC and post-combustion capture from large point sources as either/or technologies, it would be interesting to develop them both in parallel as different concepts and techniques for CO_2 capture. Moreover, the problem of carbon dioxide concentration in atmospheric air has become so vast that all the technologies able to counteract the problem in some way should be taken in careful consideration.

2.2.1 What is Direct Air Capture and why?

Based on data described in the Introduction, the risks associated to a continuous increment of GHG (and so CO_2 concentration in the atmosphere) get bigger and bigger every year. The climatic response to elevated CO_2 concentration is still uncertain, so a small risk of catastrophic impacts exists even at today's concentration, and the risk is constantly growing as emissions continue to drive up the atmospheric CO_2 burden [20].

The idea of separating CO_2 from air was introduced about 70 years ago and the first industrial use of capturing carbon dioxide from air was reported in cryogenic oxygen plants to prevent condensed carbon dioxide in air from clogging the heat exchangers [21]. Today, this technology is mainly adopted for air separation (e.g. oxygen) plants, spacecrafts and submarines. The carbon dioxide removal has always been a problem for space applications and programs, since human beings emit CO_2 at a rate of about 1 kg/person/day [21], and its concentration in the air of a space shuttle increases very quickly in the absence of systems able to eliminate it. Thus, a lot of research has been done during years to solve this problem, that has been overcome with good results.

The concept of DAC was therefore first introduced at an industrial level and only in 1999 by Lackner as a climate change mitigation opportunity. Once this concept was proposed for the first time as a climate change mitigation possibility, the subsequent years have been dedicated to the technical and scientific analyses with the aim of understanding whether it could really be a good alternative to the traditional capture systems. The considerable number of scientific publications in the 15 years following Lackner's proposal, reflects how attention has changed on DAC concept. Indeed, only 25 publications are registered in the first subsequent decade (from 2000 to 2010) while almost 100 have been published from 2010 to 2015 [9]. This wants to underline how the academics, environmentalists and the scientific community attention is shifting toward this process. Furthermore, efforts are underway to push this technology from the lab scale to the demonstration and pilot scale, but it has not yet been possible to build a real plant. This is only a part of a wider problem and discussion about the necessity of adequate energy polices; more efforts should be carried out by nations in the direction of the construction of new eco-sustainable plants or in alternative, to introduce some kind of economic penalty in case of non-retrofitting of plants with measures for carbon capture.

Anyway, the very reason to consider the direct air capture as a possible mitigation alternative is that for changing the emission's trend there is a need for some solutions able to reduce the amount of carbon dioxide already present in the atmosphere. Many years would be necessary to cut down the CO_2 load relying only on natural phenomena and sinks, therefore artificial processes that reduce the carbon dioxide concentration in the atmosphere could be important [21]. Furthermore, there is another important reason for which DAC concept should be analysed carefully. Traditional carbon capture technologies are meant to capture and separate the CO_2 from concentrated point sources only, while the direct capture of CO_2 from air would be implemented to counteract the distributed emission sources that are more than half of the total current emissions [21].

2.2.2 Pros and cons of DAC

The evaluation of the goodness of a plant or a process must consider in the proper way all the benefits and drawbacks associated to the new system. Therefore, also for the direct air capture, still today scientists are debating about the actual feasibility of the process. The main problem is always related to the costs of the technology: if they are unacceptably high, the realization of the systems results to be not convenient. Here following a list of the main pros and cons of DAC technology is proposed with the intent of providing more elements for a deepening on the topic.

As said in the first sections of this work, the concentration of CO_2 in air is estimated about 390 parts per million (ppm), which is about 300 times more diluted than the concentration of CO_2 in a flue gas stream, about 12% by volume [21]. As illustrated by Sherwood plot in next Figure 2.3 and already described in detail in paragraph 1.3, the energetic and economic costs to separate a specific compound from a mixture depend on how dilute this compound is in the starting mixture. As seen, the costs of DAC are higher than the costs of post-combustion capture especially because of the higher thermodynamic barrier due to the lower concentration of CO_2 in air.

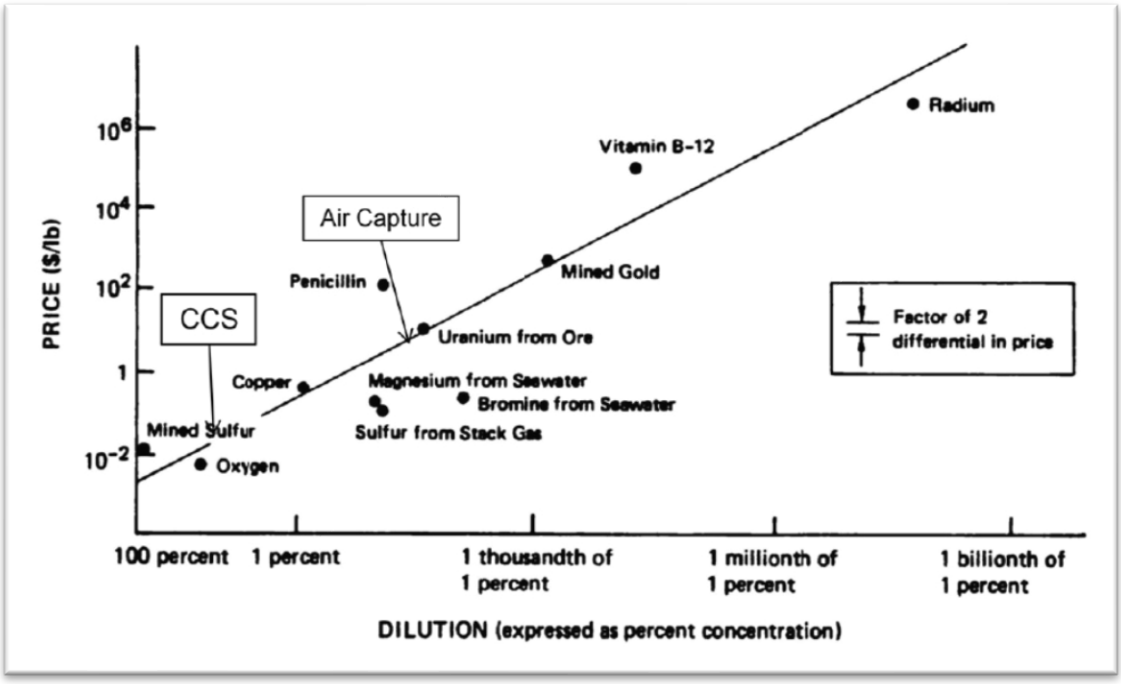

Figure 2.3 – The Sherwood Plot [23]

Once proposed, the Sherwood plot was an empirical relationship between the price of a metal and its concentration in the ore from which it was extracted, plotted on a log-log scale [21]. Since its publication, this plot was used and applied to many other substances which are extracted from mixture, as the CO_2 from the air in this case. The marks inserted in Figure 2.3 refer to the approximate concentration of carbon dioxide in power plant exhaust gas (referred to as "CCS" in the figure, broadly speaking) and CO_2 in air (Air Capture). As it is clear, the costs for DAC estimated with this approach would be 100 times higher than the cost for a traditional post-combustion capture, and it is of course the main reason for which investors are still not fully convinced of DAC concept, without considering other cons that are however inherent in the technology. Looked under this hypothesis, it seems evident that the DAC concept is characterized by intrinsic problems; but for a correct evaluation, it should be seen under a broader perspective that considers also the benefit that it could bring as a tool to mitigate the CO_2 concentration in the air. The other important factor that makes capture from air more difficult than from exhaust streams is the big amount of energy and materials cost necessary to move great quantities of air through an absorbing structure. As it will be shown in the next sections, this is one of the most demanding challenges for the implementation of a cost-effective DAC system.

If the cons are still a significative challenge to overcome, in the future the pros could potentially have greater weight in the feasibility of DAC concept. As mentioned in section 2.2.1, a prominent advantage of DAC is the fact that it has the potential to address emissions from distributed sources as well as point-like sources. In fact, considering that the annual CO_2 emissions come predominantly from distributed point sources, it is obvious that new innovative technologies able to counteract these kinds of CO_2 sources must be considered to strongly impact anthropogenic emissions [9]. Moreover, DAC processes are not location-specific, i.e., capture facilities can be located anywhere. Finally, capturing CO_2 from air has the advantage of not having to face the problem of contaminants (e.g. NO_x, SO_x) in the gas mixture, which rather cause degradation of performance of the sorbents used in flue gas post-combustion capture processes.

2.3 Scheme and operation of a DAC system

Before entering the details of the plants that realize direct capture of CO_2 from air, it is important to show all the possibilities that are currently on the table for the separation of a gas mixture. Direct air capture of CO_2 with chemicals is retained to be the solution so far more achievable considering the quantity of ambient air processed, pros and cons of the technology. It consists on a typical absorption process characterized by the preferential dissolution of a species into a liquid. Other alternatives are being tested to evaluate their effective validity. Between these, the possibility of using solid adsorbent materials (where the preferential adherence of a species onto a solid occurs) is under study to separate the CO_2 from air via an adsorption process instead of an absorption one. Finally, only few years ago a new technology that uses special filters for capturing the CO_2 directly from air has been proposed: in 2017, the first world's DAC plant of this type has been installed in Switzerland by Climeworks company.

2.3.1 DAC system based on solid sorbents

The use of solid sorbent materials to capture the carbon dioxide from air is still held in poor consideration. A lot of work will have to be done to make it a reality in the field of carbon capture. The idea of using solid filters to separate and collect the CO_2 comes from Climeworks company itself. In fact, in the last years as a part of the EU-funded CarbFix2 project, Climeworks and Reykjavik Energy have partnered to combine direct air capture technology using filters with the injection of CO_2 into basalts, for permanent storage by mineralization of the injected carbon [22].

Fundamentally, the Climeworks DAC design is based on an adsorption/desorption process on alkaline-functionalized adsorbents. CO_2 capture occurs without treating the entering atmospheric air. The subsequent CO_2 desorption is performed through a temperature-vacuum-swing (TVS) process [22]. In the following figure, the Climeworks DAC design is shown. In this process, the pressure in the system is reduced and the temperature is increased from 80 to 100°C, releasing at the same time the captured CO_2. The whole process is repeated after a cooling phase has occurred.

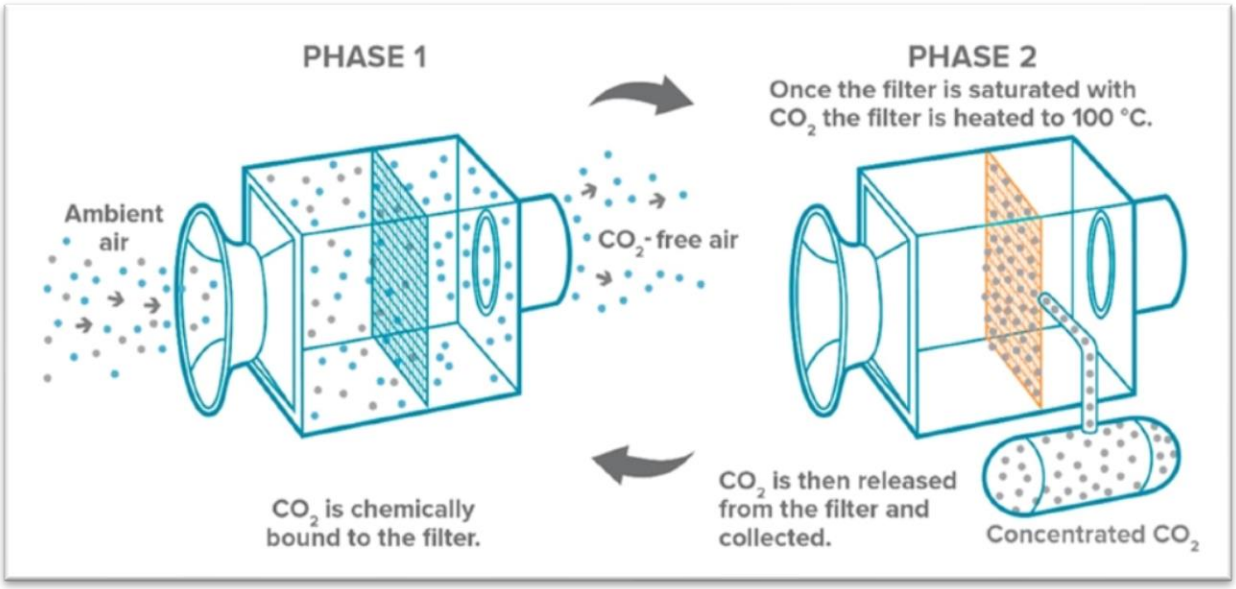

Figure 2.4 – Climeworks DAC design [24]

The reasons to choose a modular design for the filters have been established mainly for [22]:

- reducing operating costs;
- supporting scalability and diversity in deployment;

- solving transport issues and enable automated manufacturing.

Probably the most innovative solution introduced by these filters is that both the adsorption and desorption processes occur inside the same component, reducing therefore the global maintainability of the plant but affecting in some way its reliability. Furthermore, collectors are engineered to be encapsulated well into a steel frame and the only moving parts are the fans that draw in air for adsorption, and two lids at the entry and the exit of the collector which create an airtight seal for the CO_2 desorption [22].

Another important strength of this system is the collector's operating temperature. The temperature vacuum-swing process that occurs inside requires a certain amount of energy whose major share is in a range of temperature between 80°C to 120°C [22], that can be met by heat at relatively low temperature which is available from many sources such as low-grade waste heat, or heat coming from other kinds of low temperature processes.

Other possibilities for using solid sorbents are in the field of research. In 2009, Lackner proposed a new solid sorbent to overcome some drawbacks of traditional aqueous sorbents used to capture CO_2 from air [23]. He realized that the kinetic limitations of the aqueous hydroxide solutions are those of aqueous hydroxide chemistry in general, and not specific to sodium or potassium hydroxides (typically used in this field). And this is true, since for liquid sorbents the uptake rate per unit area will always be dominated by the limited reaction kinetics of CO_2 transferring from the gas phase into the aqueous liquid [23]. For this reason, the use of solid sorbents can lead to new and potentially different mechanisms to explore. Furthermore, solid sorbents, unlike fluids, have microscopic surface roughness that can improve the nominal uptake rate significantly. Lackner proposed a sorbent with lower binding energy (with respect to aqueous solutions) but able to maintain an uptake rate not worse than that of a 1-molar sodium hydroxide solution. Lackner and his co-workers chose a strong-base ion-exchange resin, so a composite material [23]. At the end of the experiments they found that the uptake rate of the resin was typically between 10 and 500 μ mol $m^{-2}s^{-1}$, exceeding that of a one molar sodium hydroxide film of equal nominal area [23]. Considering these results, it should be clear that some kinds of solid sorbents could be taken into consideration. Of course, the actual feasibility of such a solution is to be analysed, above all to understand the cost and feasibility of regenerating the solid materials and their replacement rate during real operations.

Definitively, pros and cons of solid sorbents can be summarized in the following lists, suggested by *Keith et al.* [24].

Pros:

- possibility of low energy input;
- low operating costs;
- applicability across a wide range of scales.

Cons:

- need to build a very large structure at low cost;
- need to allow the entire structure to be periodically sealed from ambient air during the regeneration step;
- need to resist to temperature, pressure and humidity cycles;
- need to overcome the conflicting requirements of high sorbent performance, low cost and long economic life in impure ambient air.

2.3.2 DAC system based on liquid sorbents

As described previously, the technologies considered for DAC are based on reversible sorbents than can be cycled many times to capture and release CO_2. Furthermore, the sorbents studied for flue gas capture have included both physisorbent and chemisorbent materials, but these materials do not perform with same results in direct air capture of CO_2. Materials such as zeolites, activated carbons, or metal-organic frameworks (MOFs) typically perform poorly at low CO_2 partial pressures, offering very small CO_2 uptake and low CO_2 selectivity [9]. As air capture deals with an extremely low CO_2 concentration (e.g. 400 ppm), chemisorbent materials have proven to be much more effective for DAC processes [9]. Therefore, the selection of the sorbent is a crucial design choice, since it influences both the rate at which CO_2 is removed from the processed gas and the energy requirements for the successive sorbent regeneration step [19].

Due to the ultradilute nature of CO_2 in the atmosphere, chemical sorbents with strong CO_2-binding affinities are typically employed for CO_2 capture. So, to face the problem of the low CO_2 concentration in air, aqueous sorbents selected for flue gas capture are still different with respect

to those used for DAC. Typical sorbents studied for DAC systems are indeed aqueous hydroxide sorbents and a basic two-step sequence (absorption of CO_2 and solvent regeneration) is used for almost the totality of systems for CO_2 capture based on liquid sorbent solutions [19].

These systems involve the interaction in a suitable contactor of the CO_2-rich mixture with a liquid solution of water and a hydroxide (mostly sodium or potassium hydroxide), characterized by a significative affinity toward CO_2 molecules. After this first step, there is always a subsequent and separate step for the solvent desorption/regeneration under different conditions. In this way, at the end of the two steps, carbon dioxide is released from the sorbent in a concentrated form. The following lines give a brief explanation of why the Kraft process has been taken as a model for developing DAC systems.

The Kraft process has become a very influential system for CO_2 capture from air by using caustic solution [9]. The term caustic is used to denote strong basis, particularly alkalis. The latter are basic, ionic salts of an alkali metal or alkaline earth metal chemical element. The main caustic solutions considered here refer to those formed by sodium hydroxide (NaOH), potassium hydroxide, (KOH) or calcium hydroxide ($Ca(OH)_2$). The Kraft process has been used in paper industry since 1884 and involves the use of a sodium hydroxide solution to extract cellulose from wood [9] but the idea of studying this process comes from the fact that the same principles for the use and recycling of the sodium solution in the Kraft process can also be applied for CO_2 capture [23].

The general scheme of a DAC system based on Kraft process is shown in the following figure adapted from the American Physical Society report on direct air capture of CO_2 with chemicals [19].

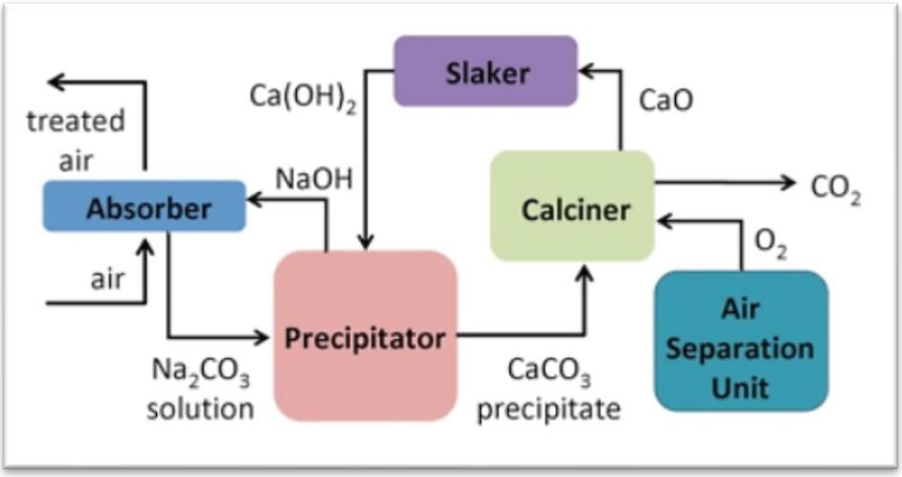

Figure 2.5 – Scheme of a plant for DAC that uses NaOH as the absorber [19]

This is a very general but sufficiently clear scheme of the plant with the only difference that in the Kraft process and in general in pulp and paper industry, the block Precipitator of Figure 2.5 is usually named 'causticizer'.

The block 'Absorber' is responsible of the contact between the CO_2-rich stream with the aqueous hydroxide solution. In the following sections this component will be described into details because its design can be very different depending on the engineering and design choices made during the project phase. The contact between carbon dioxide and sodium hydroxide generates sodium carbonate (Na_2CO_3), water, and a certain amount of heat being an exothermic reaction (R.1). Once the Na_2CO_3 is formed, it is sent to the 'Causticizer' block (or Precipitator in Figure 2.5) where the causticization reaction takes place (R.2). Sodium carbonate just formed is put in contact with calcium hydroxide to produce calcium carbonate ($CaCO_3$), to form again the sodium hydroxide that will be sent back to the absorber to restart the chemical loop. This reaction is slightly exothermic but is very important as the calcium carbonate will be able to release the CO_2 once it will be decomposed at the end of the process. The choice of using sodium hydroxide (that will produce sodium carbonate in the absorber) is also related to the fact that the exchange of carbonate ions from sodium to calcium (in the causticizer) has been calculated to be very efficient [9]. The theoretical efficiency is about 96% [25], although experimental values have not reached efficiencies close to the theoretical limit [9]. The precipitated $CaCO_3$ is then separated in a kiln ('Calciner' block), where it is thermally decomposed into quicklime (CaO), and CO_2 (R.3) that can be transferred and subsequently compressed [9]. To close the cycle, calcium hydroxide is regenerated by hydration in the 'Slaker' block (R.4) and finally reused [2].

For a question of clarity, here following the main reactions occurring in the main components of the plant described above are shown together with their enthalpy of reaction [9]:

ABSORBER	$2NaOH + CO_2 \rightarrow Na_2CO_3 + H_2O$	$\Delta H° = -109.4$ kJ mol^{-1}	1
CAUSTICIZER	$Na_2CO_3 + Ca(OH)_2 \rightarrow 2NaOH + CaCO_3$	$\Delta H° = -5.3$ kJ mol^{-1}	2
CALCINER	$CaCO_3 \rightarrow CaO + CO_2$	$\Delta H° = +179.2$ kJ mol^{-1}	3
SLAKER	$CaO + H_2O \rightarrow Ca(OH)_2$	$\Delta H° = -64.5$ kJ mol^{-1}	4

As it is clear from the enthalpy of reaction listed above, this process is associated to large energy requirements, especially for causticization reaction which is well above the calculated thermodynamic minimum [23], [25].

In Figure 2.6 the enthalpy level diagram for CO_2 absorption and regeneration by sodium hydroxide is shown. The picture has been taken from the American Physical Society report on Direct Air Capture of CO_2 with chemicals [19], and it is very helpful to understand the different energy levels at which the reactions involved in the process occur.

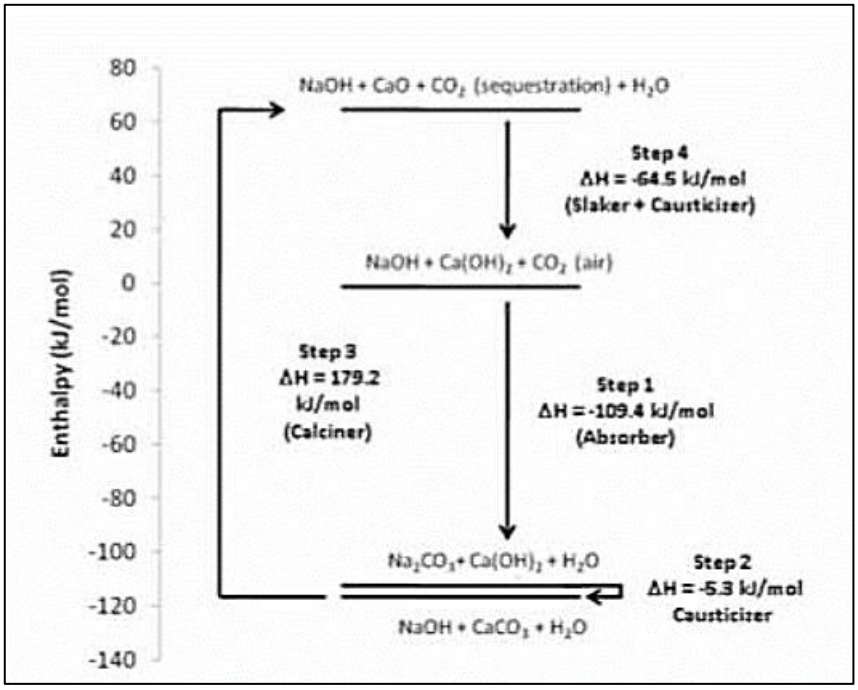

Figure 2.6 – Enthalpy level diagram for CO_2 absorption and regeneration by NaOH [19]

One observation on Figure 2.6 refers to the fact that some molecules do not participate in specific physical processes (e.g. NaOH is not transported to the calciner).

As anticipated before, the solution with sodium hydroxide is not the only caustic solution taken into consideration for direct capture of CO_2 from air using liquid solutions. As it will be shown in the following section, also potassium hydroxide is starting to take hold in DAC sector. Indeed, the DAC design proposed in a paper published on July 2018 by *Keith et al.* [24] considers the use of a solution of water and KOH. A few years ago, Bandi et al. [26] examined the use of KOH by using a 2 m packing column and a 1.5 M solution of KOH to sorb about 70% of the CO_2 in ambient air. Despite large energy penalties associated to aqueous hydroxide solutions, baseline designs will be however useful for future economical and energetic evaluations [9].

As done for solid sorbents in the previous section, the main pros and cons of aqueous sorbents are listed here [24], to provide a useful comparison with the solid sorbents presented before.

Pros:

- the contactor can operate continuously and can be built using cheap cooling-tower hardware;
- the liquid surface is continuously renewed allowing very long contactor lifetimes despite dust and atmospheric contaminants;
- CO_2 captured can be easily pumped to a central regeneration facility.

Cons:

- cost and complexity of the regeneration system;
- water loss in dry environments.

2.3.3 The reference DAC system. Design and operation description

The idea of this thesis was born after reading about a DAC design proposed in July 2018 by Keith et al. [24]. They have published a detailed description of a DAC plant which they are working on together with the Canadian company Carbon Engineering [27]. This design has been taken as the reference for the process modelling that will be described in detail in the next paragraph 3.3, so this section is fully concentrated on the plant and its main functions.

The process proposed by Keith et al. is designed to capture almost 1 Mt-CO_2/year from the atmosphere in a continuous process using an aqueous KOH sorbent, coupled with caustic recovery loop [24]. The only primary energy input of the plant is the natural gas, or in alternative natural gas and electricity. The design requires either 8.81 GJ of natural gas, or 5.25 GJ of gas and 366 kWh of electricity, per ton of CO_2 captured [24].

This plant recalls the typical DAC systems based on liquid sorbents. In fact, after the first absorption section, the second part is entirely constituted by the necessary components to perform the solvent regeneration. In the following Figure 2.7, the process chemistry is illustrated together with the energy associated to each reaction that takes place in a specific component.

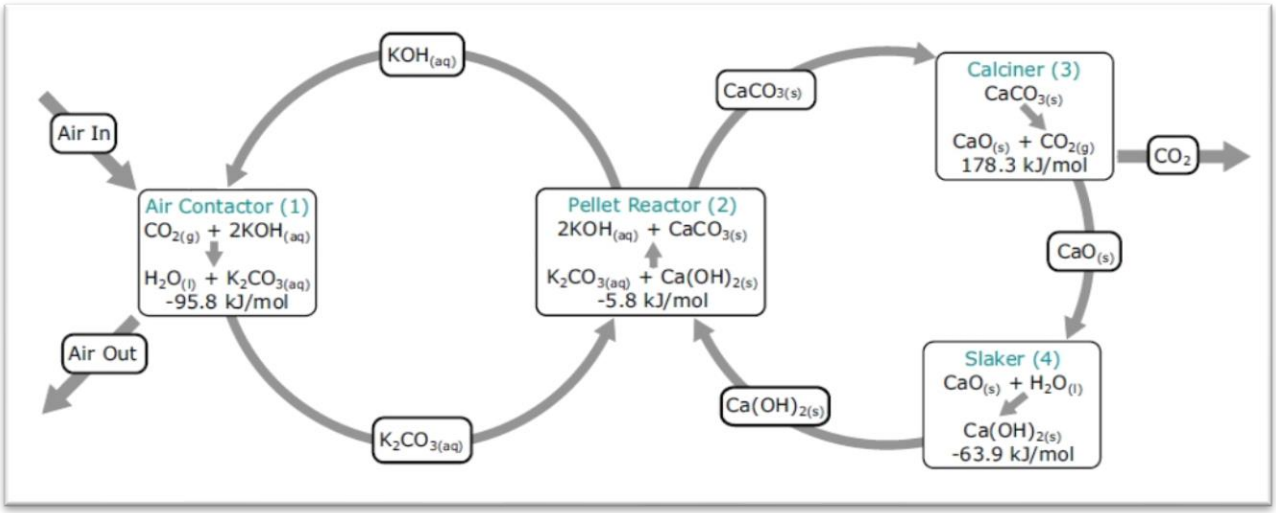

Figure 2.7 – Process chemistry and thermodynamics [24]

The first chemical loop (left part of Figure 2.7) aims at removing the CO_2 from atmospheric air using an aqueous solution composed by ionic concentrations of roughly 1.0 M OH^-, 0.5 M CO_3^{2-}, and 2.0 M K^+ [24]. Then, the calcium loop (right part of Figure 2.7) drives the removal of carbonate ion and thus the regeneration of the alkali capture solution used in the previous loop. It is

therefore responsible of the precipitation of the ion CO_3^{2-} with ion Ca^{2+}, to form $CaCO_3$ solid pellets. At the same time, Ca^{2+} ions are replenished by dissolution of $Ca(OH)_2$. At the end of the process, the $CaCO_3$ is thermally decomposed in the calciner into CO_2 and CaO: the latter is then hydrated (or 'slaked') in the slaker reactor to produce $Ca(OH)_2$ again. Furthermore, it is important to notice that water yielded in reaction 1 is consumed in reaction 4, balancing the process. Globally the full process has evaporative losses, as it will be shown in the next paragraphs.

The reactions involved in this system are very similar to the ones already reported in the previous section regarding the Kraft process. Indeed, this system is, in some respects, derived from the Kraft process but in this case the caustic solution used to perform the CO_2 absorption and recovery is based on the potassium hydroxide, KOH, and not sodium hydroxide, NaOH. The main reactions involved in the two chemical loops and shown in former Figure 2.7, are reported below for a reason of clarity. The reaction enthalpies are given in kJ per mole of carbon and referred to STP (Standard Temperature and Pressure conditions) [24].

AIR CONTACTOR	$2KOH_{(aq)} + CO_{2(g)} \rightarrow K_2CO_{3(aq)} + H_2O_{(l)}$	$\Delta H° = -95.8$ kJ mol^{-1}	5
PELLET REACTOR	$K_2CO_{3(aq)} + Ca(OH)_{2(s)} \rightarrow 2KOH_{(aq)} + CaCO_{3(s)}$	$\Delta H° = -5.8$ kJ mol^{-1}	6
CALCINER	$CaCO_{3(s)} \rightarrow CaO_{(s)} + CO_{2(g)}$	$\Delta H° = +178.3$ kJ mol^{-1}	7
SLAKER	$CaO_{(s)} + H_2O_{(l)} \rightarrow Ca(OH)_{2(s)}$	$\Delta H° = -63.9$ kJ mol^{-1}	8

Figure 2.8, reported in the next pages, provides a simplified but sufficiently detailed energy and material balance of the complete process. The numbers indicated in red refer to the electricity demands of each operation unit. Furthermore, the main chemical components that constitute gas and/or liquid streams are reported in the picture using mass fraction for gaseous streams and molar concentration for the aqueous ones.

The plant has been subdivided in 6 main sections, defined with the aim of realizing a detailed model of the whole system since many material streams are connected between one section and the others; therefore, the definition of some principal sections was fundamental to understand the exact operation of every single component of the plant.

The names of the sections are listed below.

1. Air contactor and absorber
2. Pellet reactor
3. Steam slaker
4. Calciner
5. CO_2 compression
6. Power island

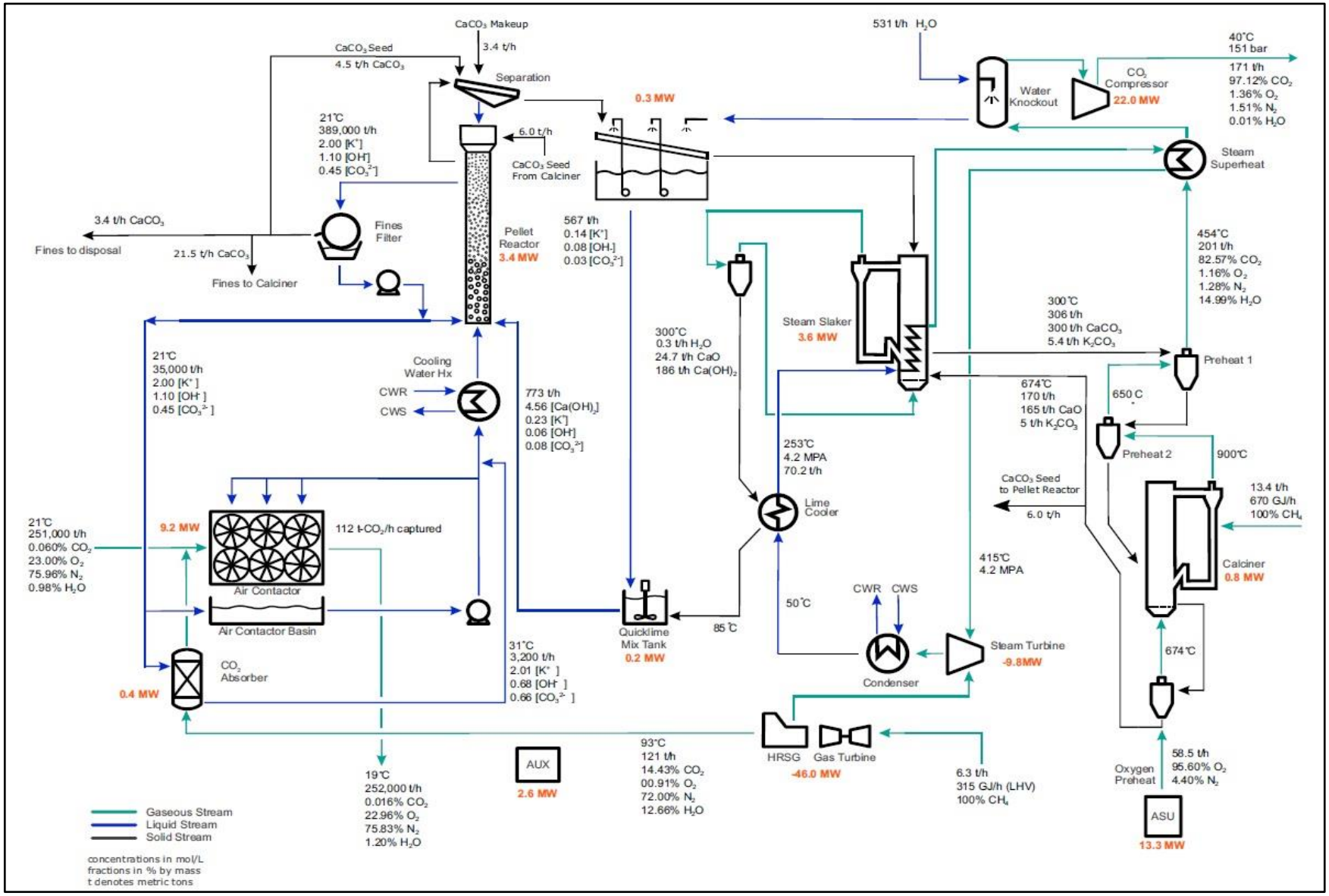

Figure 2.8 – Schematic layout of the DAC plant with energy and material balances [24]

3. DAC model

In this chapter the whole process simulation is described. The assumptions considered for each stream and component, and all the tools adopted in order to reach the desired results are provided in the following sections. The figures shown in the next paragraphs describe the layout of the plant as it was modelled on the software, trying to reproduce as close as possible the scheme of the real plant shown in Figure 2.8.

The software utilized for the simulation is Aspen Plus® (version 8.8), provided by the American company AspenTech®. The following paragraphs will provide all the explanations required for a full comprehension of the model realized.

3.1 Methods for system modelling

Before entering the details of the model, this paragraph and the next one are to explain the main physical and thermodynamic equations that describe the phenomena taking place in the components of the plant. Therefore, the two main thermodynamic models considered for this work will be presented, together with the mass transfer theory that is essential to explain the physical phenomenon of absorption that occurs inside the absorber, in the air contactor section of the plant.

3.1.1 Thermodynamic models

The accuracy of software calculations is strictly related to the correct choice of the thermodynamic models used in the simulation since all unit operation models need property calculations to generate results. In fact, flash and enthalpy calculations are often sufficient information to calculate a mass and heat balance but other thermodynamic properties (e.g. transport properties) are calculated for all process streams. For these reasons, it is fundamental to adopt specific thermodynamic models to correctly describe the physics of components modelled with a software.

One of the most recurring situations in the plant is the physical contact between a gaseous stream with an aqueous one. It occurs mainly in the air contactor and in the absorber units, where CO_2 must be stripped-off from gas mixtures, so two thermodynamic models have been applied to describe the Vapor-Liquid Equilibrium (VLE) that occurs in these components. The two methods considered for the different physical phases are listed here:

- Electrolyte NRTL (Non-Random Two-Liquid), applied for the *liquid* phase;
- SRK EoS (Soave-Redlich-Kwong Equation of State), applied for the *gas* phase.

3.1.1.1 Electrolyte-NRTL method

The Electrolyte-NRTL approach estimates the excess Gibbs free energy and the activity coefficient of an electrolyte system, considering the strong non-ideal behaviour of an ionic mixture. It correlates the activity coefficient of a compound with its mole fraction in the liquid phase concerned: so, it is very useful in chemical applications to calculate phase equilibria. The model was first proposed by *Chen et al.* and then generalized by the same author; since there is a significant number of publications about this model [28], [29], [30], only the main assumptions and equations will be described here, leaving further information to the reader.

The Electrolyte-NRTL model is based on two main assumptions, here summarized [29], [30]:

1. like-ion repulsion. This means that ions of the same electric charge are characterized by extremely large forces and the local concentration of anions around anions and cations around cations is therefore equal to zero.
2. local electroneutrality. Cations and anions are distributed around a central molecule in such a way that the net local ionic charge is equal to zero.

Moreover, the other important parameter to be introduced is the *excess* of Gibbs free energy. The Gibbs free energy is a thermodynamic potential that can be used to calculate the maximum reversible work that can be performed by a certain thermodynamic system at a constant temperature and pressure. The excess of Gibbs energy can be defined instead as a difference between the Gibbs free energy of electrolyte systems and the Gibbs energy of an ideal solution with the same condition of temperature, pressure and concentration [31]. Furthermore, this

excess of Gibbs free energy is composed by a sum of two different contributes, as reported in the following equation:

$$g_{ex} = g_{ex}^{LOCAL} + g_{ex}^{LONG} \qquad \text{(eq. 3-1)}$$

where:

- g_{ex}^{LOCAL} is the *local contribution*, which considers the existing short-range interactions in the neighbourhood of any chemical species;
- g_{ex}^{LONG} is the *long-range contribution*, which describes the ion-ion interaction existing just beyond the neighbourhood of an ionic species.

The model development for the NRTL *short-range (local) contribution* has been described in detail by *Chen et al.* in their early publications [30]. Here it is important to remember that in an electrolyte system, all the species can be categorized as one of three types: molecular species, cationic species and anionic species [31]. The first type consists of a central molecular species with cationic and anionic species in its immediate neighbourhood; in this way, the local electroneutrality is maintained. The other two types are based on the like-ion repulsion assumption and here the central species can be both a cationic or anionic species [31]. With these premises, the excess Gibbs energy for an electrolyte system, provided by the short-range contribution can be written as follow:

$$\begin{aligned}\frac{G_{ex}^{local}}{R\,T} = &\sum_I \sum_m r_{m,I}\, n_I \left(\frac{\sum_j X_j\, G_{jm}\, \tau_{jm}}{\sum_k X_k\, G_{km}}\right) + \\ &+ \sum_I \sum_c z_c\, r_{c,I}\, n_I \left(\sum_a Y_a\, \frac{\sum_j X_j\, G_{jc,ac}\, \tau_{jc,ac}}{\sum_k X_k\, G_{kc,ac}}\right) + \\ &+ \sum_I \sum_a z_a\, r_{a,I}\, n_I \left(\sum_c Y_c\, \frac{\sum_j X_j\, G_{ja,ca}\, \tau_{ja,ca}}{\sum_k X_k\, G_{ka,ca}}\right)\end{aligned} \qquad \text{(eq. 3-2)}$$

with:

$$X_j = C_j\, x_j \qquad \text{(eq. 3-3)}$$

$$x_j = \frac{\sum_j x_J\, r_{j,J}}{\sum_I \sum_i x_I\, r_{i,I}}\, x_j = \frac{\sum_j x_J\, r_{j,J}}{\sum_I \sum_i x_I\, r_{i,I}} \qquad \text{(eq. 3-4)}$$

where:

- subscripts m, c and a refer to molecular species, cations and anions, respectively; subscripts i and j denote segment-based species indexes
- subscripts I and J denote component indexes;
- n_I is the mole number of component I;
- x is the segment-based mole fraction;
- z is the charge number;
- C_j is equal to z_j for ionic species, while it is equal to 1 for molecular species;
- r represents the number of species (either molecular or anionic or cationic, depending on the specific subscript associated);
- Y is a (cationic or anionic) charge composition fraction quantity;
- τ is the asymmetric binary interaction energy parameter, related to G with a non-random factor parameter α reported in the following equation:

$$G = e^{-\alpha\tau} \quad \text{(eq. 3-5)}$$

At the same time, to estimate the excess Gibbs free energy from *long-range* interactions, another approach is followed. It is based on the unsymmetrical Pitzer-Debye-Hückel (PDH) formula, shown below [32]:

$$\frac{G_{ex}^{long}}{R\,T} = -\sum_i n_i \left(\frac{1000}{M_s}\right)^{\frac{1}{2}} \left(\frac{4\,A_\varphi\,I_x}{\rho}\right) ln\left(1 + \rho\,{I_x}^{\frac{1}{2}}\right) \quad \text{(eq. 3-6)}$$

with:

$$A_\varphi = \frac{1}{3}\left(\frac{2\,\pi\,N_A\,d_s}{1000}\right)^{\frac{1}{2}} \left(\frac{{Q_e}^2}{\varepsilon_s\,k_B\,T}\right)^{\frac{3}{2}} \quad \text{(eq. 3-7)}$$

$$I_x = \frac{1}{2}\sum_i x_i\,{z_i}^2 \quad \text{(eq. 3-8)}$$

where:

- A_φ is the Debye-Hückel parameter;
- I_x is the ionic strength;
- M_s is the molecular weight of the solvent s;

- N_A is the Avogadro's number;
- ρ is the closest approach parameter;
- d_s is the density of the solvent;
- Q_e is the electron charge;
- ε_s is the dielectric constant of the solvent s;
- k_B is the Boltzmann constant.

As written before, one of the goals of NRTL-method is the correlation of the activity coefficient of a compound with its mole fraction in the liquid phase concerned, therefore the last important parameter that should be evaluated is the activity coefficient γ_I of the component I. This can be performed by applying two different equations, where the value of the excess Gibbs free energy found before is now fundamental for the correct calculation of the activity coefficient. The first part of the equations reported below is valid for both short-range and long-range contribution, since the excess Gibbs free energy that appears in the equation already contains information about short- and long-range contribution. On the other hand, the second part considers the two contributions separately.

$$ln\,\gamma_I = \frac{1}{R\,T}\left(\frac{\partial G_{ex}}{\partial n_I}\right)_{T,p,n_{J\neq I}} = \ln\gamma_I^{local} + \ln\gamma_I^{long} \qquad \text{(eq. 3-9)}$$

3.1.1.2 Soave-Redlich-Kwong Equation of State

The Redlich-Kwong equation of state is an empirical, algebraic equation that relates temperature, pressure, and volume of gases. It is considered more accurate that the van der Waals equation and the ideal gas equation at temperatures above the critical temperature. The equation was first formulated by Redlich and Kwong in 1949 [33], but it has experienced many revisions and modifications, in order to improve its accuracy in terms of predicting gas-phase properties of more than one compound, as well as in better simulating conditions of gas mixtures at low temperatures. The original formulation is shown in the equation below:

$$p = \frac{R\,T}{V_M - b} - \frac{a}{\sqrt{T}\;V_M\,(V_M + b)} \qquad \text{(eq. 3-10)}$$

where:

- p is the gas pressure;
- R is the gas constant;
- T is the temperature;
- V_M is the molar volume;
- a is a corrective constant used to consider the attractive potential of molecules;
- b is a corrective constant for the volume.

As said above, this first equation has been revised many times and this thesis work adopted the Soave's correction of the original one. The Soave-Redlich-Kwong equation of state better describes the vapor-liquid equilibrium of fluids with respect to the first equation proposed. The final formulation is reported here below:

$$p = \frac{R\,T}{V_M - b} - \frac{a_C\,\alpha(T)}{V_M\,(V_M + b)} \qquad \text{(eq. 3-11)}$$

with:

$$a_C = 0.42747\,\frac{R^2\,T_C^2}{p_C} \qquad \text{(eq. 3-12)}$$

$$b = 0.08664\,\frac{R\,T_C}{p_C} \qquad \text{(eq. 3-13)}$$

The difference made by Soave's correction relates to the $T^{-\frac{1}{2}}$ term, which is replaced with a more general term, $\alpha(T)$, still function of temperature:

$$\alpha(T) = \left\{1 + m\left[1 - \left(\frac{T}{T_C}\right)^{\frac{1}{2}}\right]\right\} \qquad \text{(eq.3-14)}$$

with:

$$m = 0.48 + 1.574\,\omega - 0.176\,\omega^2 \qquad \text{(eq. 3-15)}$$

where ω is the acentric factor of the considered component.

The different equations listed so far are valid for each component of a vapor mixture. Of course, it is possible to calculate the pressure of the whole system. But in this case, it would be necessary to apply the appropriate mixing rule, in relation to the specific case and the different features of the mixture; some applicable rules are arithmetic rule, quadratic rule, and other more elaborated rules.

3.1.2 Mass transfer model

This paragraph is dedicated to the explanations about the mass transfer phenomenon that occurs between a gaseous and a liquid phase when they come into contact. These explanations are important because they constitute the theoretical basis of the process that takes place in the absorption column, but also in the air contactor.

As written in the previous section, the generation of ionic species involves only the liquid phase and therefore, only molecular species contributes to the vapor-liquid equilibrium. There are two different approaches through which the mass transfer and kinetics between the liquid and vapor phase in the absorption column can be explained. These models are [34]:

- equilibrium-based stage efficiency model
- rate-based model

The first one is the traditional approach which considers that in each stage of the column, vapor phase and liquid phase are in equilibrium with each other. In a real column, this never happens and therefore the approximation that it introduces is quite unrealistic. To solve this issue, the equilibrium-based method applies a factor called “stage efficiency” [35], but the results obtained, however, fail to reach the accuracy of those reached with the rate-based approach. For this reason, the rate-based model has been the adopted method for the analysed system. This method has been developed to overcome the approximations introduced by the equilibrium-based stage efficiency model, with the aim of obtaining better results from the simulations of the system.

The rate-based model is a rigorous approach. It adopts the “two-film” theory (described in the following) and it discretizes the films into different segments on each stage, obtaining in this way a complete characterization of energy balance, kinetics, heat and mass transfer, hydrodynamics

and column properties of the system [36]. Furthermore, it assumes that the separation is driven by the mass transfer between the phases and it uses the Maxwell-Stefan theory for the calculation of the mass transfer rates [35]; in this way, the phase equilibrium is achieved only at the vapor-liquid interface, and not in each stage of the column.

As mentioned above, the film theory is a fundamental basis for the application of the rate-based model. The theory was proposed by Lewis and Whitman in 1924 [37], and it is reputed to be very suitable for performing a mass transfer analysis at the liquid-vapor interface. It assumes steady-state conditions and that all the mass transfer resistances are concentrated in two films of finite thickness, located near the interface between gas and liquid [34]. The mixing by convection is not considered in these two films so any transfer of solute is regulated by the diffusion process, while the convection is very rapid in the bulk phase. The resulting concentration of solute can be therefore considered almost uniform everywhere except near the films [34]. Since the two layers are very thin, the solute inside each film can be neglected, if compared to the one that flows through them. At the same time, the solute that passes in the film of a certain phase must diffuse also in the layer of the other one. Therefore, the two films behave as 'diffusional resistances' in series [34].

At the end of the dissertation about the rate-based model and the two-film theory, the parameter of interest is the mass transfer coefficient between the two phases, k_C. In its final expression, it can be written as a function of the CO_2 diffusivity and the thickness δ of the film [38]:

$$k_c = \frac{D_{CO_2}}{\delta} \qquad \text{(eq. 3-16)}$$

3.2 Chemical reactions

In the introduction of paragraph 2.3.3, the chemical reactions involved in the global process have been listed. As it is clear, many reactions occur inside different components of the plant and this must be taken into account when modelling the process. Chemical reactions previously provided involve not only equilibrium reactions but also salts formation and dissociation reactions. Following the hint of the reference paper, the thermodynamic packages chosen in the software has been the ENTRL-RK and RK-SOAVE for the aqueous phase and gaseous phase respectively [24]. In particular, the property database APV88 has been adopted. It contains the following databanks: ASPENCPD, AQUEOUS, SOLIDS, INORGANIC, PURE26 and PURE32.

For the equilibrium reactions, the equilibrium constant can be found using the equation below:

$$lnK_j = A_j + \frac{B_j}{T} + C_j lnT + D_j T \qquad \text{(eq. 3-17)}$$

This equation shows that the equilibrium constant of a reaction is strongly dependent on temperature T, and depends also on some coefficients (A_J, B_J, C_J and D_J) which can be identified for a specific reaction.

The reactions listed in the following rows have been automatically generated by the software Aspen Plus® with the procedure of 'Electrolyte wizard'; by inserting in the 'Components' section of the software all the substances present in the system, the software is able to generate the ionic components and the reactions in which they are involved. This tool is very useful since the data in the selected databanks are exploited, and it is especially helpful when it is difficult to find in literature the parameters which characterized specific reactions, such as the coefficients to calculate equilibrium constants. In Table 3.1, the reactions generated by the software are reported, together with the type of reaction (equilibrium, salt or dissociation reaction).

Table 3.2 contains the characteristic parameters provided by Aspen Plus® wizard.

Table 3.1 – Reactions generated by Aspen Plus® "Electrolyte wizard"

REACTION	TYPE	N°
$H_2O + HCO_3^- \leftrightarrow CO_3^{2-} + H_3O^+$	Equilibrium	9
$CaOH^+ \leftrightarrow Ca^{2+} + OH^-$	Equilibrium	10
$2\ H_2O + CO_2 \leftrightarrow HCO_3^- + H_3O^+$	Equilibrium	11
$2\ H_2O \leftrightarrow OH^- + H_3O^+$	Equilibrium	12
$K_2CO_3 \leftrightarrow CO_3^{2-} + 2\ K^+$	Salt	13
$CaCO_3 \leftrightarrow CO_3^{2-} + Ca^{2+}$	Salt	14
$KOH \rightarrow OH^- + K^+$	Dissociation	15
$Ca(OH)_2 \rightarrow CaOH^+ + OH^-$	Dissociation	16

Table 3.2– Thermodynamic coefficients for reactions generated with Aspen Plus®

REACTION	COEFFICIENTS			
	A	B	C	D
9	216.05	-12431.7	-35.4819	0
11	231.465	-12092.1	-36.7816	0
12	132.899	-13445.9	-22.4773	0
13	-175.998	17765.2	21.6865	0

3.3 Process layout

The model realized tends to represent the same configuration, but it requires some modifications and additional components with respect to the real layout, in order to reduce the plant complexity. For the sake of clarity, the process layout obtained by the modelling of the plant will be shown firstly in a unique picture (Figure 3.1 in next page) and then provided using some blocks that are called 'hierarchies' in Aspen Plus®. These blocks (reported in Figure 3.2) have been defined in this way to recall the names of the plant sections already described in previous paragraphs. In this chapter, each hierarchy will be 'exploded' in order to analyse in detail the features and the blocks inside. To facilitate the comprehension, the characteristics of each component of the modelled plant have been reported in a single Table 3.3 in the next pages. In the same way, mass flow rate, temperature, pressure and chemical composition of the streams

modelled in Figure 3.1 have been collected and reported in a dedicated APPENDIX at the end of this thesis.

The layout presented in Figure 3.2 shows how the different blocks and hierarchies are linked one to each other. Slaker and calciner hierarchies are linked together by a significant number of streams, meaning that each one needs the products of the other, and vice versa.

The model employs the “electrolyte template” available on Aspen Plus®, which is good to perform chemical reactions between electrolytes. It is sufficient to write all the reactions in the Property section of the software and in its Simulation section it can make a reaction occur even when two streams are simply mixed. In other words, the reactions happen also outside specific reactors and this was very helpful for managing the many reactions that take place throughout the plant.

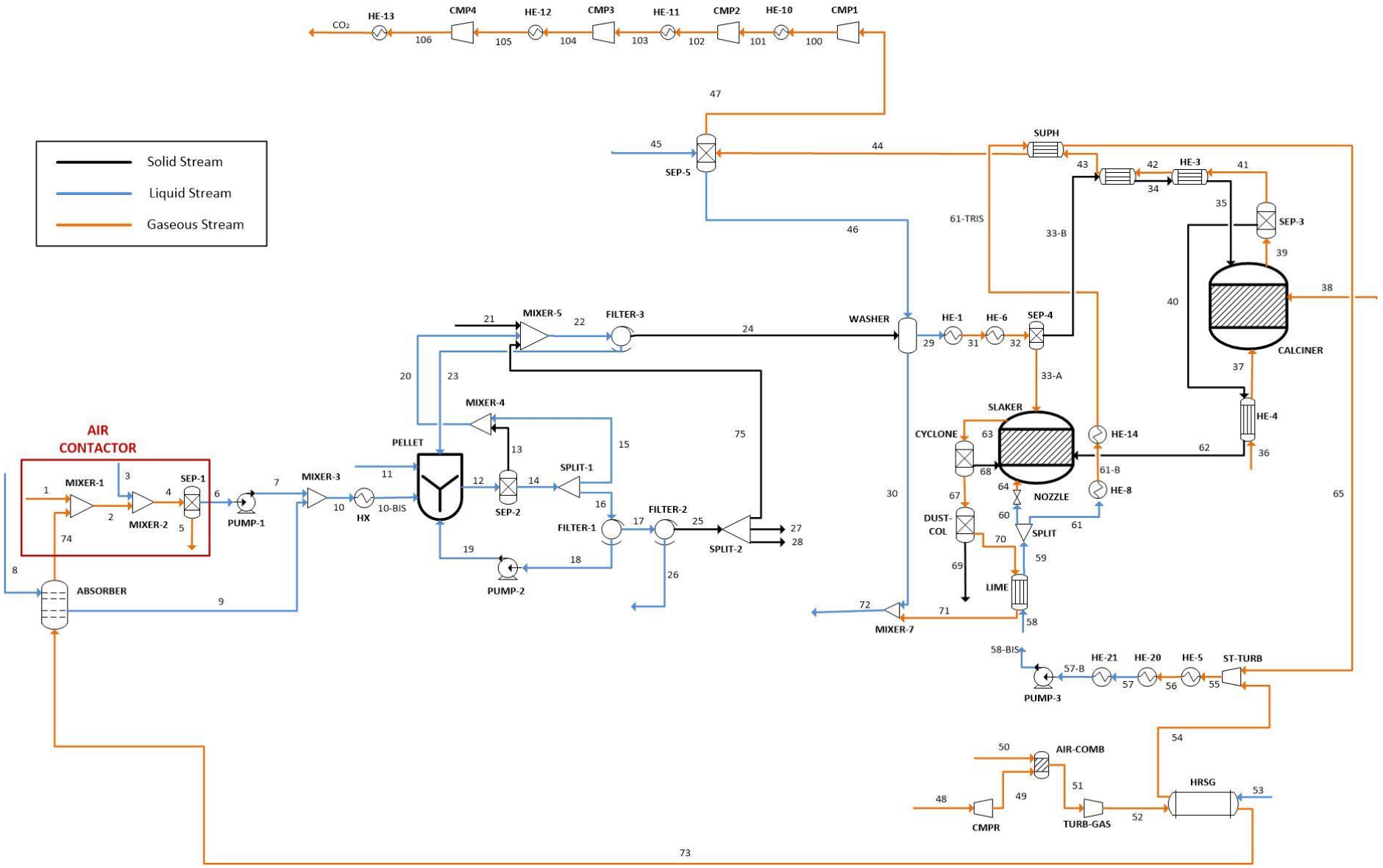

Figure 3.1 - Model of the global plant

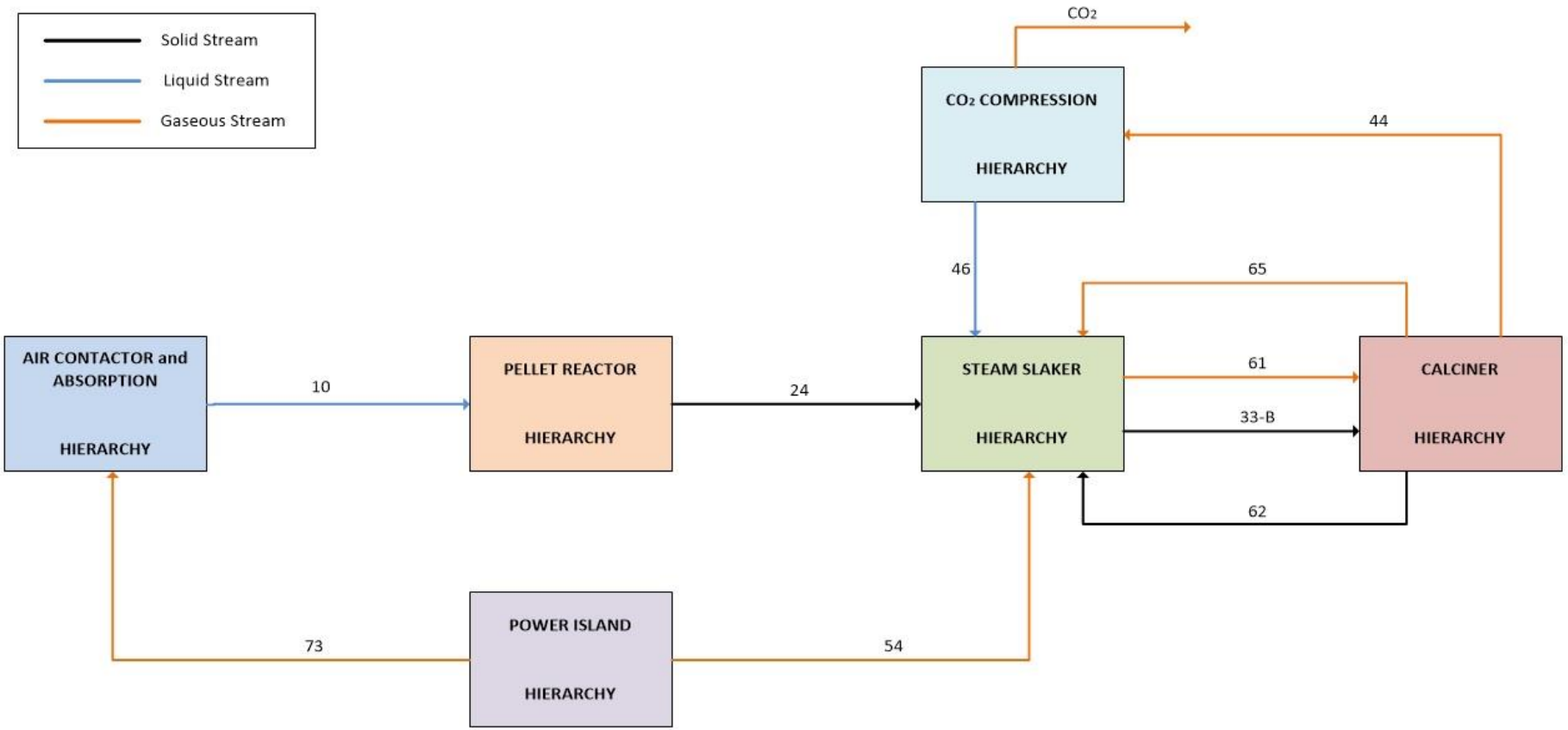

Figure 3.2 – Plant scheme with hierarchies

Table 3.3 - Main components and characteristics

BLOCK ID	CHARACTERISTICS
SEP-1	· Aspen Plus® block: Sep · Modelled with the logic 0/1 for gas-liquid separation · Pressure drop = 0.005 bar
PUMP-1	· Aspen Plus® block: Pump · Pressure increase = 0.005 bar
HX	· Aspen Plus® block: Heater · Duty = 60859.8 kW · Pressure drop = 0 bar
FILTER-2	· Aspen Plus® block: Filter · Model: solid separator · Fraction of solid to solid outlet = 1 · Fraction of liquid to liquid outlet = 0.9 · Pressure drop = 0.1 bar
PUMP-2	· Aspen Plus® block: Pump · Pressure increase = 0.1 bar
HE-1	· Aspen Plus® block: Heater · Degrees of superheating = 0°C · Pressure drop = 0 bar
SLAKER	· Aspen Plus® block: RStoic · Operating temperature = 300°C · Operating pressure = 1 bar · CaO fractional conversion = 0.85

BLOCK ID	CHARACTERISTICS
ABSORBER	· Aspen Plus® block: RadFrac · Calculation type: rate-based · Operating pressure = 1 bar · Packing column with BERL Ceramic · Height = 12 m · Diameter = 7.5 m · Number of stages = 16 · Reaction condition factor = 0.9 · Film discretization ratio = 5 · Interfacial area factor = 1.2 · Liquid film discretization points = 5
PELLET	· Aspen Plus® block: Crystallizer · Operating temperature = 25°C · Operating pressure = 1 bar · Saturation calculation method: chemistry
FILTER-1	· Aspen Plus® block: Filter · Model: solid separator · Fraction of solid to solid outlet = 1 · Fraction of liquid to liquid outlet = 0.9 · Pressure drop = 0.1 bar
FILTER-3	· Aspen Plus® block: Filter · Model: solid separator · Fraction of solid to solid outlet = 1 · Fraction of liquid to liquid outlet = 0.9 · Pressure drop = 0.1 bar
WASHER	· Aspen Plus® block: Swash · Liquid-to-solid mass ratio · Mixing efficiency = 1
HE-6	· Aspen Plus® block: Heater · Outlet temperature = 300°C · Pressure drop = 0 bar
LIME	· Aspen Plus® block: MHeatX · Hot side outlet temperature = 85°C

NOZZLE	· Aspen Plus® block: Valve · Calculation type: adiabatic flash for specified outlet pressure · Outlet pressure = 1 bar
HE-25	· Aspen Plus® block: Heater · Outlet temperature = 300°C · Pressure drop = 0 bar
HE-5	· Aspen Plus® block: Heater · Degrees of superheating = 0°C · Pressure drop = 0 bar
HE-21	· Aspen Plus® block: Heater · Outlet temperature = 50°C · Pressure drop = 0 bar
CALCINER	· Aspen Plus® block: RStoic · Operating temperature = 900°C · Operating pressure = 1 bar · $CaCO_3$ fractional conversion = 0.98
HE-3	· Aspen Plus® block: MHeatX · Hot side outlet temperature = 650°C
HE-2	· Aspen Plus® block: MHeatX · Hot side outlet temperature = 674°C
CMP1	· Aspen Plus® block: Compr · Type: isentropic · Pressure ratio = 3.5 · Isentropic efficiency = 0.85 · Mechanical efficiency = 0.9
CMP3	· Aspen Plus® block: Compr · Type: isentropic · Pressure ratio = 3.5 · Isentropic efficiency = 0.85 · Mechanical efficiency = 0.9
HE-10	· Aspen Plus® block: Heater · Outlet temperature = 45°C · Pressure drop = 0 bar
HE-12	· Aspen Plus® block: Heater · Outlet temperature = 45°C · Pressure drop = 0 bar
CMPR	· Aspen Plus® block: Compr

HE-8	· Aspen Plus® block: Heater · Degrees of superheating = 0°C · Pressure drop = 0 bar
ST-TURB	· Aspen Plus® block: Turbine · Type: isentropic · Discharge pressure = 1 bar
HE-20	· Aspen Plus® block: Heater · Degrees of subcooling = 0°C · Pressure drop = 0 bar
PUMP-3	· Aspen Plus® block: Pump · Discharge pressure = 42 bar
HE-4	· Aspen Plus® block: MHeatX · Hot side outlet temperature = 674°C
HE-2	· Aspen Plus® block: MHeatX · Hot side outlet temperature = 450°C
SUPH	· Aspen Plus® block: MHeatX · Hot side outlet temperature = 370°C
CMP2	· Aspen Plus® block: Compr · Type: isentropic · Pressure ratio = 3.5 · Isentropic efficiency = 0.85 · Mechanical efficiency = 0.9
CMP4	· Aspen Plus® block: Compr · Type: isentropic · Pressure ratio = 3.5 · Isentropic efficiency = 0.85 · Mechanical efficiency = 0.9
HE-11	· Aspen Plus® block: Heater · Outlet temperature = 45°C · Pressure drop = 0 bar
HE-13	· Aspen Plus® block: Heater · Outlet temperature = 45°C · Pressure drop = 0 bar
AIR-COMB	· Aspen Plus® block: RGibbs

	· Type: isentropic · Discharge pressure = 10 bar · Isentropic efficiency = 0.85 · Mechanical efficiency = 0.9
TURB-GAS	· Aspen Plus® block: Turbine · Type: isentropic · Discharge pressure = 1 bar · Isentropic efficiency = 0.85 · Mechanical efficiency = 0.9

	· Operating temperature = 1000°C · Operating pressure = 10 bar · Calculation option: calculate phase equilibrium and chemical equilibrium
HRSG	· Aspen Plus® block: MHeatX · Cold side outlet temperature = 415°C

3.3.1 Air contactor and absorption section

The modelling of this hierarchy has tried to reproduce the functions of the air contactor section. In the following page, in Figure 3.3, the model layout for this section is proposed. Since the air contactor is an innovative component of the real plant, Aspen Plus® software does not provide the specific component to be used directly for the model implementation. This has required an additional work to describe in the proper way the functioning of the block. As it is possible to see in Figure 3.3, the red rectangle represents the air contactor which has been modelled using three different Aspen blocks. MIXER-1, MIXER-2 and SEP-1 perform the functions required for the separation of CO_2 from atmospheric air. MIXER-1 is used to mix the ambient air (stream 1) with the gas turbine exhausts once they have been stripped-off about 90% of the initial CO_2 content in the ABSORBER block (stream 74). Stream 2 is then mixed with stream 3 which is composed of the liquid solution described in the previous chapters, used to capture the CO_2. The liquid solution stream has been implemented using the molar composition of the stream provided by the reference paper that is 2.00 M K^+, 1.10 M OH^- and 0.45 CO_3^{2-}. At the same time, also the mass flow rates of the streams and their mass fractions tend to respect the values provided by the reference publication.

The only difference observed between the model and some values given in the publication refers to the mass flow rates of solvent streams. To respect the values of CO_2 capture in the absorber and in the air contactor, some *design specifications* have been used in the software to reach the desired results. The software Aspen Plus® provides indeed a tool in which it is possible to assign a certain specification to a property of a stream or a block (e.g. numerical value, equivalence), varying properly another variable in a chosen range. All the design specifications implemented in the model will be described properly in the last paragraph 3.4 of this chapter. A design specification is used here to vary the mass flow rate of solvent (stream 3) to reach a CO_2 capture of about 75% in the block SEP-1. Looking at the results, it has been found that the mass flow rate obtained results to be much lower than the value given in the source. This can be explained looking at Figure 2.8 where it is visible an 'air contactor basin'; this could mean that the air contactor works with a high surplus of solvent that is stored somehow to ensure a continuous functioning of the component.

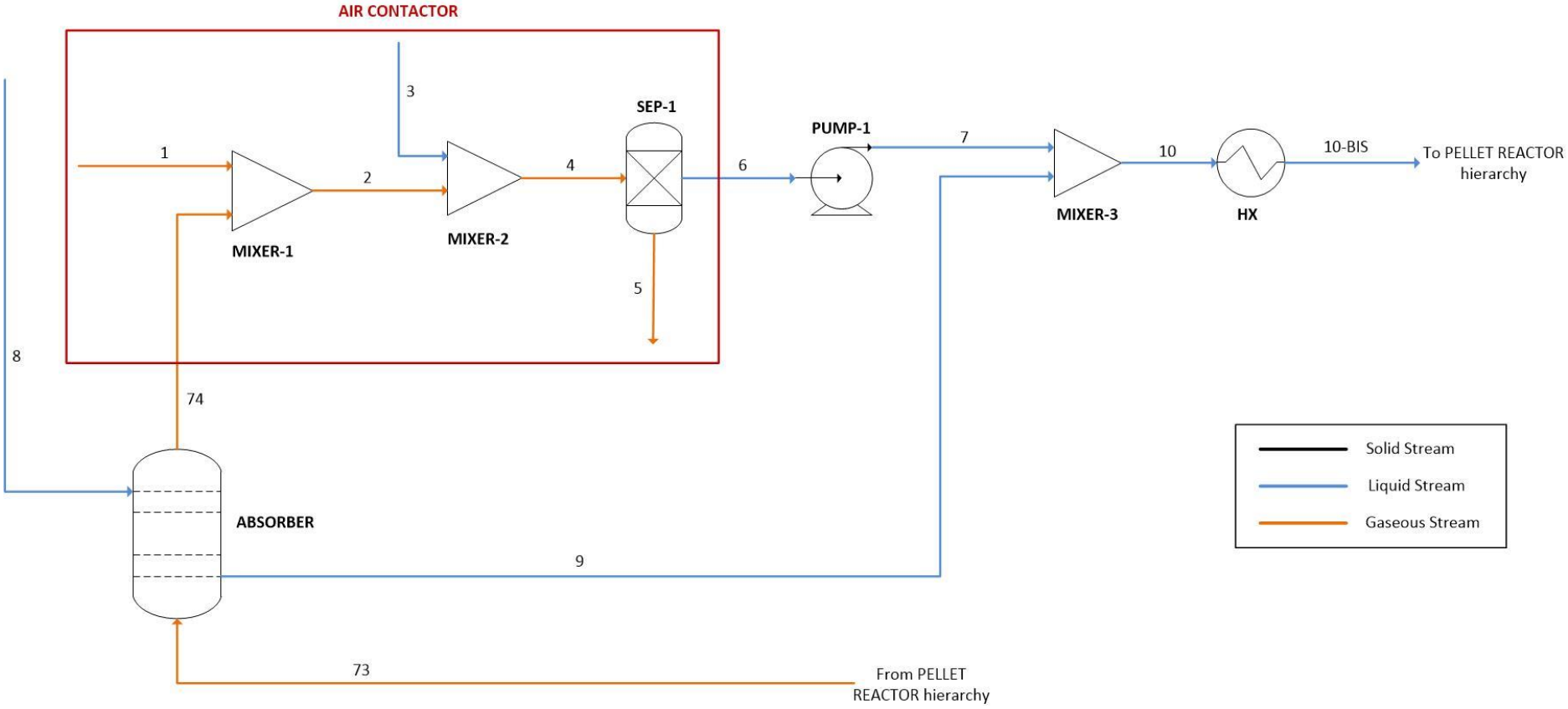

Figure 3.3 – Air contactor and absorber hierarchy

This thesis is corroborated by the fact that same results are obtained in the absorber block, where the capture phenomenon is nearly the same. Absorber columns considered for typical post-combustion capture use similar solvents and, in these applications, the values of solvent mass flow rates are of the same order of magnitude of the values obtained in the model rather than the values given in the paper.

Once the CO_2 has reacted in stream 4 with the liquid solution contained in stream 3 to form potassium carbonate, then, the block SEP-1 has been modelled with the logic 0/1. This means that it performs a simple gas-liquid separation, where the gaseous compounds such as CO_2, O_2 and N_2 are separated in stream 5, whereas the liquid substances continue toward the block PUMP-1. In this way, stream 5 represents the ambient air which exits the air contactor: as a result of the design specification fixing the desired CO_2 capture ratio, stream 5 is characterized by a much lower CO_2 content with respect to the ambient air that enters the first MIXER-1 (stream 1). Furthermore, block SEP-1 has been modelled with a pressure drop of 500 Pa with the aim of reproducing the real operation of the air contactor. For this reason, the subsequent PUMP-1 is required to recover the pressure drop of 500 Pa occurred before, and therefore restoring the pressure of 1 bar in the downstream components.

After the block PUMP-1, block MIXER-3 has been used to put together the remaining liquid solution coming out of the air contactor with the liquid solution which exits the ABSORBER block. The liquid solvent solution used in this section of the plant is used in both the air contactor and the absorber. In the real plant, this solution is recovered from the pellet reactor in a closed loop. To reduce complexity and to avoid any convergence problems, the streams containing the solution have been modelled with an open loop, using two different streams (stream 3 and stream 8). This choice has been done also considering the greater ease in managing the design specifications of this section.

Then, stream 10 is heated-up in the first heat exchanger of the plant, named HX. This component has been modelled by setting its heat duty and no pressure drop. All the heat exchangers of the plant have been modelled with the assumption of “ideal” heat exchangers, therefore characterized by zero pressure drop. The heat exchanger HX is ideally used in pairs with another heat exchanger of the plant, HE-5. Since they are characterized by the same heat exchange, the heat duty of the heater HX is firstly set with a “guess” value and then overwritten with a calculator block with the actual heat duty delivered by the cooler HE-5. The calculator is another tool

provided by Aspen Plus® which is used to insert a FORTRAN code (or Excel sheet calculations) into the simulation. The variables type need to be defined as either import or export variable. Import variables are read from the simulation while the export variables are written to the simulation. In this specific case, the heat duty generated by HE-5 would be defined as an export variable to be written to the attempt value assigned previously to the heat duty of HX.

The last component of this section is the block ABSORBER. This is one of the most critical components of the simulation mainly because of the high number of performance parameters required. The column is filled with structured packing material provided by BERL Ceramic and the size of the column has been set to 12 x 7.5 m (height x diameter), as indicated on the reference paper. For the calculations, a rate-based model calculation has been applied. Therefore, the column has been subdivided into 16 stages; the flow model and the film characterization have been considered as established formerly by the theory: well mixed flow (both liquid and vapor phase), configuration with a discretized film with reactions in the liquid phase and simple film without reactions in the vapor phase have been the hypothesis adopted.

To simulate an absorption column with a rate-based model, other parameters were required. The values chosen for the reaction condition factor, film discretization ratio, liquid film discretization points and interfacial area factor, shown in Table 3.3, have been taken from literature [35], [39], [40].

The *reaction condition factor* is a value that gives a weight to the condition of a reaction. Its value ranges between 0 and 1, where a lower factor represents liquid condition closer to the interface whereas higher factor indicates liquid condition closer to the bulk. It can be expressed using the following expression:

$$factor \cdot bulk + (1 - factor) \cdot interface$$

The *film discretization ratio* is the ratio of the thickness of the adjacent discretization regions; a value greater than 1 means thinner film regions near the vapor-liquid interface [35]. The *interfacial area factor* is a corrective parameter that is multiplied by the value of the simple interfacial area and finally, the correlations used for the absorber simulation are the ones suggested by the software: *Onda et al. (1968)* [41], has been selected for the calculation of mass transfer coefficient, interfacial area and holdup method, and *Chilton and Colburn* for the calculation of the heat transfer coefficient.

In former Table 3.3 the parameters used for modelling the absorption column are summarized. The values chosen for some parameters have been taken from the literature for CO_2 absorption using amines: it has been considered a good approximation, being the absorption processes with amines very similar to that with hydroxides.

3.3.2 Pellet Reactor section

Pellet reactor is used to remove carbonate ion (CO_3^{2-}) formed in the air contactor. Figure 3.4 in the next page represents the pellet reactor hierarchy 'exploded', where all the streams involved are shown. The reaction that takes place in the reactor is the crystallization reaction (R.6), which is slightly exothermic. In the real plant, the pellet reactor will be a fluidized bed reactor, but the already existing component 'FLUIDBED' on Aspen Plus® required too much parameters and details that the reference publication did not provide. Furthermore, in literature it has been very difficult to find specific works on this block. So, considering the nature of the reaction occurring inside the reactor (crystallization of $CaCO_3$), it has been decided to model this component through the block crystallizer (PELLET block) provided by the software. On one hand, this component requires the specifications of temperature and pressure (25°C, 1 bar), on the other hand also the "saturation calculation method" must be provided to perform the crystallization of the compounds. Considering that the chemical reactions had been already inserted at the beginning of the simulation in the "Property" section of the software, here it has been possible to refer directly to the chemistry previously implemented. Otherwise, solubility data or a solubility function should be inserted manually in the dedicated section.

As it is shown in Figure 3.4, the block PELLET is fed by four streams. Stream 10 is constituted by the solvent that comes from the air contactor hierarchy, while stream 11 is a liquid stream which contains mainly $Ca(OH)_2$, required to sustain the reaction inside the crystallizer. Stream 11 has been modelled as an "open" stream, but it should correspond to stream 72, modelled in the successive section (Steam slaker hierarchy). This has been done to prevent possible problems of convergence between the two sections during the simulation; however, stream 10 has been set with the same chemical composition and mass flow rate of stream 72, not to alter the results of the simulation.

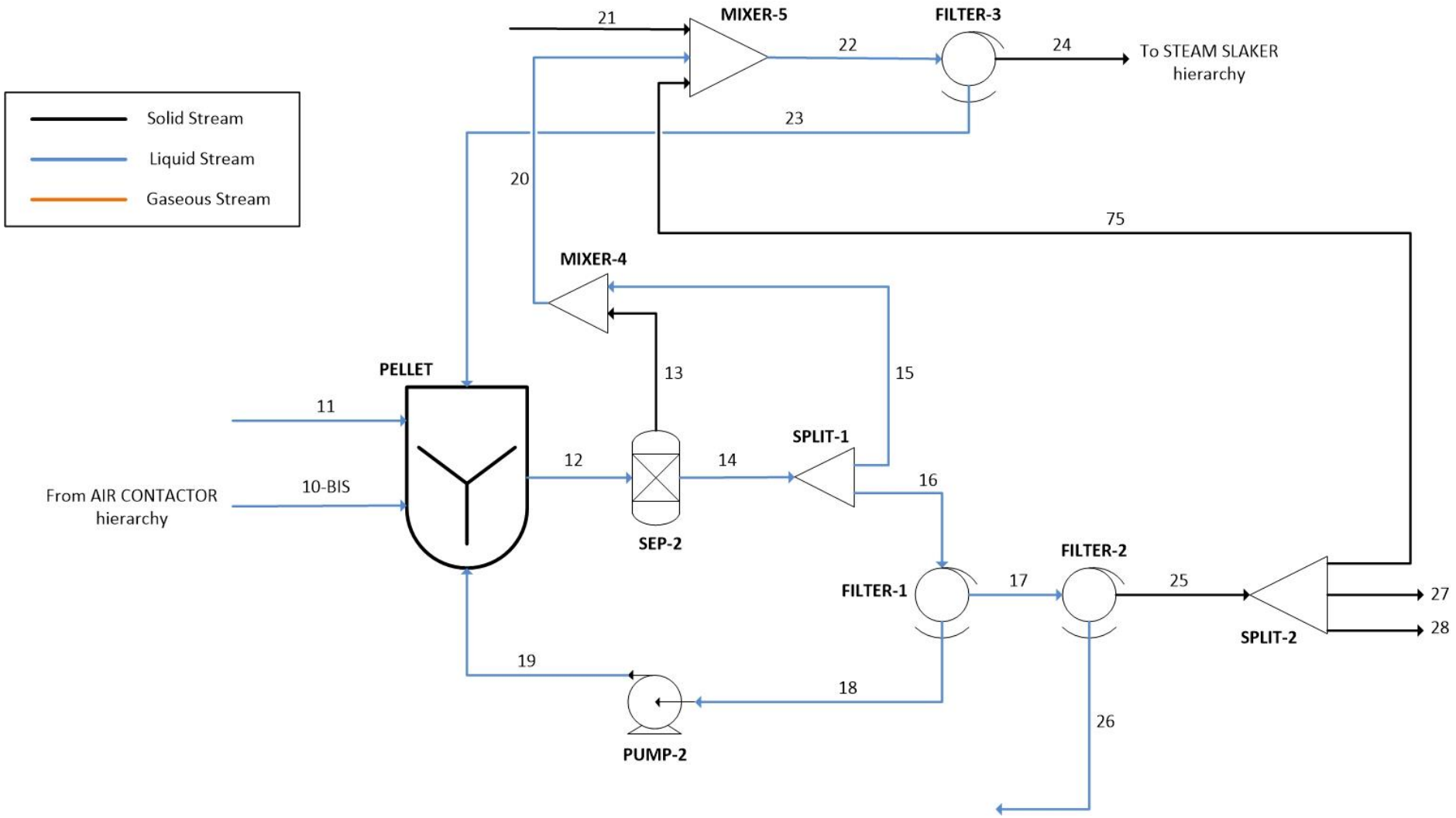

Figure 3.4 – Pellet reactor hierarchy

One important parameter for this section is the calcium retention. In the modelling of the two recirculation loops connected to the pellet reactor (upper and lower recirculation loops), it is necessary to respect this parameter and block SEP-2 was introduced for this scope. The problem is related to the fact that the greater quantity of liquid solution is recirculated in the lower loop, in which the smallest share of solid calcium carbonate should be present. For this reason, a simple separator (block SEP-2) has been used to model a sort of sieve (inside the reactor) that is able to collect only the solid $CaCO_3$ formed in the reactor to be sent afterward to the upper recirculation loop. From mass balances, $CaCO_3$ split fraction of block SEP-2 has been set to 80% but then modified by a design specification; this means that the result of the design specification will provide the amount of calcium carbonate present in stream 12 that continues in stream 14, whereas the remaining percentage is sent to the MIXER-4 to be mixed with the liquid solvent solution that arrives from the upper recirculation loop (stream 15). Moreover, to respect the mass balances on the pellet reactor given by Keith et al., the block SPLIT-1 has been modelled in order to split 99.9% of liquid stream 14 to the stream 16, and only 0.1% to the upper stream 15.

Therefore, by means of a design specification (explained in the following paragraph 3.4) and using an intermediate “ideal” separator block, the value of calcium retention (fixed at 90%) has been respected in the model.

Following the description of the upper recirculation loop, once the solid $CaCO_3$ flow (stream 13) has been mixed in the block MIXER-4 with the liquid stream 15, the resulting stream 20 is sent to the subsequent MIXER-5. This component is used because the pellet reactor needs a ‘makeup’ of solid calcium carbonate to sustain the reaction in the reactor. Stream 21 is composed of $CaCO_3$ only and, in addition to stream 21 and 20, also the stream 75 is mixed with the other two in the mixer. Stream 75 is constituted by a fraction of solid $CaCO_3$ that is filtered in the lower loop (by FILTER-1 and FILTER-2) and then recirculated to the upper loop. Stream 22 is therefore a mixed stream, composed by liquid solution and solid $CaCO_3$ pellets. This final stream is filtered in the subsequent FILTER-3 (a solid separator), where almost the totality of solid calcium carbonate is filtered and sent to the Steam slaker section (stream 24) while the liquid separated in the block is recirculated to the pellet reactor again (stream 23).

As introduced before, stream 16 is almost all liquid but it still contains a small amount of solid calcite ($CaCO_3$) that must be removed before sending the liquid again to the reactor. For this

purpose, in the lower recirculation loop, FILTER-1 and FILTER-2 are used to separate the remaining quantity of $CaCO_3$. Both the blocks have been modelled as standard “solid separators”. FILTER-1 can separate a certain amount of solid $CaCO_3$, with a certain pressure drop inside established by the data of the reference publication. Therefore, the liquid stream which exits FILTER-1 (stream 18) is pumped through the block PUMP-2 before being sent in the Pellet reactor again. After the first filtration step, a second filter, FILTER-2, is used to remove all the amount of solid $CaCO_3$ from the liquid stream 17. Once the solid fraction has been removed in stream 25, also in this case, as done in the air contactor section, stream 26 has been modelled as an “open stream”. It should be connected to the blocks that represent the air contactor and the absorber column but for reasons of convergence of the simulation, and to implement the design specification in the air contactor section more easily, it has been decided to model it as an “open” flow. However, this is an acceptable approximation, especially because the high flow rates indicated by the reference paper in this part of the plant give greater freedom during the modelling phase, being sure not to overestimate the solvent flow rate.

Finally, the solid $CaCO_3$ flow (stream 25) is split in three streams (27, 28 and 75). Stream 75 has already been discussed, while stream 27 could be sent to the calciner block and stream 28 is made of $CaCO_3$ to be disposed-off.

3.3.3 Steam slaker section

The slaker is the fluidized bed reactor used to hydrate the quicklime (CaO) that comes from the calciner, and to preheat the $CaCO_3$ pellets which arrive from pellet reactor in stream 24. In the real plant, solid calcite pellets pass through the steam reactor and are heated thanks to the heat generated by the high exothermicity of the slaking reaction (R.8). Aspen Plus® does not provide a component that matches all the functions of the real reactor, so this section of the plant has been modelled trying to reproduce all the functionalities of the real reactor making the appropriate changes. Once stream 24 (containing solid $CaCO_3$) has passed the block FILTER-3 in the pellet reactor hierarchy, it is washed in the WASHER block using water. Water (stream 46) is provided by an external flow that will be described in the CO_2 compression hierarchy (paragraph 3.3.5); here it has the role of 'separating' the solid $CaCO_3$ from the liquid hydroxide solution in which it is still absorbed. Therefore, all the liquids exit the washer in stream 30 while the calcite in stream 29 is dried and heated up to 300°C to evaporate the remaining content of water; this is performed in the heaters HE-1 and HE-6. Two heat exchangers have been considered in order to facilitate the calculations in the pinch analysis. The first one (HE-1) is used to heat the $CaCO_3$ and the water associated, set with a number of degrees of superheating equal to 0°C. The second one (HE-6) is used instead to perform the function of the real slaker, i.e., heat up $CaCO_3$ to 300°C.

Then, to remove completely H_2O from the solid, stream 31 (at 300°C) is passed through a separator, SEP-4, which is modelled again with the 0/1 logic. In this case, all the compounds that are in the vapor phase are removed and sent in the slaker (stream 33-A) to sustain the slaking reaction, while the stream 33-B containing only solid $CaCO_3$ is sent toward the calciner where it will be thermally decomposed. Since the software does not provide a reactor block able to heat a stream leaving it intact from a chemical and physical point of view, as it happens in the real reactor, therefore the reader should imagine that both heaters HE-1 and HE-6 are fictitious components, used only to simulate the passage and heating of $CaCO_3$ through the reactor. Moreover, stream 33-A (that contains only water) enters the slaker: if $CaCO_3$ could pass into the slaker, the evaporated water would increase the vapor content in the reactor.

Even if in the real plant it will be a fluidizing bed reactor, the slaker has been modelled using another kind of component, for the same reasons mentioned in the case of the pellet reactor: to

reduce complexity, and mainly because block RStoic provided by Aspen Plus® is able to manage in the proper way the reaction occurring inside the slaker.

In fact, this block requires very little information about the reactor:

- operating temperature;
- operating pressure;
- reactions that occur inside;
- fractional reactants conversion.

Furthermore, the fractional reactants conversion required by the software perfectly matched with the datum about CaO conversion provided by the reference paper. Following the data found in the source, a conversion of 85% of incoming CaO has been set. Moreover, the steam slaker works at 300°C and atmospheric pressure, and the only reaction specified in the block has been the slaking reaction (R.8) between quicklime and water.

As it is possible to see in Figure 3.5, the SLAKER block is fed by water stream 33-A, stream 62, stream 64 and CaO recirculation in the stream 68. Stream 62 comes from the calciner hierarchy and is composed only of calcium oxide, fundamental to sustain the slaking reaction. Stream 64 comes from the initial stream 58; they have been used to model a 42-bar steam line at 253°C that is used in the real plant to provide to the slaker a certain amount of heat. Slaker reactors usually work with water but sometimes they can be heated to a specific temperature (in this case, 300°C) through water vapor. The thermodynamic advantage of steam slaking over conventional water slaking used in the Kraft process is that the slaking reaction enthalpy is released at higher temperatures [24].

Therefore, to model the contribute of this line, blocks SPLIT, NOZZLE and HE-8 and HE-25 have been included in the simulation. Since vapor at 42 bar is injected only in a small quantity inside the reactor, the splitter SPLIT has been used to this purpose; this block divides the incoming stream 59 in two sub-streams, 60 and 61. Stream 60 is then expanded from 42 bar to 1 bar (the slaker pressure) in a simple throttle valve (block NOZZLE) that simulates the expansion of the water vapor when it exits the vapor line and enters the reactor. During the expansion it cools down, but its final temperature is still high enough to increase the temperature of the reactor. In the real design of the plant, the amount of steam that is not sparged in the slaker passes through the

slaker and heats up. Being the steam at 253.3°C, it is fully vaporized passing inside the reactor and ideally reaches the thermal equilibrium with the slaker (this should not be possible unless the residence time is very high, but this is an acceptable approximation). This phenomenon has been modelled using two heaters (HE-8 and HE-25), again for facilitating pinch analysis calculations. In the heat exchangers, water changes its phase, and this must be considered with some techniques in the pinch analysis; the use of two heaters is therefore carried out to simplify the process. These components are characterized by no pressure drop and are modelled to heat the steam from 253.3°C to 300°C.

Following the line of the steam (stream 61-B), it is sent to the calciner hierarchy where it passes through the heat exchanger SUPH. This component is used to extract heat from the calciner exhausts, but it will be explained in the next hierarchy. Here it is sufficient to say that the steam is heated further in the superheater up to the temperature of 415°C before entering in the steam turbine ST-TURB with the name of stream 65. The steam turbine has the role of producing the remainder of the power required by the plant and has been modelled with the proper block (block Turbine) provided by the software. The turbine data, together with data about the other components of this hierarchy, can be found in Table 3.3 of paragraph 3.3. The steam contained in stream 65 is expanded in turbine with stream 54, composed by the steam generated by the HRSG, described in the further power island hierarchy. Once the steam has been expanded in turbine, it is condensed up to 50°C by three coolers, HE-5, HE-20, HE-21. The condensation is a single phenomenon, but three coolers have been used in order to account for the latent heat of condensation in the calculation of the pinch analysis. The steam exits the turbine in stream 55 and is pumped to 42 bar again to be recirculated in the slaker, thanks to the centrifugal pump modelled with the block PUMP-3. Streams 58-BIS and 58 are actually the same stream in the real plant, but they have been modelled as different flows to solve a problem of convergence of the simulation. However, the results have been not altered since stream 58 which enters the heat exchanger LIME has been set with the same flow rate and the same chemical composition of stream 58-BIS.

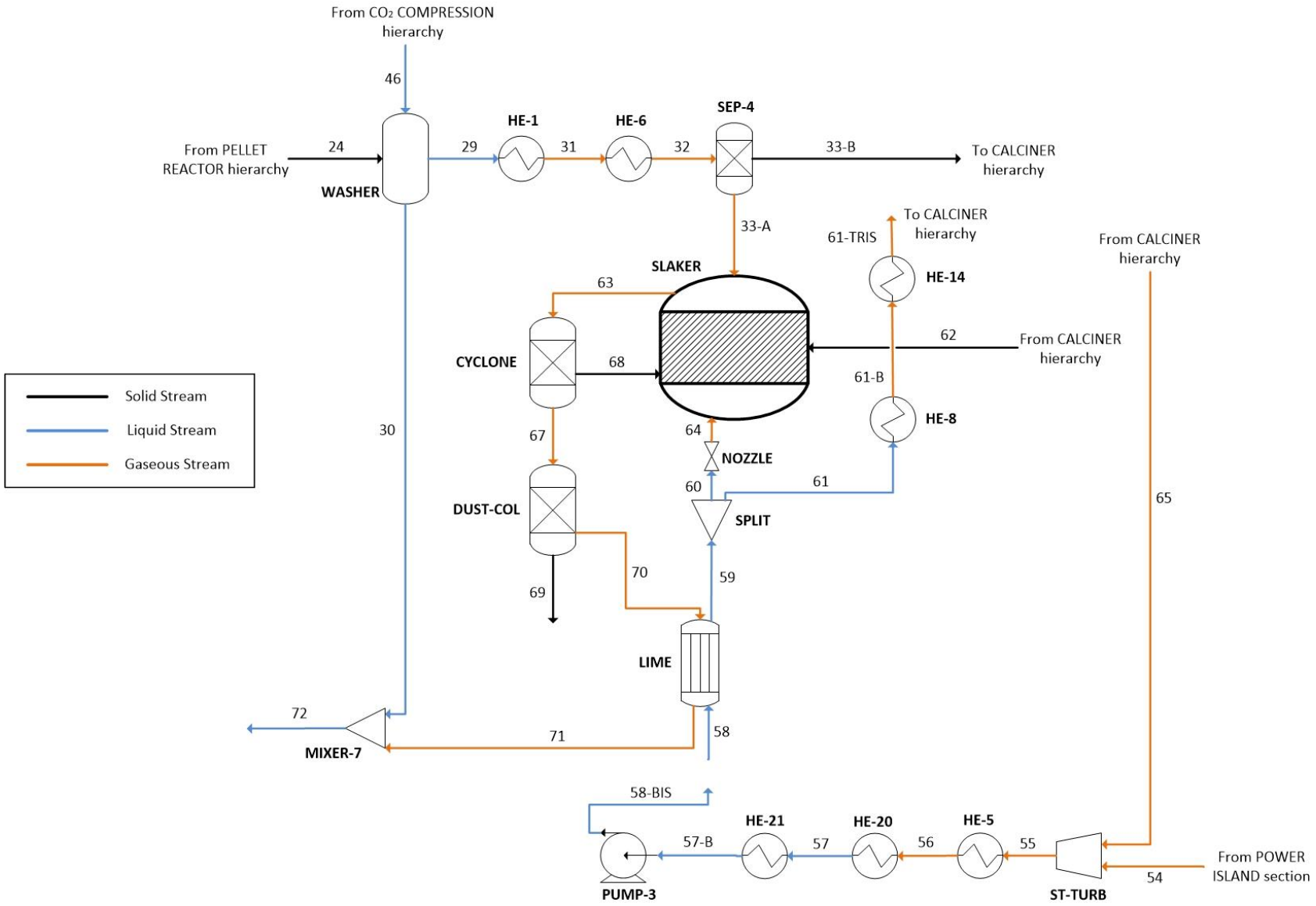

Figure 3.5 – Steam slaker hierarchy

Finally, the recirculation loop at the left of the steam slaker must be analysed. As written in the previous page, CaO conversion in the slaker reactor has been fixed to 85%; it means that a small amount of CaO will still be found at the exit of the slaker. The small quicklime particles contained in stream 63 are therefore separated in the first separator named CYCLONE and the remaining amount of CaO that "bypassed" the previous block is finally removed in the stream 69 by the subsequent block DUST-COL. The first separator (CYCLONE) has been considered to simulate the behaviour of the 'primary cyclone', used in the real plant to elutriate and recirculate small quicklime particles that leave the slaker; the second separator (DUST-COL) is used instead to simulate a "dust collector", used to capture all the CaO "survived" to the first separator. This hierarchy contains only two more components, that are the lime cooler (modelled in the software with the block LIME) and the MIXER-7; this is a traditional counterflow heat exchanger used to recover the sensible heat from the hydrated lime that is then sent back to the pellet reactor hierarchy: here, it feeds the pellet reactor for restarting the chemical cycle. MIXER-7 mixes the $Ca(OH)_2$ contained in stream 71 with the liquid solution coming out of the WASHER. Stream 72 is therefore a mixed stream (liquid and solid) and will be sent to the pellet reactor to make the lime reacting with the potassium carbonate.

3.3.4 Calciner section

The calciner reactor is the centre of this hierarchy, whose layout is shown in Figure 3.6 at the end of this paragraph. In this reactor, the calcination of $CaCO_3$ occurs (R.7). This reaction is fundamental to close the cycle of the solvent regeneration and to produce CO_2 in a concentrated form at the same time. Calciners are large steel vessels in which the fluidizing gas is supplied at the bottom of the reactor. Here it works at ambient pressure and 900°C and the real fluidized bed reactor has been modelled using again a simple stoichiometric reactor provided by Aspen Plus® (RStoic block). This choice fits particularly well with the kind of reactor since the little specifications provided by the reference source refer to the operating conditions of the reactor and to the $CaCO_3$-to-CaO conversion efficiency. This last parameter is required by the block RStoic in the software, and it has been set to 98%, according to the data given by the reference source.

The calciner receives $CaCO_3$ pellets from the steam slaker hierarchy at a temperature of 300°C (stream 33-B). Before entering the reactor, solid calcite passes through two heat recovery cyclones arranged in counterflow configuration with the outgoing gas stream. These two cyclones have been modelled with simple counterflow heat exchangers (HE-2 and HE-3), where the inlet and outlet temperatures of the streams have been fixed as design values to respect the data provided by Keith et al. Once the gaseous stream 41 produced by the calciner has been cooled by HE-3 and HE-2, it is then sent toward the superheater (block SUPH already mentioned in the Steam slaker hierarchy, paragraph 3.3.3), where it is used to preheat the water vapor (stream 44) to the temperature required for its successive expansion in the steam turbine.

The stoichiometric reactor chosen in the software can receive more than one incoming flow, but it generates only one product stream. As said, the reactor is fed by solid $CaCO_3$ contained in stream 35 (and almost completely converted), almost pure oxygen from ASU (Air Separation Unit, not modelled here) in stream 37, and natural gas in stream 38. The considered component is not a Gibbs reactor (RGibbs on the software), which is rather able to make the reactions happen autonomously without further specifications. So, in addition to the thermal decomposition reaction of $CaCO_3$ (R.7), the combustion reactions of natural gas must be provided manually. Natural gas is mainly composed of CH_4 and C_2H_6: therefore, the reactions between these two compounds with oxygen have been inserted in the proper section of the software considering their complete conversion.

The presence of both solid and gas inside the reactor means that the product stream will contain a solid and a gaseous fraction. For this reason, the block SEP-3 has been used to model a solid-gas separator working with the usual 0/1 logic. The calcium carbonate is produced by the calciner at about 900°C (operating temperature of the reactor); once released, it is therefore separated in the stream 40 and sent to the heat exchanger HE-4 where it is cooled to 674°C in a single cyclone, again modelled as a conventional heat exchanger. HE-4 preheats the incoming oxygen (stream 36) to the same temperature of CaO (674°C) before sending it to the steam slaker.

The amount of incoming oxygen has been fixed looking at the values proposed by the source, since the ASU has been not modelled in this thesis; its energy consumptions have been set equal to those proposed by Keith and accounted in the assessment of energy performance (chapter 4). Moreover, the mass flow rate of natural gas injected in the calciner (stream 38) has been varied by a design specification, described in the paragraph 3.4. The design specification used here aims at obtaining a mass flow rate of natural gas capable of realizing an adiabatic calciner. The calcination reaction is highly exothermic, and an excessive natural gas flow rate would make the reactor even more exothermic, with a straightforward increase of energy consumption. To reduce as much as possible the energy consumption, it has been decided to consider the reactor adiabatic, therefore introducing the mentioned design specification.

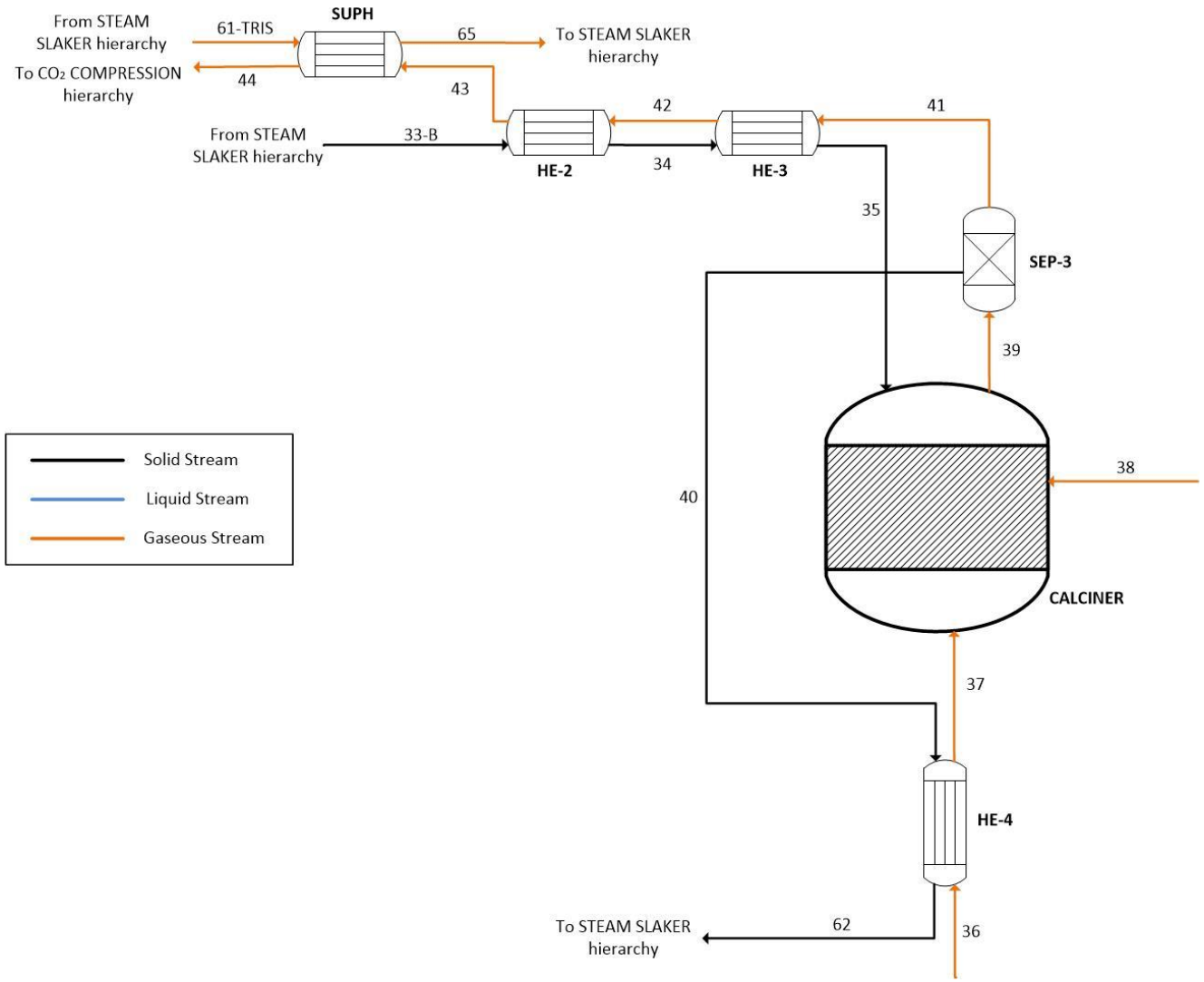

Figure 3.6 – Calciner hierarchy

3.3.5 CO_2 compression section

The concentrated CO_2 gas stream (stream 44) that arrives from the calciner reactor is characterized by a significant CO_2 mass fraction but still not sufficient to be directly considered for further uses. So, before entering the compressor section, it is "cleaned-up" in a water knockout. It is a simple separator where the stream 44 is put in contact with water (stream 45) to cool the calciner's off-gas and to condense the water content inside it. Removing water by condensation in SEP-5, the outgoing stream 47 is therefore characterized by an even higher CO_2 concentration. The separator has been modelled to send only the gaseous compounds in the stream 47, and in the stream 46 the water injected with stream 45 and the H_2O separated from the stream 44.

After passing the separator block, the stream 47 is compressed from atmospheric pressure up to 150 bar, as indicated by the source. The compression has been realized by a 4-stages compressor [24], modelled with the four distinct compressors shown in Figure 3.7 (CMP1, CMP2, CMP3 and CMP4). The stages modelled all have the same pressure ratio of 3.5 in order to obtain a flow of concentrated CO_2 at 150 bar. Moreover, each compressor used in the model has been considered as an isentropic compressor, with the same isentropic and mechanical efficiency. It was possible to consider each compressor as isentropic since no external heat is being added or extracted during the pressure increase. Furthermore, a step of inter-cooling between a compression stage and the other has been realized thanks to four coolers. The coolers have been modelled with no pressure drop and aim to bring CO_2 stream back to the same temperature (45°C) between one compression stage and the next. The inter-refrigeration is considered in engineering applications whenever the fluid pressure must be increased a lot, mainly to reduce the compression work of each stage and to avoid reaching too high temperature that would lead to harmful consequences on materials. This is explained in the next equation where it is shown that the isentropic compression work is directly proportional to the inlet temperature of the fluid (T_{in}) and the compressor pressure ratio (β). Then, to evaluate the compressor "useful work" it is sufficient considering also the compressor efficiency.

$$L_{is} = \frac{k}{k-1} \cdot R^* \cdot T_{in} \cdot (\beta^{\frac{k}{k-1}} - 1) \qquad \text{(eq. 3-18)}$$

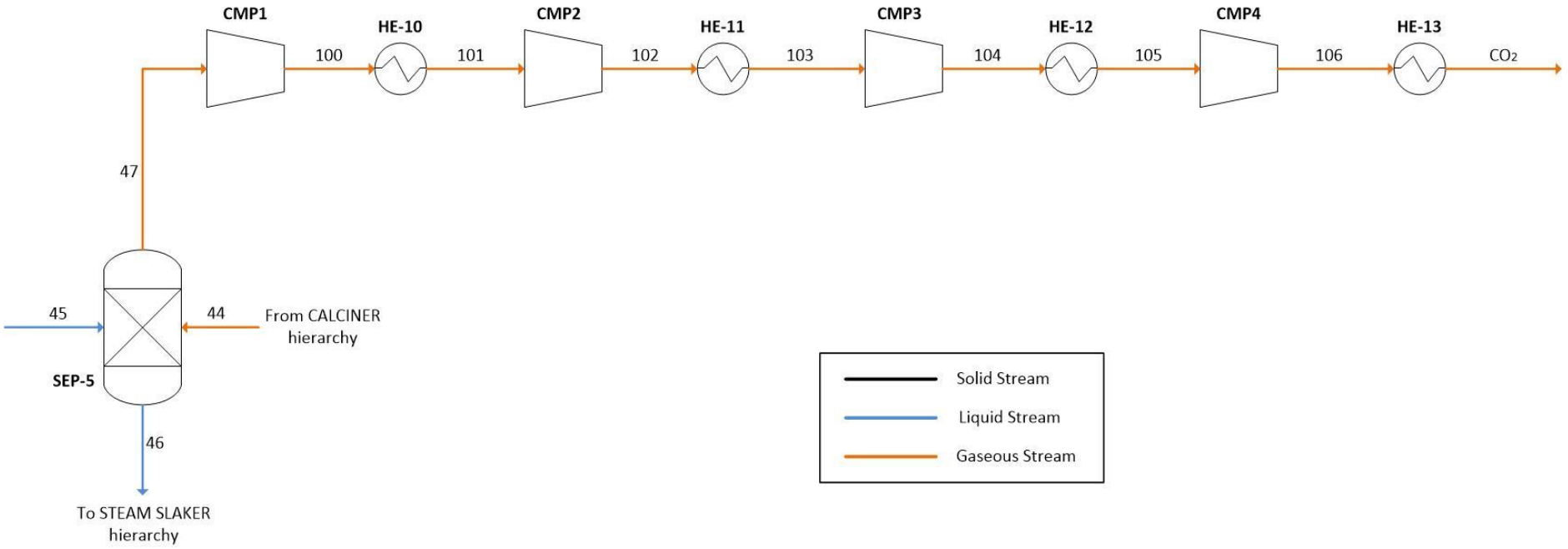

Figure 3.7 – CO_2 compression hierarchy

3.3.6 Power Island section

This is the last hierarchy of the model and it has been modelled to take into consideration the internal power demand of the plant, especially for the pellet reactor and the other auxiliary equipment. The power island consists of a combined cycle, i.e., a natural gas turbine followed by a heat recovery steam generator (HRSG); the HRSG steam is used to produce power whereas the gas turbine exhaust stream is stripped of CO_2 using a conventional counterflow gas-liquid column in the air contactor and absorber section, already described in paragraph 3.3.1.

The block CMPR represents the compressor of the gas turbine section. It compresses ambient air from atmospheric conditions up to 10 bar and it has been modelled with an isentropic compressor characterized by an isentropic efficiency of 85% and a mechanical efficiency of 90%. Then, the real combustor of a gas turbine plant has been modelled with the block AIR-COMB. The Aspen Plus® component chosen is a Gibbs reactor (block RGibbs) that automatically considers all components present in the "Property" section of the software as possible products. This means that the products composition depends on the components that enters the block. In this case, the two inlet streams are the number 49 and 50, where the first corresponds to the air compressed to 10 bar in the previous compressor CMPR, and the second is the natural gas stream that enters the block at 25°C and 10 bar. The block AIR-COMB works at temperature of about 1000 °C and a pressure of 10 bar; it means that the products of the combustion reactions will be at the same operating conditions of the reactor. This block is very useful to avoid writing all the chemical reactions that occur inside the block; on the other hand, it is fundamental to consider all the possible components involved in the reactions that can occur inside the reactor since the software is not able to individuate possible missing components. The products obtained from this block are then sent to the gas turbine TURB-GAS to be expanded to atmospheric conditions. The gas turbine has been modelled with the proper component in Aspen Plus® with the specification of the discharge pressure, fixed therefore to 1 bar. The gas turbine resulting stream 52 is then sent to the HRSG block, that aims at simulating the behaviour of a real heat recovery steam generator. In this model it has been considered only as a simple heat exchanger where the cold side outlet temperature of the water has been fixed to 415°C equal to the temperature of stream 65. In this way, streams 54 and 65 enter the successive steam turbine (block ST-TURB) at the same temperature.

In this section one design specification has been implemented on the mass flow rate of the stream 48. The natural gas flow rate which feeds the combustor (block AIR-COMB) is fixed and equal to that of the reference publication while the flow rate of stream 48 is varied by the software in order to obtain a mass flow rate of 121 ton/hr in the stream 71. This value has been set to respect the mass flow rates indicated by Keith et al. in their work. The layout of the section is provided in Figure 3.8 which can be found in the following page.

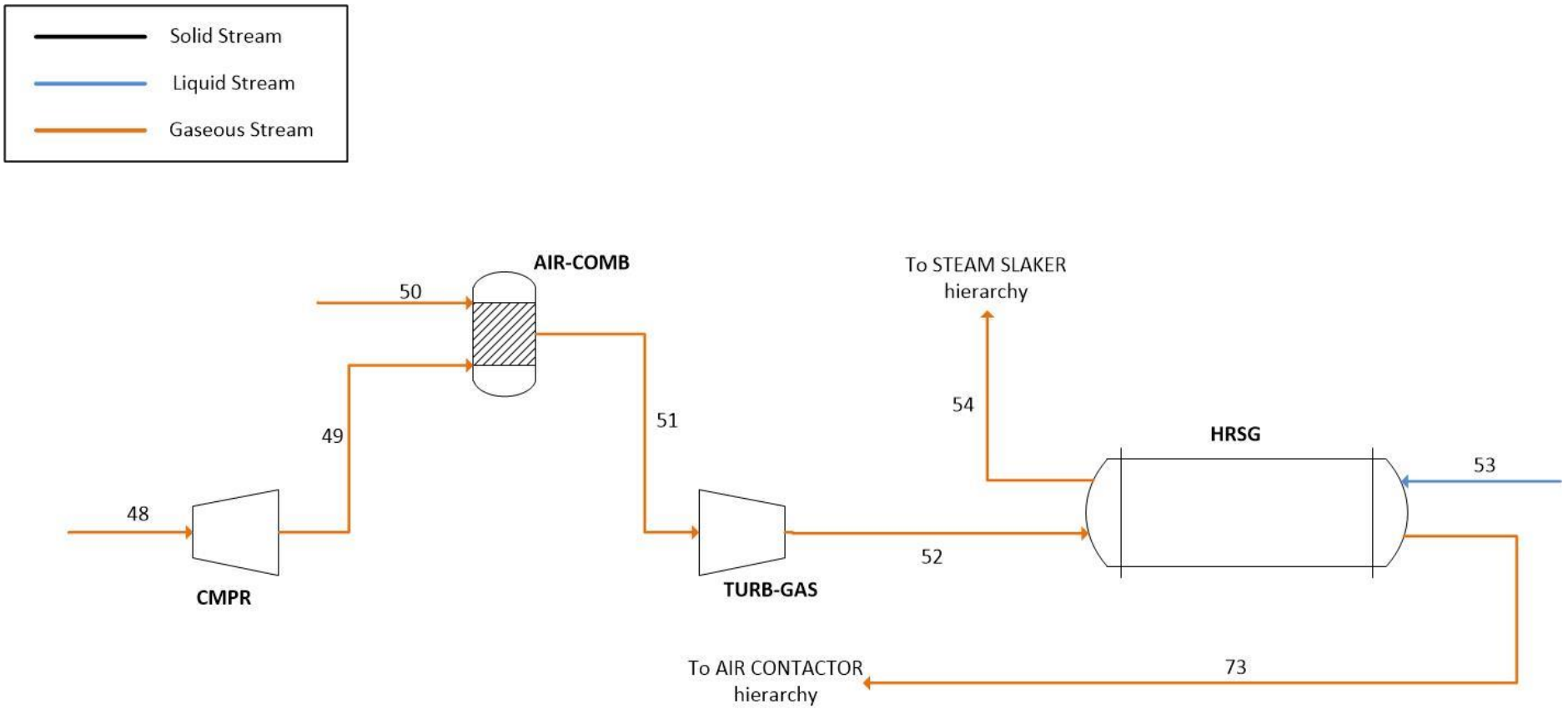

Figure 3.8 – Power island hierarchy

3.4 Design specifications

The "design specification" is a tool provided by the software Aspen Plus®, already mentioned in previous sections, that can be now explained in more detail. In other words, a design specification is a tool through which it is possible to assign a certain specification to a stream property or a block (e.g. numerical value, equivalence, split ratio), varying properly another variable in a set range. If used properly, it can solve simulation problems that would be otherwise difficult to overcome.

Table 3.4 below indicates the design specifications implemented for the simulation with the number of the section in which they were applied.

Table 3.4 - Design specifications

Design specification	Description and target	Variable	Section
1. AC-RATIO	$\frac{\dot{m}_{CO_2\_out}}{\dot{m}_{CO_2\_in}} = 0.2561$	Mass flow rate of stream 3 (liquid solvent to the air contactor)	3.3.1
2. CA-RETEN	$\frac{Calcium\ (Ca)_{out}}{Calcium\ (Ca)_{in}} = 0.9$	$CaCO_3$ split fraction of SEP-2	3.3.2
3. GAS-TURB	$\dot{m}_{natural\ gas\_out} = 121\ \frac{ton}{hr}$	Mass flow rate of stream 48 (ambient air)	3.3.6
4. NAT-GAS	$\phi_{th\_CALCINER} = 0\ W$	Mass flow rate of stream 38 (natural gas to calciner)	3.3.4
5. SOLV-ABS	$\frac{\dot{m}_{CO_2\_out}}{\dot{m}_{CO_2\_in}} = 0.1$	Mass flow rate of stream 8 (liquid solvent to the absorber)	3.3.1

1. *AC-RATIO*: the software varies iteratively the mass flow rate of stream 3 which contains the liquid solvent used to separate the CO_2 from the air, with the aim of obtaining a carbon dioxide capture of 74.39% in the blocks that simulate the air contactor. This design specification is set in the air contactor and absorber hierarchy.
2. *CA-RETEN*: this specification has been implemented in the pellet reactor hierarchy and aims at simulating the calcium retention datum given by the reference source. Both the numerator and denominator of the fraction in Table 3.4 contain values of mass flow rates. Only the streams containing calcium at the inlet and the outlet section of the block PELLET have been considered and the software varies only the amount of $CaCO_3$ separated in SEP-2 to reach the desired amount of $CaCO_3$ in the upper recirculation loop, fixed at 90% of the incoming calcium carbonate.
3. *GAS-TURB*: in the power island hierarchy, this specification modifies iteratively the mass flow rate of ambient air (stream 48) compressed by compressor CMPR to obtain a mass flow rate of 121 ton/hr in stream 73. This stream is then sent to the air contactor section to be stripped-off the CO_2 generated by the combustion; this design specification has been therefore introduced mostly to respect the amount of CO_2 which will be extracted in the subsequent absorption column (ABSORBER), value provided by the reference source. Moreover, this specification has been important for producing further reliable energy performance assessments.
4. *NAT-GAS*: the amount of natural gas injected in the calciner is overwritten by Aspen Plus® to obtain an adiabatic reactor.
5. *SOLV-ABS*: this design specification is conceptually equal to the previous *AC-RATIO* specification. The mass flow rate of liquid solvent (stream 8) in the air contactor and absorber hierarchy is varied to realize a CO_2 capture of 90% in the absorber column (block ABSORBER).

4. Energy performance of the plant. Results and discussion

After the simulation, all the results have been collected and analysed to evaluate the energy performance of the plant. The aim of this thesis was firstly to reproduce a possible layout of a DAC plant (in the specific case, the one proposed by Keith and Carbon Engineering) with the software Aspen Plus® and then to calculate its energy performance for validating the model, according to the reference system.

The key energy performance indicator used in the field of carbon capture is a parameter that gives the amount of primary energy spent (usually in kJ or kWh) to separate a mole (or kg) of CO_2. The energy costs furnished by the reference paper included only the primary energy provided by natural gas, used to feed the calciner reactor and the power island. The paper does not mention thermal energy needs, while the electricity demand is said to be satisfied by the power produced by the combined cycle. Therefore, the only energetic expenditure refers to the natural gas. In particular, Keith et al. do not consider a traditional natural gas but pure methane. The value given in CE's paper is 8.81 GJ/$mol_{CO2,\ captured}$ or 5.25 GJ/$mol_{CO2,\ captured}$ and 366 kWh of electricity. An analysis of the simulation results has been done with the aim of verifying that the primary energy consumption of the modelled plant coincided with the reference plant, or that it was at least a comparable value.

First of all, it has been necessary to evaluate the molar flow of CO_2 captured in the model of the plant. Analysing the simulation results, a value of 716.91 $mol_{CO2,\ captured}$/s has been calculated and the values are shown in the following Table 4.1.

Table 4.1 - CO_2 captured in the model

	CO_2_in [mol/s]	**CO_2_out [mol/s]**
Stream 2	957.21	-
Stream 5	-	240.3
CO_2 CAPTURED [mol/s]	716.91	

Then, also the calciner and power island modelled with Aspen Plus® are fed by natural gas, so its energy content must be taken into consideration. This thesis has not considered pure methane, but a conventional natural gas with the following composition and with a LHV of 43.054 MJ/kg.

Considering the mass flow rates of natural gas to the calciner and to the power island, the total power associated to natural gas is 216.27 MW.

Table 4.2 - Natural gas composition

Chemical species	Composition [% vol]
CH_4	87
C_2H_6	6
CO_2	3
N_2	4

Even if the reference paper does not mention an energy integration between different sections of the plant, the pinch analysis of the plant modelled on Aspen Plus® has been realized to assess the possible availability of internal thermal energy. In a plant, there are always streams which need to warm up and others that need to cool down. So, before using an external heat source to heat the cold streams, pinch analysis assesses the possibility of realizing an internal heat recovery network between the streams using simple heat exchangers. In this way, it is possible to recover a certain amount of heat from some hot streams and transfer it to the cold streams that must be heated up. Pinch analysis is a widespread methodology used for the minimization of the energy consumption and for the optimization of the heat recovery system [42].

Before applying the methodology, it is necessary to individuate both the cold and the hot streams inside the plant to get the values of the minimum heat supply and the minimum heat removal, as main results. In Figure 4.1 and Figure 4.2 the main values calculated before getting the results are shown, where the number of the stream correspond to the number assigned to the same stream in the model shown in former paragraph 3.3. The minimum heat supply and heat removal result to be 51.82 MW and 48.24 MW, respectively. If the “cold” demand can be satisfied by a conventional cold stream (e.g. water at ambient conditions), the heat demand which is not satisfied by an internal heat recovery must be provided from an external source. After the calculation, Figure 4.3 shows the scheme of the heat exchangers among the streams selected in the first step of the analysis. Table 4.3 summarizes the energy results for each heat exchanger.

Stream	c_p [kJ/kg/K]	Mass flow rate [kg/s]	Hot/Cold	T_{in} [°C]	T_{out} [°C]	T_{in}* [°C]	T_{out}* [°C]	G·c_p [kW/K]	Φ [kW]
10	3,74	1330,46	C	19,2	31,4	24,2	36,4	4973,59	60677,76
29	2,37	108,85	C	57	99,6	62	104,6	258,40	11007,81
31	1,94	108,85	C	99,6	300	104,6	305	211,65	42414,70
61	-	17,55	C	253,3	254,3	258,3	259,3	21443,00	21443,00
61-B	2,28	17,55	C	254,3	300	259,3	305	40,01	1828,64
55	1,91	24,49	H	104,3	99,6	99,3	94,6	46,76	219,77
56	-	24,49	H	99,6	98,6	94,6	93,6	55539,50	55539,50
57	4,20	24,49	H	98,6	50	93,6	45	102,80	4996,23
100	0,95	144,24	H	181,6	45	176,6	40	136,74	18678,88
102	0,98	144,24	H	163,3	45	158,3	40	141,00	16679,89
104	1,07	144,24	H	131,2	45	126,2	40	154,41	13310,23
106	2,12	144,24	H	124,6	45	119,6	40	306,08	24364,09

Figure 4.1 - Streams definition

T* [°C]	ΔT	G·c_p [kW/K]	Φ [kW]	$Φ_{cum}$ [kW]	$Φ_{cum}$ final [kW]
305				0	51818,35
259,3	45,7	-251,66	-11501,05315	-11501,05	40317,30
258,3	1	-21654,65	-21654,65	-33155,70	18662,65
176,6	81,7	-211,65	-17291,82	-50447,52	1370,83
158,3	18,3	-74,91	-1370,83	-51818,35	0,00
126,2	32,1	66,09	2121,42	-49696,94	2121,42
119,6	6,6	220,50	1455,29	-48241,64	3576,71
104,6	15	526,58	7898,71	-40342,94	11475,42
99,3	5,3	479,83	2543,11	-37799,83	14018,52
94,6	4,7	526,59	2474,98	-35324,85	16493,50
93,6	1	56019,33	56019,33	20694,48	72512,83
62	31,6	582,63	18411,25	39105,72	90924,08
45	17	841,03	14297,57	53403,30	105221,65
40	5	738,23	3691,15	57094,45	108912,80
36,4	3,6	0	0,00	57094,45	108912,80
24,2	12,2	-4973,59	-60677,76	-3583,31	48235,04

Figure 4.2 - Grand composite curve definition

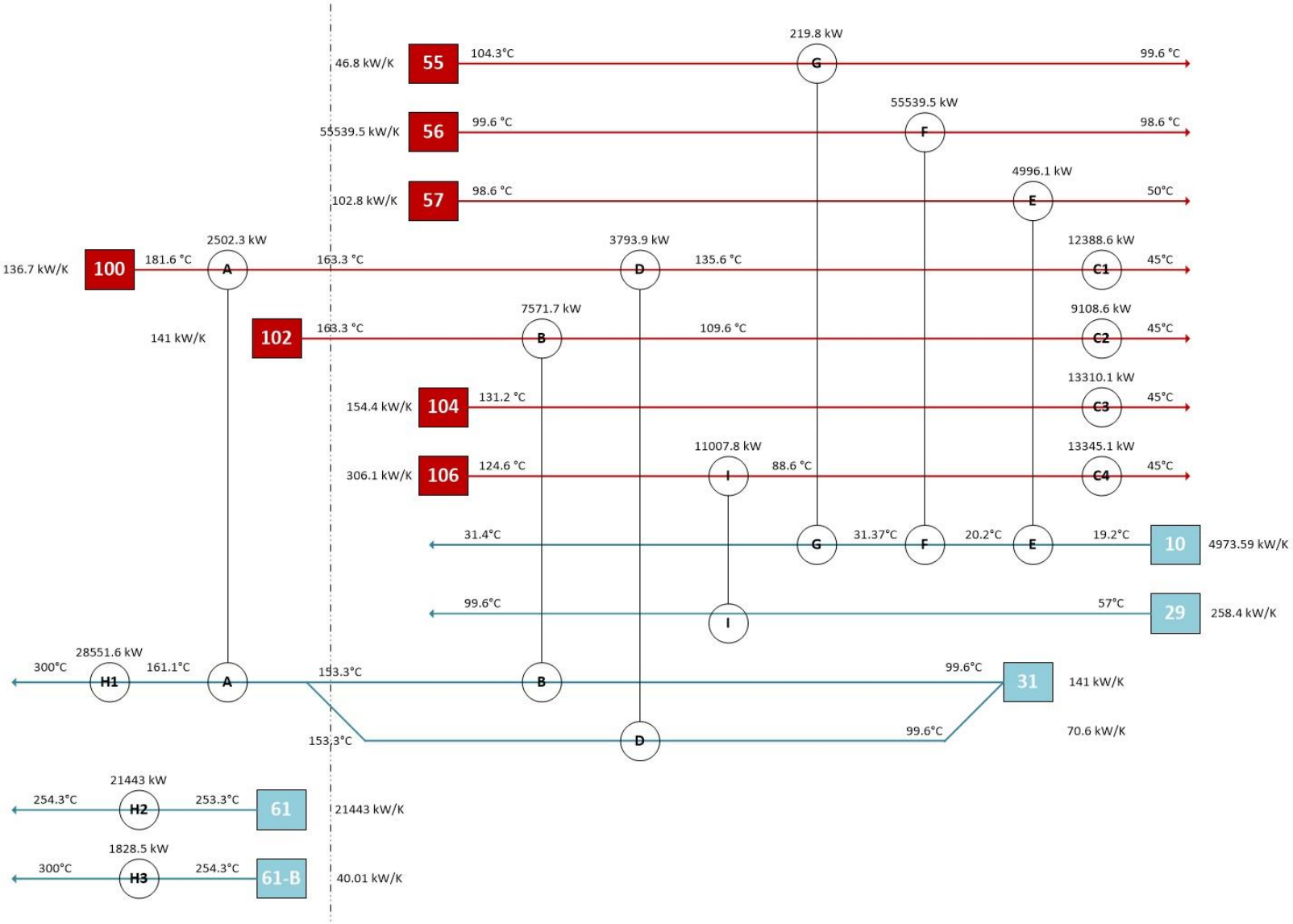

Figure 4.3 - Schematization of the thermal integration between the streams

Table 4.3 - Thermal power for each heat exchanger

HEAT EXCHANGER	Heat duty [MW]
A	2.5
B	7.57
D	3.79
E	4.99
F	55.54
G	0.22
I	11.01
H_1	28.55
H_2	21.44
H_3	1.83
C_1	12.34
C_2	9.11
C_3	13.31
C_4	13.35

The grand composite curve obtained with this configuration is shown in the following figure. Figure 4.5 highlights the total heat recovered.

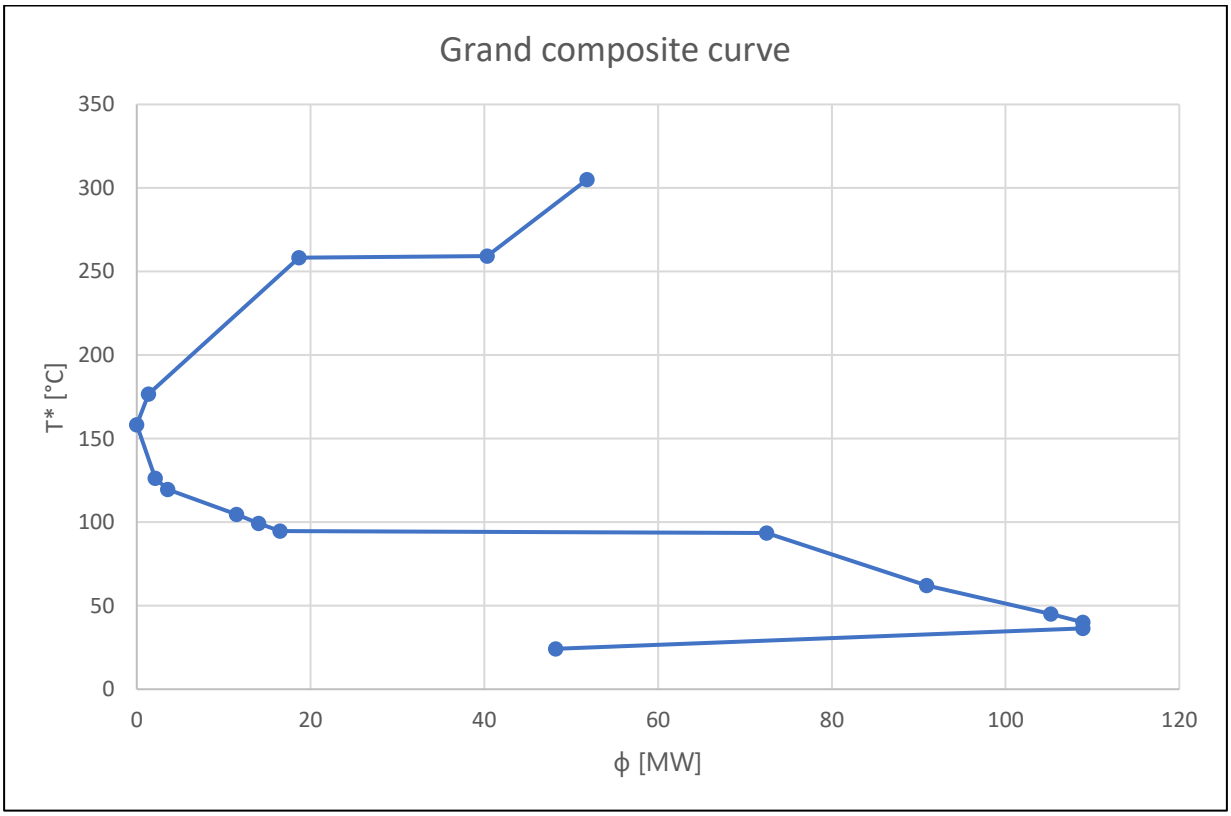

Figure 4.4 - Grand composite curve

The grand composite curve is used to determine the possibility of reducing the quality of external energy sources required to satisfy the heat demand of the plant, and it is a useful tool also to understand the minimum temperature at which heat from the external sources must be provided.

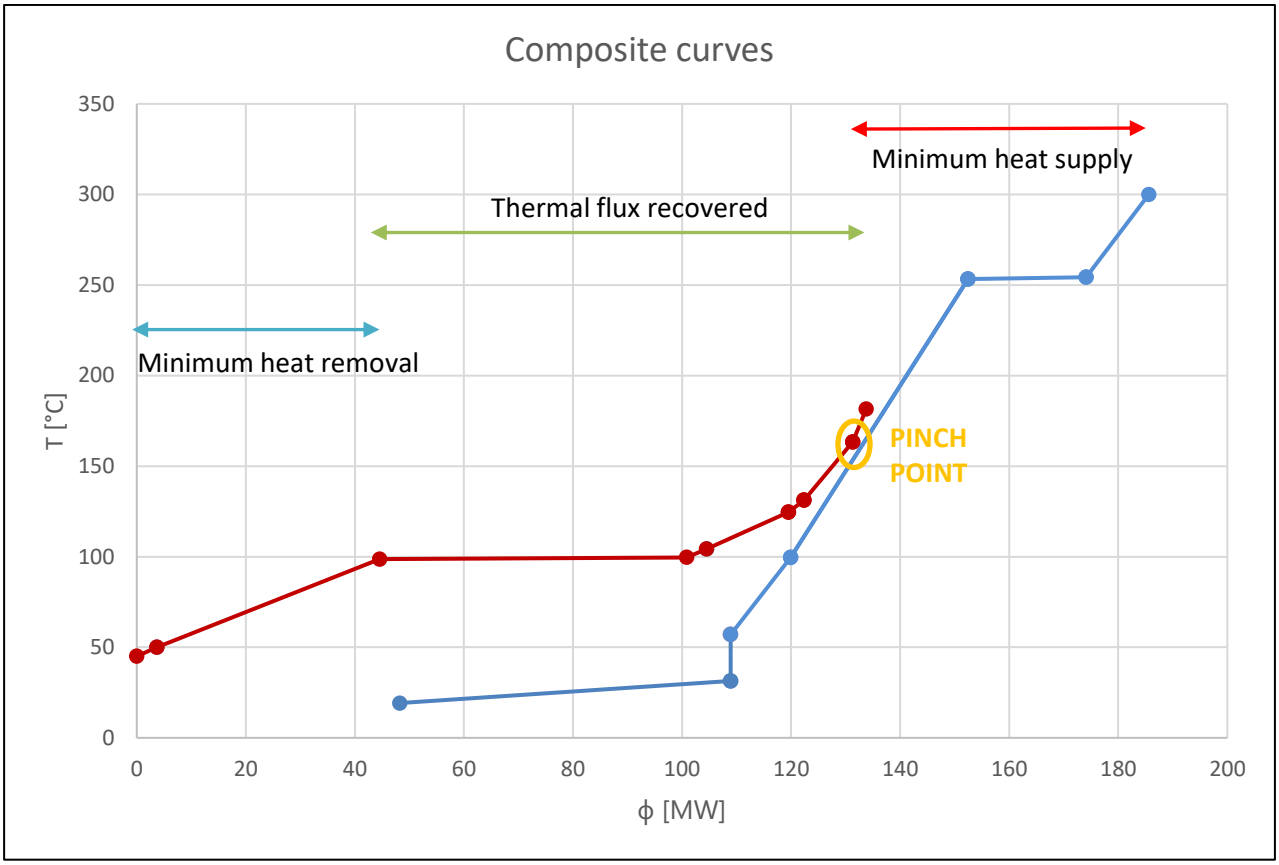

Figure 4.5 - Composite curves

The minimum temperature difference between the two streams flowing in each of the designed heat exchangers ("pinch point" T) has been set to 10 °C. The results obtained by the application of the pinch analysis methodology are interesting, especially looking at the green arrow of Figure 4.5. It represents the internal thermal energy demand that can be satisfied simply by realizing a heat exchange network. This amount of energy is recovered inside the plant and therefore not required by an external source with a significant saving in terms of primary energy to be employed.

Once the pinch analysis is applied, it is possible to consider other possible heat sources inside the plant. As already known, the slaker is highly exothermic: assuming 75% efficiency for the direct utilization of the thermal energy produced, the amount of heat duty recovered from the reactor

is 45.36 MW. At the end, the heat demand that is not satisfied by the heat recovery system of the plant is 6.46 MW that must be therefore provided by natural gas. All these results can be found in the following table.

Table 4.4 - Final heat demand after pinch analysis and thermal recovery

	Heat demand/availability [MW]
From pinch analysis	51.82
Slaker reactor	-45.36
TOTAL	**6.46**

To obtain the total primary energy consumption needed to generate the heat which must be provided with an external source, a conversion factor of 1.1 has been considered to pass from thermal energy to primary energy. Therefore, the calculated primary energy consumption is 0.3116 $MJ/mol_{CO2,\ captured}$.

Table 4.5 shows a comparison between the key energy performance indicator given by the reference paper of Keith and CE, and the value calculated with the model developed in this thesis.

Table 4.5 - Final comparison with reference paper

Comparison with other papers		
	[MJ/mol_CO_2]	[kWh/kg_CO_2]
Minimum work of separation	0.0210	0.1326
Keith [24]	0.3876	2.45
DAC plant – THESIS WORK	0.3116	1.97

The value obtained in this paper (last row) has been calculated under these hypothesis:

- application of pinch analysis methodology;
- adiabatic calciner;
- natural gas instead of pure CH_4.

The difference between the number obtained in this paper and Keith's value is mainly due to the last point, because the LHV of the pure methane is of course higher than LHV of natural gas; to

compensate this difference, the mass flow rates of natural gas used in this thesis are only slightly higher than in the case of Keith and this is the reason why the value obtained here is below the one of the reference source which uses pure CH_4.

4.1 Future developments

The field of direct air capture incorporates ideas and works of many different types. This paper has been written with the aim of giving a model to allow further assessments by third parties and to provide a solid basis to develop and improve when steps forward in the field of direct air capture will be carried out.

Some other academic works have been already published on this topic, but the values of the same energy performance indicator calculated in this chapter, have been significantly different with respect to the one obtained here. Therefore, a first interesting start could be the comparison between this paper and those works [2], [25], [26], with the aim of investigating the reasons of such differences and understanding the possibility of merging the strengths between the various solutions proposed.

Furthermore, the plant analysed requires a certain amount of external energy here provided by a conventional fossil fuel (natural gas). In the perspective of reducing the consumption of all kinds of fossil fuels, a very innovative and promising development could refer to the use of synthetic hydrocarbons instead of natural gas. Synthetic hydrocarbons can be generated through the Fischer-Tropsch process, starting from a different carbon capture system. In fact, re-using the CO_2 converted in CO, together with H_2, it is possible to produce synthetic fuels; this could be interesting mainly with the goal of creating a net-zero carbon dioxide emission. For this reason, it is an attractive concept that should be studied in future insights.

5. Conclusions

In this thesis, a reference DAC plant has been analysed whit the aim of reproducing it with an Aspen Plus® model to provide a basis for future developments and to assess its feasibility from an energy point of view.

The plant has been subdivided in different sections, each of them reproduced in the software. The components adopted in the model tried to reproduce as much as possible the real behaviour of the plant. To fulfil this requirement, some design specifications have been implemented to modify mainly mass flow rates of some streams or split fractions of specific blocks.

Once the model has been completed, its accuracy has been tested only from the energy point of view as to carry out a tecno-economic analysis, data that are not yet available in the DAC field would have been necessary, such as the cost of components. The absence of already existing plants is indeed one of the major problems that must be faced to evaluate also the economic feasibility of a DAC system.

However, the energy analysis has been performed firstly considering the thermal integration inside the plant: pinch analysis has been realized to evaluate possible thermal recovery between the streams of the plant. Thanks to the integration, about 90% of thermal recovery has been estimated, thus confirming the goodness of this kind of solution in such a system. In this plant, several streams must be either cooled or heated: these are the perfect conditions for implementing a thermal integration with the pinch analysis methodology. At the end of the calculations, it has been found that the minimum heat supply is 51.82 MW whereas the minimum heat removal is 48.24 MW. The “cold demand” can be satisfied by an external cold stream (e.g. water at ambient conditions), while the heat demand is covered with the same natural gas used to feed the calciner and the power island section. Moreover, the electricity demand of the plant is completely satisfied by the gas turbine of the power island and the steam turbine of the steam slaker section.

The energy performance indicator calculated gives a value of primary energy consumed to separate a unit of CO_2. A value of 0.3116 $MJ/mol_{CO2,captured}$ has been obtained considering the best operating conditions to reduce the energy demand of the plant, that are listed in the next page:

- application of pinch analysis methodology;
- use of an adiabatic calciner;
- use of natural gas instead of pure methane.

The result has been validated through the comparison with the same performance index provided by the reference source (0.3876 MJ/$mol_{CO2,captured}$).

To conclude, since there is still a lack of detailed technical documentations concerning the Direct Air Capture sector, this work can be a starting point for further studies, which can focus on other issues related to the analysed process, such as the utilization of other types of solvents (e.g. NaOH) and the exploitation of the captured CO_2.

References

[1] IPCC, *Climate Change 2014: Synthesis Report*. .

[2] R. Baciocchi, G. Storti, and M. Mazzotti, “Process design and energy requirements for the capture of carbon dioxide from air,” vol. 45, pp. 1047–1058, 2006.

[3] UNFCCC (United Nations Framework Convention on Climate Change), “The Paris Agreement,” 2015. [Online]. Available: https://unfccc.int/process-and-meetings/the-paris-agreement/the-paris-agreement. [Accessed: 18-Nov-2018].

[4] United Nations, “Transforming our world: the 2030 Agenda for Sustainable Development,” *Gen. Assem. 70 Sess.*, vol. 16301, no. October, pp. 1–35, 2015.

[5] EU (European Union), “Strategic Energy Technology (SET) Plan,” 2015. [Online]. Available: https://ec.europa.eu/research/energy/index.cfm?pg=policy&policyname=set. [Accessed: 08-Nov-2018].

[6] G. Cinti, A. Baldinelli, A. Di Michele, and U. Desideri, “Integration of Solid Oxide Electrolyzer and Fischer-Tropsch: A sustainable pathway for synthetic fuel,” *Appl. Energy*, vol. 162, pp. 308–320, 2016.

[7] M. Samavati, A. Martin, V. Nemanova, and M. Santarelli, “Integration of solid oxide electrolyser, entrained gasification, and Fischer-Tropsch process for synthetic diesel production: Thermodynamic analysis,” *Int. J. Hydrogen Energy*, pp. 1–19, 2018.

[8] IPCC, *Carbon Dioxide Capture and Storage*. 2005.

[9] C. R. Murdock, S. A. Didas, and C. W. Jones, “Direct Capture of CO2 from Ambient Air,” 2016.

[10] E. Tzimas and S. Peteves, *Controlling emissions: the option of Carbon Sequestration*. 2003.

[11] M. J. Prins, K. J. Ptasinski, and F. J. J. G. Janssen, “Exergetic optimisation of a production process of Fischer-Tropsch fuels from biomass,” *Fuel Process. Technol.*, vol. 86, no. 4, pp. 375–389, 2005.

[12] I. Dimitriou, P. García-Gutiérrez, R. H. Elder, R. M. Cuéllar-Franca, A. Azapagic, and R. W. K. Allen, “Carbon dioxide utilisation for production of transport fuels: process and economic analysis,” *Energy Environ. Sci.*, vol. 8, no. 6, pp. 1775–1789, 2015.

[13] C. Pritchard, A. Yang, P. Holmes, and M. Wilkinson, “Thermodynamics, economics and systems thinking: What role for air capture of CO2?,” *Process Saf. Environ. Prot.*, vol. 94, no. C, pp. 188–195, 2015.

[14] K. Z. House, A. C. Baclig, M. Ranjan, E. A. van Nierop, J. Wilcox, and H. J. Herzog, “Economic and energetic analysis of capturing CO2 from ambient air,” *Proc. Natl. Acad. Sci.*, vol. 108, no. 51, pp. 20428–20433, 2011.

[15] P. Viglierco, “Techno-economic analysis of an amine scrubbing based biogas upgrading process for biomethane injection into the gas grid,” 2017.

[16] F. R. H. Abdeen, M. Mel, M. S. Jami, S. I. Ihsan, and A. F. Ismail, “A review of chemical absorption of carbon dioxide for biogas upgrading,” *Chinese J. Chem. Eng.*, vol. 24, no. 6, pp. 693–702, 2016.

[17] F. Bauer, C. Hulteberg, T. Persson, and D. Tamm, “Biogas upgrading – Review of commercial technologies,” *Swedish Gas Technol. Centre, SGC*, p. 82, 2013.

[18] FNR, M. Beil, W. Beyrich, U. Holzhammer, and T. Krause, “Biomethane,” p. 48, 2013.

[19] American Physical Society, “Direct Air Capture of CO2 with Chemicals,” *Am. Phys. Soc.*, 2011.

[20] D. W. Keith, “Why Capture CO 2 from the Atmosphere ?,” vol. 1654, no. 2009, pp. 1654–1656, 2012.

[21] M. Ranjan and H. J. Herzog, “Feasibility of air capture,” *Energy Procedia*, vol. 4, no. 2010, pp. 2869–2876, 2011.

[22] V. Gutknecht, S. Ó. Snæbjörnsdóttir, B. Sigfússon, E. S. Aradóttir, and L. Charles, “Creating a carbon dioxide removal solution by combining rapid mineralization of CO 2 with direct air capture,” *Energy Procedia*, vol. 146, pp. 129–134, 2018.

[23] K. S. Lackner, “Capture of carbon dioxide from ambient air,” *Eur. Phys. J. Spec. Top.*, vol. 176, no. 1, pp. 93–106, 2009.

[24] D. W. Keith, G. Holmes, D. St. Angelo, and K. Heidel, “A process for capturing CO2 from the atmosphere,” *Joule*, 2018.

[25] F. Zeman, “Energy and material balance of CO2 capture from ambient air,” *Environ. Sci. Technol.*, vol. 41, no. 21, pp. 7558–7563, 2007.

[26] A. Bandi, T. Weimer, K. Schaber, and M. Specht, “CO2 Recycling for Hydrogen Storage and Transportation-Electrochemical CO2 Removal and Fixation,” *Transportation (Amst).*, vol. 36, no. 95, 1995.

[27] CE (Carbon Engineering), “Carbon Engineering website,” 2009. [Online]. Available: http://carbonengineering.com/. [Accessed: 20-Nov-2018].

[28] C. Chen, H. Britt, J. F. Boston, and L. B. Evans, “Extension and Application of the Pitzer Equation for Vapor-Liquid Equilibrium of Aqueous Electrolyte Systems with Molecular Solutes,” vol. 25, no. 5, pp. 820–831, 1979.

[29] C. Chen, H. Britt, and J. F. Boston, “Local Composition Model for Excess Gibbs Energy of Electrolyte Systems,” vol. 28, no. 4, pp. 588–596, 1982.

[30] B. Mock, L. B. Evans, and C. Chen, “Thermodynamic Representation of Phase Equilibria of Mixed-Solvent Electrolyte Systems,” vol. 32, no. 10, pp. 1655–1664, 1986.

[31] C. Chen and Y. Song, “Generalized Electrolyte-NRTL Model for Mixed-Solvent Electrolyte Systems,” vol. 50, no. 8, 2004.

[32] J. E. Crooks and J. P. Donnellan, “Kinetics and Mechanism of the Reaction between Carbon Dioxide and Amines in Aqueous Solution.” .

[33] O. Redlich and J. N. S. Kwong, “On the thermodynamics of solutions,” *Chem. Rev.*, vol. 44,

no. 1, pp. 233–244, 1949.

[34] S. Moioli, L. A. Pellegrini, and S. Gamba, “Simulation of CO2 capture by MEA scrubbing with a rate-based model,” vol. 42, no. August, pp. 1651–1661, 2012.

[35] Y. Zhang, H. Chen, C. C. Chen, J. M. Plaza, R. Dugas, and G. T. Rochelle, “Rate-based process modeling study of CO2 capture with aqueous monoethanolamine solution,” *Ind. Eng. Chem. Res.*, vol. 48, no. 20, pp. 9233–9246, 2009.

[36] G. Qi, S. Wang, H. Yu, P. Feron, and C. Chen, “Rate-Based Modeling of CO2 Absorption in Aqueous NH3 in a Packed Column,” *Energy Procedia*, vol. 37, no. x, pp. 1968–1976, 2013.

[37] W. K. Lewis and W. G. Whitman, “Principles of Gas Absorption,” *Ind. Eng. Chem.*, vol. 16, no. 12, pp. 1215–1220, 1924.

[38] A. Benamor, B. S. Ali, and M. K. Aroua, “Kinetic of CO2absorption and carbamate formation in aqueous solutions of diethanolamine,” *Korean J. Chem. Eng.*, vol. 25, no. 3, pp. 451–460, 2008.

[39] M. R. M. Abu Zahra, *Carbon dioxide capture from flue gas: Development and evaluation of existing and novel process concepts*. 2009.

[40] G. Léonard, “Optimal design of a CO 2 absorption unit and assessment of solvent degradation,” no. June, p. 55, 2011.

[41] K. Onda, H. Takeuchi, and Y. Okumoto, “Mass transfer coefficients between gas and liquid phases in packed columns,” 1968.

[42] I. C. Kemp, *Pinch analysis and process integration: A user guide on process integration for the efficient use of energy*. 2007.

APPENDIX

		10	24	33-B	44	46	54	61	62	65	73
Temperature	[°C]	19,2	24,9	300,0	369,4	59,7	415,0	300,0	674,0	415,1	26,1
Pressure	[bar]	1,0	1,0	1,0	1,0	1,0	42,0	42,0	1,0	42,0	1,0
Mass flow	[tonne/hr]	4789,7	217,7	217,7	163,1	549,8	25,0	63,2	123,9	63,2	121,0
Mass fraction	[%]										
H_2O		0,904	0	0	0,126	1	1	1	0	1	0,109
KOH		0	0	0	0	0	0	0	0	0	0
K_2CO_3		0	0	0	0	0	0	0	0	0	0
O_2		0	0	0	0,117	0	0	0	0	0	0,021
N_2		0	0	0	0,02	0	0	0	0	0	0,743
CO_2		0	0	0	0,737	0	0	0	0	0	0,127
$CaCO_3$		0	1	1	0	0	0	0	0,035	0	0
Ca++		0	0	0	0	0	0	0	0	0	0
H_3O+		0	0	0	0	0	0	0	0	0	0
CaOH+		0	0	0	0	0	0	0	0	0	0
K+		0,044	0	0	0	0	0	0	0	0	0
KOH (S)		0	0	0	0	0	0	0	0	0	0
K_2CO_3 (S)		0	0	0	0	0	0	0	0	0	0
$Ca(OH)_2$		0	0	0	0	0	0	0	0	0	0
HCO_3-		0,036	0	0	0	0	0	0	0	0	0
OH-		0	0	0	0	0	0	0	0	0	0
CO_3--		0,016	0	0	0	0	0	0	0	0	0
CaO		0	0	0	0	0	0	0	0,965	0	0
CH_4		0	0	0	0	0	0	0	0	0	0
C_2H_6		0	0	0	0	0	0	0	0	0	0

AIR CONTACTOR section		1	2	3	4	5	6	7	8	9	10	10-BIS	73	74
Temperature	[°C]	21,0	21,0	21,0	17,9	17,8	17,8	17,8	21,0	55,2	19,2	19,2	26,1	55,9
Pressure	[bar]	1,0	1,0	1,0	1,0	1,0	1,0	1,0	1,0	1,0	1,0	1,0	1,0	1,0
Mass flow	[tonne/hr]	250000,0	250103,8	2760,6	252864,4	248266,5	4597,9	4597,9	174,6	191,8	4789,7	4789,7	121,0	103,8
Mass fraction	[%]													
H_2O		0,01	0,01	0,887	0,019	0,003	0,908	0,908	0,887	0,813	0,904	0,904	0,109	0,104
KOH		0	0	0	0	0	0	0	0	0	0	0	0	0
K_2CO_3		0	0	0	0	0	0	0	0	0	0	0	0	0
O_2		0,23	0,23	0	0,227	0,232	0	0	0	0	0	0	0,021	0,024
N_2		0,76	0,76	0	0,751	0,765	0	0	0	0,005	0	0	0,743	0,857
CO_2		0,001	0,001	0	0	0	0	0	0	0,016	0	0	0,127	0,015
$CaCO_3$		0	0	0	0	0	0	0	0	0	0	0	0	0
Ca++		0	0	0	0	0	0	0	0	0	0	0	0	0
H_3O+		0	0	0	0	0	0	0	0	0	0	0	0	0
CaOH+		0	0	0	0	0	0	0	0	0	0	0	0	0
K+		0	0	0,071	0,001	0	0,043	0,043	0,071	0,065	0,044	0,044	0	0
KOH (S)		0	0	0	0	0	0	0	0	0	0	0	0	0
K_2CO_3 (S)		0	0	0	0	0	0	0	0	0	0	0	0	0
$Ca(OH)_2$		0	0	0	0	0	0	0	0	0	0	0	0	0
HCO_3-		0	0	0	0,001	0	0,032	0,032	0	0,1	0,036	0,036	0	0
OH-		0	0	0,017	0	0	0	0	0,017	0	0	0	0	0
CO_3--		0	0	0,025	0	0	0,017	0,017	0,025	0	0,016	0,016	0	0
CaO		0	0	0	0	0	0	0	0	0	0	0	0	0
CH_4		0	0	0	0	0	0	0	0	0	0	0	0	0
C_2H_6		0	0	0	0	0	0	0	0	0	0	0	0	0

PELLET REACTOR section - 1		10	11	12	13	14	15	16	17	18	19
Temperature	[°C]	19,2	21,0	25,0	25,0	25,0	25,0	25,0	25,0	25,0	25,0
Pressure	[bar]	1,0	1,0	1,0	1,0	1,0	1,0	1,0	0,9	0,9	1,0
Mass flow	[tonne/hr]	4789,7	770,0	53010,3	192,0	52818,3	52,8	52765,5	5367,4	47398,1	47398,1
Mass fraction	[%]										
H_2O		0,904	0,706	0,93	0	0,934	0,934	0,934	0,918	0,935	0,935
KOH		0	0	0	0	0	0	0	0	0	0
K_2CO_3		0	0	0	0	0	0	0	0	0	0
O_2		0	0	0	0	0	0	0	0	0	0
N_2		0	0	0	0	0	0	0	0	0	0
CO_2		0	0	0	0	0	0	0	0	0	0
$CaCO_3$		0	0,007	0,006	1	0,002	0,002	0,002	0,019	0	0
Ca++		0	0	0	0	0	0	0	0	0	0
H_3O+		0	0	0	0	0	0	0	0	0	0
CaOH+		0	0	0	0	0	0	0	0	0	0
K+		0,044	0,007	0,041	0	0,041	0,041	0,041	0,04	0,041	0,041
KOH (S)		0	0	0	0	0	0	0	0	0	0
K_2CO_3 (S)		0	0	0	0	0	0	0	0	0	0
$Ca(OH)_2$		0	0,277	0	0	0	0	0	0	0	0
HCO_3-		0,036	0	0	0	0	0	0	0	0	0
OH-		0	0,003	0,01	0	0,01	0,01	0,01	0,01	0,01	0,01
CO_3--		0,016	0	0,014	0	0,014	0,014	0,014	0,014	0,014	0,014
CaO		0	0	0	0	0	0	0	0	0	0
CH_4		0	0	0	0	0	0	0	0	0	0
C_2H_6		0	0	0	0	0	0	0	0	0	0

PELLET REACTOR section - 2		20	21	22	23	24	25	26	27	28	75
Temperature	[°C]	25,0	21,0	24,9	24,9	24,9	25,0	25,0	25,0	25,0	25,0
Pressure	[bar]	1,0	1,0	1,0	1,0	1,0	1,0	1,0	1,0	1,0	1,0
Mass flow	[tonne/hr]	244,9	9,4	270,4	52,7	217,7	101,0	5266,5	11,5	73,3	16,2
Mass fraction	[%]										
H_2O		0,201	0	0,182	0,935	0	0	0,935	0	0	0
KOH		0	0	0	0	0	0	0	0	0	0
K_2CO_3		0	0	0	0	0	0	0	0	0	0
O_2		0	0	0	0	0	0	0	0	0	0
N_2		0	0	0	0	0	0	0	0	0	0
CO_2		0	0	0	0	0	0	0	0	0	0
$CaCO_3$		0,785	1	0,805	0	1	1	0	1	1	1
Ca++		0	0	0	0	0	0	0	0	0	0
H_3O+		0	0	0	0	0	0	0	0	0	0
CaOH+		0	0	0	0	0	0	0	0	0	0
K+		0,009	0	0,008	0,041	0	0	0,041	0	0	0
KOH (S)		0	0	0	0	0	0	0	0	0	0
K_2CO_3 (S)		0	0	0	0	0	0	0	0	0	0
$Ca(OH)_2$		0	0	0	0	0	0	0	0	0	0
HCO_3-		0	0	0	0	0	0	0	0	0	0
OH-		0,002	0	0,002	0,01	0	0	0,01	0	0	0
CO_3--		0,003	0	0,003	0,014	0	0	0,014	0	0	0
CaO		0	0	0	0	0	0	0	0	0	0
CH_4		0	0	0	0	0	0	0	0	0	0
C_2H_6		0	0	0	0	0	0	0	0	0	0

STEAM SLAKER section - 1		24	29	30	31	32	33-A	33-B	46	54	55	56	57	57-B	58	58-BIS
Temperature	[°C]	24,9	57,0	57,0	99,6	300,0	300,0	300,0	59,7	415,0	104,3	99,6	99,6	50,0	50,0	51,4
Pressure	[bar]	1,0	1,0	1,0	1,0	1,0	1,0	1,0	1,0	42,0	1,0	1,0	1,0	1,0	42,0	42,0
Mass flow	[tonne/hr]	217,7	391,8	375,7	391,8	391,8	174,2	217,7	549,8	25,0	88,2	88,2	88,2	88,2	70,2	88,2
Mass fraction	[%]															
H_2O		0	0,444	1	0,444	0,444	1	0	1	1	1	1	1	1	1	1
KOH		0	0	0	0	0	0	0	0	0	0	0	0	0	0	0
K_2CO_3		0	0	0	0	0	0	0	0	0	0	0	0	0	0	0
O_2		0	0	0	0	0	0	0	0	0	0	0	0	0	0	0
N_2		0	0	0	0	0	0	0	0	0	0	0	0	0	0	0
CO_2		0	0	0	0	0	0	0	0	0	0	0	0	0	0	0
$CaCO_3$		1	0,556	0	0,556	0,556	0	1	0	0	0	0	0	0	0	0
Ca++		0	0	0	0	0	0	0	0	0	0	0	0	0	0	0
H_3O+		0	0	0	0	0	0	0	0	0	0	0	0	0	0	0
CaOH+		0	0	0	0	0	0	0	0	0	0	0	0	0	0	0
K+		0	0	0	0	0	0	0	0	0	0	0	0	0	0	0
KOH (S)		0	0	0	0	0	0	0	0	0	0	0	0	0	0	0
K_2CO_3 (S)		0	0	0	0	0	0	0	0	0	0	0	0	0	0	0
$Ca(OH)_2$		0	0	0	0	0	0	0	0	0	0	0	0	0	0	0
HCO_3-		0	0	0	0	0	0	0	0	0	0	0	0	0	0	0
OH-		0	0	0	0	0	0	0	0	0	0	0	0	0	0	0
CO_3--		0	0	0	0	0	0	0	0	0	0	0	0	0	0	0
CaO		0	0	0	0	0	0	0	0	0	0	0	0	0	0	0
CH_4		0	0	0	0	0	0	0	0	0	0	0	0	0	0	0
C_2H_6		0	0	0	0	0	0	0	0	0	0	0	0	0	0	0

STEAM SLAKER section - 2		59	60	61	61-B	61-TRIS	62	63	64	65	67	68	69	70	71	72
Temperature	[°C]	253,3	253,3	253,3	253,3	300,0	674,0	300,0	99,6	415,1	300,0	300,0	300,0	300,0	85,0	99,6
Pressure	[bar]	42,0	42,0	42,0	42,0	42,0	1,0	1,0	1,0	42,0	1,0	1,0	1,0	1,0	1,0	1,0
Mass flow	[tonne/hr]	70,2	7,0	63,2	63,2	63,2	123,9	305,9	7,0	63,2	305,1	0,8	17,6	287,4	287,4	663,2
Mass fraction	[%]															
H_2O		1	1	1	1	1	0	0,485	1	1	0,487	0	0	0,516	0,516	0,79
KOH		0	0	0	0	0	0	0	0	0	0	0	0	0	0	0
K_2CO_3		0	0	0	0	0	0	0	0	0	0	0	0	0	0	0
O_2		0	0	0	0	0	0	0	0	0	0	0	0	0	0	0
N_2		0	0	0	0	0	0	0	0	0	0	0	0	0	0	0
CO_2		0	0	0	0	0	0	0	0	0	0	0	0	0	0	0
$CaCO_3$		0	0	0	0	0	0,035	0,016	0	0	0,014	0,574	0	0,015	0,015	0,007
Ca++		0	0	0	0	0	0	0	0	0	0	0	0	0	0	0
H_3O+		0	0	0	0	0	0	0	0	0	0	0	0	0	0	0
CaOH+		0	0	0	0	0	0	0	0	0	0	0	0	0	0	0
K+		0	0	0	0	0	0	0	0	0	0	0	0	0	0	0
KOH (S)		0	0	0	0	0	0	0	0	0	0	0	0	0	0	0
K_2CO_3 (S)		0	0	0	0	0	0	0	0	0	0	0	0	0	0	0
$Ca(OH)_2$		0	0	0	0	0	0	0,44	0	0	0,441	0	0	0,468	0,468	0,203
HCO_3-		0	0	0	0	0	0	0	0	0	0	0	0	0	0	0
OH-		0	0	0	0	0	0	0	0	0	0	0	0	0	0	0
CO_3--		0	0	0	0	0	0	0	0	0	0	0	0	0	0	0
CaO		0	0	0	0	0	0,965	0,059	0	0	0,058	0,426	1	0	0	0
CH_4		0	0	0	0	0	0	0	0	0	0	0	0	0	0	0
C_2H_6		0	0	0	0	0	0	0	0	0	0	0	0	0	0	0

CALCINER section		33-B	34	35	36	37	38	39	40	41	42	43	44	61-BIS	62	65
Temperature	[°C]	300,0	471,7	685,5	200,0	652,0	25,0	900,0	900,0	900,0	650,0	450,0	369,4	300,0	674,0	415,1
Pressure	[bar]	1,0	1,0	1,0	1,0	1,0	1,0	1,0	1,0	1,0	1,0	1,0	1,0	42,0	1,0	42,0
Mass flow	[tonne/hr]	217,7	217,7	217,7	58,5	58,5	10,8	287,0	123,9	163,1	163,1	163,1	163,1	63,2	123,9	63,2
Mass fraction	[%]															
H_2O		0	0	0	0	0	0	0,071	0	0,126	0,126	0,126	0,126	1	0	1
KOH		0	0	0	0	0	0	0	0	0	0	0	0	0	0	0
K_2CO_3		0	0	0	0	0	0	0	0	0	0	0	0	0	0	0
O_2		0	0	0	0,956	0,956	0	0,067	0	0,117	0,117	0,117	0,117	0	0	0
N_2		0	0	0	0,044	0,044	0,064	0,011	0	0,02	0,02	0,02	0,02	0	0	0
CO_2		0	0	0	0	0	0,075	0,419	0	0,737	0,737	0,737	0,737	0	0	0
$CaCO_3$		1	1	1	0	0	0	0,015	0,035	0	0	0	0	0	0,035	0
Ca++		0	0	0	0	0	0	0	0	0	0	0	0	0	0	0
H_3O+		0	0	0	0	0	0	0	0	0	0	0	0	0	0	0
CaOH+		0	0	0	0	0	0	0	0	0	0	0	0	0	0	0
K+		0	0	0	0	0	0	0	0	0	0	0	0	0	0	0
KOH (S)		0	0	0	0	0	0	0	0	0	0	0	0	0	0	0
K_2CO_3 (S)		0	0	0	0	0	0	0	0	0	0	0	0	0	0	0
$Ca(OH)_2$		0	0	0	0	0	0	0	0	0	0	0	0	0	0	0
HCO_3-		0	0	0	0	0	0	0	0	0	0	0	0	0	0	0
OH-		0	0	0	0	0	0	0	0	0	0	0	0	0	0	0
CO_3--		0	0	0	0	0	0	0	0	0	0	0	0	0	0	0
CaO		0	0	0	0	0	0	0,417	0,965	0	0	0	0	0	0,965	0
CH_4		0	0	0	0	0	0,796	0	0	0	0	0	0	0	0	0
C_2H_6		0	0	0	0	0	0,065	0	0	0	0	0	0	0	0	0

CO_2 COMPRESSION section		44	45	46	47	100	101	102	103	104	105	106	CO_2
Temperature	[°C]	369,4	21,0	59,7	59,7	181,6	45,0	163,3	45,0	131,2	45,0	124,6	45,0
Pressure	[bar]	1,0	1,0	1,0	1,0	3,5	3,5	12,3	12,3	42,9	42,9	150,1	150,1
Mass flow	[tonne/hr]	163,1	531,0	549,8	144,2	144,2	144,2	144,2	144,2	144,2	144,2	144,2	144,2
Mass fraction	[%]												
H_2O		0,126	1	1	0,012	0,012	0,012	0,012	0,012	0,012	0,012	0,012	0,012
KOH		0	0	0	0	0	0	0	0	0	0	0	0
K_2CO_3		0	0	0	0	0	0	0	0	0	0	0	0
O_2		0,117	0	0	0,133	0,133	0,133	0,133	0,133	0,133	0,133	0,133	0,133
N_2		0,02	0	0	0,023	0,023	0,023	0,023	0,023	0,023	0,023	0,023	0,023
CO_2		0,737	0	0	0,833	0,833	0,833	0,833	0,833	0,833	0,833	0,833	0,833
$CaCO_3$		0	0	0	0	0	0	0	0	0	0	0	0
Ca++		0	0	0	0	0	0	0	0	0	0	0	0
H_3O+		0	0	0	0	0	0	0	0	0	0	0	0
CaOH+		0	0	0	0	0	0	0	0	0	0	0	0
K+		0	0	0	0	0	0	0	0	0	0	0	0
KOH (S)		0	0	0	0	0	0	0	0	0	0	0	0
K_2CO_3 (S)		0	0	0	0	0	0	0	0	0	0	0	0
$Ca(OH)_2$		0	0	0	0	0	0	0	0	0	0	0	0
HCO_3-		0	0	0	0	0	0	0	0	0	0	0	0
OH-		0	0	0	0	0	0	0	0	0	0	0	0
CO_3--		0	0	0	0	0	0	0	0	0	0	0	0
CaO		0	0	0	0	0	0	0	0	0	0	0	0
CH_4		0	0	0	0	0	0	0	0	0	0	0	0
C_2H_6		0	0	0	0	0	0	0	0	0	0	0	0

POWER ISLAND section		48	49	50	51	52	53	54	73
Temperature	[°C]	20,0	315,4	25,0	1000,0	581,3	25,0	415,0	26,1
Pressure	[bar]	1,0	10,0	1,0	10,0	1,0	1,0	42,0	1,0
Mass flow	[tonne/hr]	114,7	114,7	6,3	121,0	121,0	25,0	25,0	121,0
Mass fraction	[%]								
H_2O		0,01	0,01	0	0,109	0,109	1	1	0,109
KOH		0	0	0	0	0	0	0	0
K_2CO_3		0	0	0	0	0	0	0	0
O_2		0,21	0,21	0	0,021	0,021	0	0	0,021
N_2		0,78	0,78	0,064	0,743	0,743	0	0	0,743
CO_2		0	0	0,075	0,127	0,127	0	0	0,127
$CaCO_3$		0	0	0	0	0	0	0	0
Ca++		0	0	0	0	0	0	0	0
H_3O+		0	0	0	0	0	0	0	0
CaOH+		0	0	0	0	0	0	0	0
K+		0	0	0	0	0	0	0	0
KOH (S)		0	0	0	0	0	0	0	0
K_2CO_3 (S)		0	0	0	0	0	0	0	0
$Ca(OH)_2$		0	0	0	0	0	0	0	0
HCO_3-		0	0	0	0	0	0	0	0
OH-		0	0	0	0	0	0	0	0
CO_3--		0	0	0	0	0	0	0	0
CaO		0	0	0	0	0	0	0	0
CH_4		0	0	0,796	0	0	0	0	0
C_2H_6		0	0	0,065	0	0	0	0	0